UNIVERSIDADE FEDERAL DO RIO GRANDE DO SUL
INSTITUTO DE GEOCIÊNCIAS
PROGRAMA DE PÓS-GRADUAÇÃO EM GEOCIÊNCIAS

EVOLUÇÃO PETROLÓGICA DO MAGMATISMO TTG PALEOPROTEROZOICO DO COMPLEXO ARROIO DOS RATOS, DISTRITO DE QUITÉRIA, SÃO JERÔNIMO/RS

TIAGO RAFAEL GREGORY

ORIENTADOR – Profª. Drª. Maria de Fátima Bitencourt

CO-ORIENTADOR – Prof. Dr. Lauro Valentim Stoll Nardi

Porto Alegre – 2014

Gregory, Tiago Rafael
Evolução Petrológica do Magmatismo TTG paleoproterozoico do Complexo Arroio dos Ratos, Distrito de Quitéria, São Jerônimo/RS . / Tiago Rafael Gregory. - Porto Alegre: IGEO/UFRGS, 2014.
[99 f.] il.

Tese (Doutorado).- Universidade Federal do Rio Grande do Sul.Programa de Pós-Graduação em Geocências.Instituto de Geociências. Porto Alegre, RS - BR,2014.

Orientador(es):Maria de Fátima Bitencourt
Coorientador(es):Lauro Valentim Stoll Nardi

1.Associações tipo TTG.2.U-Pb LA-MC-ICP-MS em zircão.3.Isótopos de Sr-Nd-Pb.4.Magmatismo paleoproterozoico no ESrg.I. Título.

CDU 56

Catalogação na Publicação
Biblioteca Instituto de Geociências – UFRGS
Renata Cristina Grun CRB 10/1113

Universidade Federal do Rio Grande do Sul - Campus do Vale Av. Bento Gonçalves, 9500 - Porto Alegre - RS - Brasil CEP: 91501-970 / Caixa Postal: 15001.
Fone: +55 51 3308-6329 Fax: +55 51 3308-6337
E-mail: bibgeo@ufrgs.br

UNIVERSIDADE FEDERAL DO RIO GRANDE DO SUL
INSTITUTO DE GEOCIÊNCIAS
PROGRAMA DE PÓS-GRADUAÇÃO EM GEOCIÊNCIAS

EVOLUÇÃO PETROLÓGICA DO MAGMATISMO TTG PALEOPROTEROZOICO DO COMPLEXO ARROIO DOS RATOS, DISTRITO DE QUITÉRIA, SÃO JERÔNIMO/RS

TIAGO RAFAEL GREGORY

ORIENTADOR – Profª. Drª. Maria de Fátima Bitencourt

CO-ORIENTADOR – Prof. Dr. Lauro Valentim Stoll Nardi

BANCA EXAMINADORA

Prof. Dr. Márcio Martins Pimentel – Instituto de Geociências – Universidade de Brasília

Profª. Drª. Ignez Pinho Guimarães – Departamento de Geologia – Universidade Federal de Pernambuco

Prof. Dr. Edinei Koester – Instituto de Geociências – Universidade Federal do Rio Grande do Sul

Tese de Doutorado apresentada como requisito parcial para a obtenção do Título de Doutor em Ciências.

Porto Alegre – 2014

Epígrafe

"Levantou água minha linhada, bateu no meio do rio, quem *tá* pescando não pensa nada, *tá* procurando o que não viu." Miguel Bicca

Dedicatória

Este trabalho é dedicado às pessoas que acreditaram na minha jornada geológica e acadêmica. Não é fácil virar doutor. Também é dedicado às pessoas que fazem geologia com paixão, sem detrimento do seu caráter científico.

Agradecimentos

Agradeço aos meus familiares por tudo que me dispuseram nesta jornada que é a vida.

Agradeço ao pessoal da Universidade Federal do Rio Grande do Sul (UFRGS) – colegas, professores e funcionários – pela convivência e por tudo que me auxiliaram, de alguma forma ou de outra, para concluir minha tese de doutorado.

Agradeço ao pessoal dos laboratórios que me acolheram durante os procedimentos analíticos na UFRGS, na Universidade de São Paulo e na Universidade de Brasília (UnB).

Em especial aos geólogos Maria de Fátima Bitencourt, Lauro Valentim Stoll Nardi e Luana Moreira Florisbal pelas incansáveis revisões de texto, processo no qual nunca tinha imaginado que aprenderia tanto. Também ao professor Márcio Martins Pimentel pelo auxílio na obtenção dos dados geocronológicos na UnB.

E por fim, mas não menos importante, à Calu, paixão e amor da minha vida.

Resumo

No sul do Brasil, três associações do tipo tonalito-trondhjemito-granodiorito (TTG) foram identificadas no Complexo Arroio dos Ratos (CAR), e sua idade determinada (U-Pb em zircão por LA-MC-ICP-MS). Os metatonalitos da Associação 1 (A1 – 2.148 ± 33 Ma) têm trama resultande de deformação no estado sólido. Os tonalitos e granodioritos da Associação 2 (A2 – 2.150 ± 28 Ma) são intrusivos na A1 e têm composição similar, mas são menos deformados e preservam parcialmente suas estruturas primárias. Ambas as associações coexistem com magmas básicos a intermediários. Os gnaisses granodioríticos da Associação 3 (A3 – 2.077 ± 13 Ma) não têm magmatismo máfico associado, e seu bandamento bem desenvolvido localmente mostra feições de fusão parcial. As características geoquímicas das três associações são similares e indicam fontes relacionadas a ambiente de arco magmático continental. As razões $^{87}Sr/^{86}Sr_{(i)}$ (0,701 a 0,703), os valores positivos de $\varepsilon Nd_{(t)}$ (+1,45 a +5,19) e as idades T_{DM} próximas das de cristalização indicam fontes juvenis para A1 e A2. As rochas da A3 têm razão $^{87}Sr/^{86}Sr_{(i)}$ de 0,715, valores de $\varepsilon Nd_{(t)}$ de +0,47 e idades T_{DM} próximas das de cristalização, indicando fonte de composição similar à das outras associações, embora mais rica em Rb, porém sua origem permanece em discussão. As razões isotópicas de Pb de A1 e A2 são similares e compatíveis com a evolução do manto e orógeno ($^{208}Pb/^{204}Pb$ = 37,3-37,6; $^{207}Pb/^{204}Pb$ = 15,62-15,65; $^{206}Pb/^{204}Pb$ = 18,0-18,2). As razões isotópicas de Pb da A3 são diferentes das da A1 e A2, indicando fonte mais pobre em Th ($^{208}Pb/^{204}Pb$ = 37,1; $^{207}Pb/^{204}Pb$ = 15,64; $^{206}Pb/^{204}Pb$ = 18,5). A geoquímica de A1 e A2 sugere fonte juvenil com contaminação por material crustal. Contudo, a assinatura isotópica de Sr-Nd-Pb desse material crustal é similar à da fonte que gerou essas associações, e pode ter sido a crosta gerada no arco magmático, o que é compatível com os resultados geocronológicos. O conjunto de dados aponta para processos de auto-canibalismo na geração das rochas do CAR. Os dados geoquímicos e isotópicos sugerem fusão de manto metassomatizado (tipo E-MORB) como fonte geradora das rochas do CAR. Neste caso, a geração de associações de rochas com as típicas características de associações TTG (e.*g.*, depleção em elementos terras raras pesadas) pode ter resultado da fusão de um manto tipo granada-lherzolito, o que também é indicado pelas relações de contemporaneidade com magmas básicos a intermediários. Um volume subordinado de paragnaisses foi identificado no CAR,

representado por metapelitos, com rochas calcissilicáticas subordinadas, ambos de estruturação similar à das associações TTG. Estas rochas são cortadas por anfibolitos, interpretados como antigos diques máficos, 1.716 ± 72 Ma (U-Pb em zircão por LA-MC-ICP-MS). Esses dados são inéditos no Escudo Sul-rio-grandense e, juntamente com dados geoquímicos preliminares, permitem comparar esse magmatismo ao enxame de diques máficos anorogênicos da região de Florida, Uruguai, que cortam o Cráton Rio de La Plata. Os dados obtidos são compatíveis com a evolução geológica do CAR como registro de um arco magmático meso- a tardi-rhyaciano seguido de um período intraplaca (anorogênico, ou mesmo tafrogênico), estateriano.

Abstract

In southern Brazil, three TTG-type associations have been identified within the Arroio dos Ratos Complex (ARC) and their ages determined by LA-MC-ICP-MS U-Pb in zircons. The metatonalites of Association 1 (A1 – 2,148 ± 33 Ma) have strong solid-state fabric. The tonalites and granodiorites of Association 2 (A2 – 2,150 ± 28 Ma) are intrusive in A1 and have similar composition, but are less deformed, and their primary structures are partly preserved. Both associations display coeval basic to intermediate magmas. Association 3 (A3 – 2,077 ± 13 Ma) tonalitic to granodioritic gneisses have no coeval mafic magmas, and its characteristic banding shows local partial melting features. The geochemical characteristics of the three associations are similar and indicate sources related to continental magmatic arc environment. The $^{87}Sr/^{86}Sr_{(i)}$ ratios (0.701 to 0.703), positive $\varepsilon Nd_{(t)}$ values (+1.45 to +5.19), and T_{DM} ages close to crystallization ages indicate juvenile sources for A1 and A2. The A3 rocks have $^{87}Sr/^{86}Sr_{(i)}$ ratio of 0.715, $\varepsilon Nd_{(t)}$ value of +0.47 and a T_{DM} age that is close to the crystallization age, indicating source composition similar to that of the other associations, although richer in Rb, but its origin remains under discussion. Pb isotopic ratios of A1 and A2 are similar and compatible with the evolution of the mantle and orogen ($^{208}Pb/^{204}Pb$ = 37.3-37.6; $^{207}Pb/^{204}Pb$ = 15.62-15.65; $^{206}Pb/^{204}Pb$ = 18.0-18.2). A3 Pb isotopic ratios differ from A1 and A2, indicating a source that was poorer in Th ($^{208}Pb/^{204}Pb$ = 37.1; $^{207}Pb/^{204}Pb$ = 15.64; $^{206}Pb/^{204}Pb$ = 18.5). A1 and A2 geochemichal characteristics suggest juvenile source with contamination by crustal material. However, the Sr-Nd-Pb isotopic signature of this crustal material is similar to the source material that originates these associations, and that may be the crust generated in the magmatic arc, which is compatible with the geochronological results. The dataset points to processes of self-cannibalism during the generation of the ARC rocks. The geochemical and isotopic data suggest melting of metasomatized mantle (E-MORB type) as source for the ARC rocks. In this case, the generation of rock associations with typical TTG characteristics *(e.g.,* the depletion in heavy rare earth elements) may have arisen from the melting of a garnet-lherzolite-type mantle, which is also indicated by their coexistence with basic to intermediate magmas. A subordinate volume of ARC rocks comprises high-grade paragneisses, mostly pelitic but also calc-silicate, which exhibit similar structural relations as observed in the TTG-type associations. They are crosscut by amphibolites interpreted as former

mafic dykes dated at 1,716 ± 72 Ma (U-Pb LA-MC-ICP-MS zircon).The data presented here represents the first Staterian age value obtained from mafic rocks in southern Brazil, and together with preliminary geochemical data indicate that they may be correlated in age and composition with the well-known anorogenic Florida dyke swarm in Uruguay, wich crosscuts the Rio de la Plata Craton. The ARC is here interpreted to represent the register of a mid- to late Rhyacian magmatic arc, followed by a Staterian intraplate (anorogenic, or maybe even tafrogenic) stage.

Sumário

1. Texto Explicativo da Estrutura da Tese

Esta tese de Doutorado está estruturada em torno de artigos publicados em periódicos internacionais. Conseqüentemente, sua organização compreende as seguintes partes principais:

a) Introdução sobre o tema e descrição do objeto da pesquisa de Doutorado, onde estão sumarizados os objetivos e a filosofia de pesquisa desenvolvidos, o estado da arte sobre o tema de pesquisa, seguidos de uma discussão integradora contendo os principais resultados e interpretações deles derivadas.

b) Os três artigos publicados ou submetidos a periódicos internacionais com corpo editorial permanente e revisores independentes, escritos pelo autor durante o desenvolvimento de seu Doutorado.

2. Introdução

O Complexo Arroio dos Ratos (CAR), localizado no distrito de Quitéria, município de São Jerônimo/RS, representa um segmento de crosta que registra uma complexa evolução tectono-magmática e estratigráfica em um espaço relativamente pequeno, materializada em sua complexa variação litológica. A ocorrência de tonalitos, granodioritos e dioritos deformados sob diferentes condições estruturais demonstra a necessidade de estudos de detalhamento de campo e aplicação de tecnologias que nos permitam o maior número de informações de uma determinada rocha, sempre comparando os dados de laboratório com a realidade vista em campo.

Durante o trabalho de dissertação do autor da presente tese foi identificada e caracterizada uma associação de metatonalitos e metadioritos semelhantes às associações do tipo TTG (tonalito, trondhjemito, granodiorito), com assinatura de ambiente geotectônico de arco magmático, que representa parte do magmatismo precoce do CAR.

A ocorrência de tonalitos e dioritos com assinatura de arco, semelhantes às associações TTGs, estão muito em discussão na literatura internacional, principalmente no que se refere à gênese das associações TTG (*e.g.* Condie, 2005; Martin *et al.*, 2014), às fontes e processos envolvidos na atividade magmática relacionada a ambientes com subducção de crosta oceânica, ou seja, arcos magmáticos (*e.g.* Wilson, 1989, Rollinson, 2007) e à evolução da crosta continental ao longo do tempo geológico (*e.g.* Condie, 1989; Rollinson, 2007).

2.1 Objetivos

O objetivo deste trabalho é um estudo petrológico de investigação das fontes e processos envolvidos na evolução do magmatismo do Complexo Arroio dos Ratos (CAR), procurando identificar a sua composição, os seus principais aspectos estruturais e determinar a sua idade de formação e evolução ao longo do tempo geológico. Como parte da campanha, também procurou-se identificar novas

associações dentro do CAR, em continuidade aos trabalhos propostos por Gregory *et al.* (2011), base de dados inicial deste projeto.

Os objetivos só foram alcançados graças aos trabalhos de campo com coleta de dados e amostras e às análises geoquímicas, isotópicas e geocronológicas, segundo os procedimentos apresentados nesta tese.

Acredita-se que a investigação das fontes e processos petrogenéticos envolvidos na gênese e evolução das rochas estudadas é importante para o entendimento do Paleoproterozoico da região e da evolução da crosta na porção leste do Escudo Sul-rio-grandense e tem o seu papel na discussão atual sobre as associações TTG, o magmatismo de arco e a evolução da crosta continental.

2.2 Estado da Arte: O magmatismo de arco e as associações TTG

O magmatismo de arco resulta da fusão parcial que ocorre nos limites de placas tectônicas convergentes (ou limites destrutivos), onde há subducção de assoalho oceânico sob manto litosférico de placa continental ou oceânica. Relacionado a um dos ambientes geológicos mais complexos do planeta, o magmatismo de arco é o maior responsável pela adição de material juvenil (mantélico) à crosta, contribuindo para o seu crescimento e evolução, provavelmente, desde os primórdios da Terra. Comparando-se os arcos continentais e oceânicos, pode-se dizer que os primeiros são uma evolução dos últimos e apresentam maior complexidade estrutural e diversidade composicional (Condie, 1989; Wilson, 1989; Moores & Twiss, 1995; Rollinson, 2007).

A diversidade de modelos petrogenéticos propostos para o arco magmático é diretamente proporcional à complexidade tectono-termal deste ambiente, citando-se as discussões a respeito da fusão do manto ou da placa subductada como fonte do magmatismo (Barker, 1979; Condie, 1989; Wilson, 1989; Defant & Drummond, 1990; Condie, 2005; Martin *et al.*, 2005; Moyen & Martin, 2012), da contribuição dos sedimentos subductados (Condie, 1989; Marschall & Schumacher, 2012; Castro, 2014), da estrutura hidrotermal gerada pela atividade dos fluidos liberados da placa submetida ao metamorfismo progressivo na zona de subducção e consequente metassomatismo do manto sobrejacente (Abers 2005; Peacock *et al.*, 2005; Hasenclever *et al.*, 2011), da ocorrência de bacia de retro-arco ou cinturão de

deformação de acordo com o regime tectônico do ambiente (Heuret & Lallemand, 2005; Lister & Foster, 2009; Acocella & Funiciello, 2010; Ramos, 2010) e de todas as diversidades decorrentes da geometria e estrutura térmica desta situação geológica singular. De igual complexidade é o resgate da assinatura deste tipo de ambiente em associações petrotectônicas mais antigas, onde as relações espaciais originais estão obliteradas por eventos tectônicos posteriores. Neste ponto, a geoquímica elemental e isotópica tem sido ferramenta indispensável na identificação de assembleias de arcos magmáticos antigos.

Dado que o acesso ao registro atual do magmatismo de arco se dá nas capas vulcânicas, o interesse pelos equivalentes plutônicos e sua relação com a tectônica tem sido essencial para a identificação de assembleias de arco antigas, uma vez que as capas vulcânicas têm menor potencialidade de preservação no registro geológico, e que o plutonismo é, em larga escala, o responsável pelo maior volume de rochas de um arco. Entre associações plutônicas típicas de ambiente de arco é muito comum a associação espacial de vulcânicas cálcio-alcalinas e rochas intrusivas representadas por gabros e também dioritos, tonalitos e granodioritos até granitos, com os termos intermediários a ácidos também denominados conjuntamente de granitoides (Condie, 1989; Wilson, 1989). Segundo Wilson (1989): “A predominância de tonalitos e granodioritos associados com enxames de diques de andesitos basálticos segue um curso linear bem marcado dentro dos batólitos de arco e sugere um controle estrutural profundo no seu alojamento, provavelmente relacionado às falhas translitosféricas que servem como condutos de transporte dos magmas ascendentes.”

O vínculo entre a tectônica e o magmatismo no ambiente de arco tem sido demonstrado em diversos trabalhos, indicando profundas falhas que conectam a zona de subducção com os vulcões em superfície (Wilson, 1989; Papazachos & Panagiotopoulos, 1993), frequentemente com deformação sinmagmática dos termos plutônicos durante a construção do arco (Paterson *et al.*, 1991; Saint-Blanquat *et al.*, 2011; Symington *et al.*, 2014) estabelecendo um vínculo direto entre magmatismo e tectônica em arco magmático (Cembrano & Lara, 2009; Ramos, 2010). O vínculo entre tectônica e magmatismo é bem demonstrado em ambientes colisionais (Reichardt & Weinberg, 2012; Sawyer *et al.*, 2011) e em situações transpressivas (D´Lemos *et al.*, 1992; Bitencourt, 1996; Nardi & Bitencourt, 2007; Florisbal *et al.*, 2012; Vernon, 2012), destacando-se o papel das zonas de cisalhamento

transcorrentes como ativadoras do manto (Nardi & Bitencourt, 2007; Florisbal *et al.*, 2012). O volume de ocorrência e a relação com o magmatismo tem demonstrado a importância de estruturas de deslizamento direcional em regime transpressivo ou transtrativo na evolução de arcos magmáticos (Acocella & Funiciello, 2010), como é o caso da zona de falha transpressional intra-arco Liquiñe-Ofqui (Thomson, 2002), nos Andes. A relação entre esse sistema de falhas e o vulcanismo tem sido evidenciada (Thomson, 2002; Ramos, 2010), destacando-se a sua influência na composição do magmatismo, principalmente quanto à ocorrência ou não de basaltos segundo a alimentação em crosta atenuada ou apertada, sob regime transtrativo ou transpressivo, respectivamente (Ramos, 2010).

Considerando o magmatismo plutônico relacionado a arco magmático, principalmente continental, é muito comum a referência a associações compostas de dioritos, tonalitos e granodioritos, ou também a associações do tipo TTG (tonalito, trondhjemito, granodiorito). Já nos trabalhos pioneiros de Barker (1979), tonalitos, trondhjemitos, granodioritos, quartzo-dioritos e rochas intermediárias a básicas associadas são descritos como importantes componentes de adição juvenil à crosta, sendo vinculados com arcos magmáticos, principalmente de margem continental, envolvendo subducção de crosta oceânica. As concepções acerca de uma fusão de composição basáltica hidratada em grandes profundidades, que gera um resíduo eclogítico contendo granada e/ou anfibólio, é apontada por aquele autor como responsável pela depleção em ETRs pesados característica destas associações. Entre os processos petrogenéticos sugeridos para a geração dessas rochas, destacam-se: fusão parcial da parte basáltica da crosta oceânica subductada; indução à fusão da cunha mantélica ou da crosta inferior por líquidos oriundos da desidratação da placa subductada, produzindo uma composição basáltica; líquido basáltico gerado por fusão parcial de peridotito, que sofre fracionamento de hornblenda e outras fases sólidas.

Jahn *et al.* (1980) utilizam o termo TTG em referência à comum associação plutônica de tonalitos, trondhjemitos e granodioritos em terrenos arqueanos. Destacam a sua importância na acresção crustal e consideram uma fonte basáltica (eclogitos, granulitos ou anfibolitos), descartando fusão do manto. O termo TTG desde então é amplamente utilizado, inclusive para rochas de idades mais recentes. Já Defant & Drummond (1990) utilizam o termo adakito (em referência à ilha de Adak, nas Ilhas Aleutas) para definir uma série de rochas vulcânicas interpretadas

como o produto da fusão de placa oceânica subductada. Os membros extrusivos são representados principalmente por dacitos, mas também andesitos e riolitos sódicos, e seus equivalentes plutônicos são representados por tonalitos e trondhjemitos, sendo rara a associação com magmas parentais basálticos. Segundo aqueles autores, a gênese de adakitos estaria mais restrita atualmente, ocorrendo onde há subducção de placa jovem ainda quente em um ambiente de condições térmicas relativamente mais altas ou anômalas quando comparadas com a maioria dos arcos magmáticos atuais, onde a fusão da cunha mantélica induzida por fluidos da placa subductada é o principal processo gerador de magmas. Defant & Drummond (1990) fazem referência à semelhança entre estes tipos litológicos e associações do tipo TTG arqueanas, compostas de trondhjemitos, tonalitos e granodioritos com alto alumínio, inferindo semelhantes processos petrogenéticos e concluem que os altos gradientes termais vigentes no Arqueano teriam promovido a rápida geração e subducção de crosta jovem ainda quente. Com isso, a fusão parcial de basaltos transformados em eclogitos, com ou sem anfibolitos, poderia explicar a depleção em ETRP. Entre parâmetros geoquímicos característicos de adakitos, são destacados: $SiO_2 \geq 56\%$; $Al_2O_3 \geq 15\%$; $MgO < 3\%$; $Y < 18$ ppm; $Yb < 1,9$ ppm; $Sr > 400$ ppm; e baixos teores em HFSE (*high-field strength elements*). O termo adakito também se tornou muito difundido após este trabalho, e TTGs e adakitos são utilizados como sinônimos por diversos autores (Martin *et al.*, 2005; Samsonov *et al.*, 2005; De Souza *et al.*, 2007; Naqvi & Rana Pra, 2007). Modelos baseados em tectônica de placas, com fluxo térmico relativamente maior e subducção rasa de placas quentes relativamente menores, têm sido os cenários arqueanos propostos por diversos autores (*e.g.* Defant & Drummond, 1990; Martin *et al.*, 2005).

Estudos experimentais de Rapp *et al.* (1991) indicaram uma fonte crustal máfica para a gênese de tonalitos e trondhjemitos das associações TTG, ou por processos de fusão parcial de anfibolitos, granada-anfibolitos e eclogitos, nos quais anfibólio e/ou granada são a fase residual principal, ou ainda, fracionamento controlado por hornblenda de magmas basálticos hidratados. Os autores destacam que o grau de fusão requerido em condiçoes de pressão alta deve ser maior, citando 10-15% de fusão em 8 kbar, com um resíduo dominado por anfibólio, e 25-35% de fusão em 22-32 kbar, onde granada domina o resíduo. Tais cenários não estariam restritos a um ambiente relacionado à subducção durante o Arqueano, segundo aqueles autores. Já os experimentos de Springer & Seck (1997) com granulitos básicos entre 5 e 15 kbar demonstram que a composição das fusões varia de

tonalito e trondhjemito para diorito com o aumento do grau de fusão parcial e concluem que as pressões não devem ultrapassar os 12,5 kbar, levando-se em conta os padrões de ETR típicos de tonalitos. Estes mesmos autores concluem que processos de fusão parcial de metagabros cumuláticos, com um resíduo rico em granada e pobre em plagioclásio, seriam responsáveis pela origem dos magmas tonalíticos em margens de placas convergentes. Por analogia, uma origem em altas pressões para as associações do tipo TTG na crosta arqueana é também inferida (Springer & Seck, 1997).

Atualmente há um consenso entre diversos pesquisadores (Barker, 1979; Jahn *et al.*, 1980; Defant & Drummond, 1990; Rapp *et al.*, 1991; Springer & Seck, 1997; Condie, 2005; Martin *et al.*, 2005; Moyen & Martin, 2012; Martin *et al.*, 2014) sobre a fonte basáltica das associações do tipo TTG ou adakíticas, onde processos de fusão parcial de eclogitos, granulitos ou anfibolitos deixariam um resíduo rico em granada. Tal resíduo contendo granada, com ou sem anfibólio, seria responsável pela depleção nos ETRP. Porém, os ambientes geotectônicos e os processos petrogenéticos geradores destas associações, bem como o uso dos termos TTG e adakitos como sinônimos, são ainda objeto de muito debate. Um panorama geral deste debate é revisado por Rollinson & Martin (2005), que destacam a imprecisão no uso do termo adakito, o qual tem sido utilizado para rochas de variadas composições e origens. Da mesma forma, Castillo (2012) salienta que o sinal adakítico utilizado para caracterizar as associações do tipo TTG ou adakíticas é baseado em poucos elementos traços, em detrimento de uma vasta similaridade que há entre estas associações com o resto das associações de arco, ou cálcio-alcalinas clássicas, recomendando extrema cautela no uso do termo em função das concepções genéticas a ele relacionadas. Smithies (2000) argumenta que as associações do tipo TTG arqueanas não são análogas a adakitos modernos e não apresentam indícios de interação com material do manto, e que processos modernos de subducção seriam mais restritos durante o Arqueano. Segundo aquele autor, a fusão parcial de material basáltico hidratado na base de crosta espessada seria mais apropriada para a geração destas litologias durante o Arqueano. Condie (2005) também sugere que adakitos e TTGs não seriam tipos litológicos análogos e, consequentemente, teriam origens diferentes. As diferenças geoquímicas não poderiam ser explicadas por simples mecanismos de cristalização fracionada em níveis rasos. Enquanto adakitos seriam provavelmente fusões de placa oceânica subductada, TTGs com alto Al poderiam ser produzidos por fusão parcial da crosta

inferior em sistemas de arco ou nas zonas de raiz de platôs oceânicos. Para Coldwell *et al.* (2011) adakitos refletem condições geológicas e podem ocorrer em mais de um tipo de ambiente e Moyen (2009) argumenta que o sinal adakítico (*e.g.* depleção em ETRP) pode ser gerado por vários processos genéticos. Ainda, Castro (2014) argumenta que a contaminação dos magmas oriundos da zona de subducção por material crustal se dá na cunha mantélica, através da ascenção de diápiros de materiais crustais que foram arrancados do prisma de acresção e carregados para o manto pela placa subductada.

Embora o modelo de dois estágios não possa ser descartado para a gênese de associações TTGs, principalmente arqueanas, algumas questões permanecem em aberto quando da ocorrência de rochas com essa assinatura e contendo magmatismo básico contemporâneo associado, também referido como adakitos baixa sílica por Martin *et al.* (2005), e o conjunto referido como magmatismo cálcio-alcalino clássico e vinculado à fusão do manto metassomatizado (Martin, 1999). Castillo (2012) argumenta que o termo adakito refere-se a um largo espectro de rochas vulcânicas e plutônicas cuja composição, mineralogia e aspectos petrográficos seriam indistinguíveis de outras rochas de arco, e que a relevância ou a utilização de poucos elementos traços (La/Yb e Sr/Y) para distinguí-los seria um dos motivos dos grandes desacordos vistos na referência a este termo. Argumenta também que a alta viscosidade desse tipo de magma dificulta sua migração através do manto. Martin *et al.* (2005) observa que o elevado teor de Mg dos adakitos é devido à reação dos fundidos da placa com o manto peridodítico, e Castillo (2012) cita os resultados experimentais de Rapp *et al.* (1999), que apontam as grandes proporções fusão/rocha necessárias (2:1) para que todo o fundido de placa não seja consumido pela reação com o manto. Posto todas estas observações, sugere-se como processo de geração de TTG mais plausível a fusão de manto litosférico que herda um determinado sinal geoquímico do agente que o metassomatizou, como largamente referido para a cunha do manto localizada logo acima da zona de subducção.

Em revisões mais recentes, Martin *et al.* (2014) argumentam que a gênese das associações TTG via dois estágios (geração e consumo de crosta oceânica) requer uma fonte enriquecida em LILEs, o que não seria esperado para o assoalho oceânico normal (tipo N-MORB). Com isso, aquele autor postula que a gênese destas associações seria esporádica, através da fusão de platôs oceânicos

subductados, cuja fonte seria um manto enriquecido (tipo E-MORB), ou manto inferior não depletado (tipo OIB). Para Martin *et al.* (2014), este crescimento esporádico estaria em acordo com a distribuição temporal de eventos tectônicos registrada nos cristais de zircão, interpretada como picos episódicos de crescimento crustal por alguns autores (Condie & Aster, 2010; Guitreau *et al.*, 2012), ou refletindo os diferentes potenciais de preservação de rochas geradas em diferentes ambientes geotectônicos e a aglomeração de grandes continentes dentro de um contínuo processo de crescimento crustal, cuja taxa vem diminuindo com o tempo, dado o progressivo aumento da reciclagem crustal (Cawood *et al.*, 2013).

Entre argumentos apontados para a origem dos TTG por fusão de basaltos da crosta oceânica subductada estão a ausência de magmatismo básico associado tanto aos adakitos modernos (Defant & Drummond, 1990) como às associações TTG arqueanas (Jahn *et al.*, 1980), a ocorrência de inclusões vítreas de composição adakítica em xenólitos peridodíticos hospedados em lavas relacionadas à subducção (Schiano *et al.*, 1995) e veios adakíticos em ofiolitos (Sorensen & Grossman, 1989). Outros argumentos vêm da petrologia experimental, que demonstram que a típica assinatura geoquímica adakítica seria obtida em tonalitos gerados por fusão de basaltos em alta pressão com um resíduo rico em granada (Rapp *et al.*, 1991; Springer & Seck, 1997). A evolução a partir de magmas basálticos derivados do manto por processos de cristalização fracionada é descartada dado o grande volume de fracionados máficos que seria produzido, e que não é verificado no registro geológico (Smithies, 2000). Já o modelamento por assimilação de fragmentos crustais e cristalização fracionada (DePaolo, 1981) produziria uma diferenciação até composições equivalentes aos TTG. Este, no entanto, implicaria grande perda de calor pelo sistema magmático ao consumir e fundir pedaços de rochas. Por outro lado, a consideração dos sistemas graníticos como sistemas abertos e que processos de AFC envolvendo fusões da rocha encaixante, em vez de pedaços das mesmas, tem se demonstrado uma alternativa viável para o entendimento da evolução de sistemas plutônicos, não necessitando grandes cumulados e nem consumindo grande parte da energia do sistema (Bohrson & Spera, 2001; Spera & Bohrson, 2001). Para sistemas magmáticos de arco continental, tais evidências têm sido verificadas, onde processos de refusão, novas intrusões e remobilização de elementos dentro de plútons em estágios avançados de cristalização têm sido identificados (Saint-Blanquat *et al.*, 2011; Symington *et al*, 2014), e são plausíveis considerando-se a grande anomalia termal intracrustal intrínseca ao arco

magmático. Adicionalmente, as revisões de Ramos (2010) demonstram a grande variação na composição global do vulcanismo quando o arco encontra-se em regime tectônico extensivo ou contrativo, com presença ou ausência de basaltos.

Condie (2005) ressalta que dados geoquímicos não devem ser usados de forma isolada para reconstruir ambientes tectônicos antigos. Embora a discussão dos modelos de fusão de placa *versus* fusão do manto ainda não esteja bem resolvida, a integração de dados geoquímicos de elementos maiores e traços com dados isotópicos tem sido fundamental na discussão da evolução de rochas de arco (Peccerillo *et al.*, 2004; Machado *et al.*, 2005; Castillo *et al.*, 2009; Hidalgo *et al.*, 2012), frequentemente apontando um papel secundário, como agente contaminante ou de metassomatismo, para fluidos ou fusões derivadas da placa subductada ou dos sedimentos por ela carregados. Da mesma forma, a integração de diferentes áreas do conhecimento tem demonstrado eficácia na investigação de assembleias plutônicas antigas, principalmente quando acompanhadas de deformação (D'Lemos, 1992; Bitencourt, 1996; Nardi & Bitencourt, 2007; Florisbal, 2012), integrando dados de geologia estrutural, petrografia, geoquímica, isotopia e geocronologia numa abordagem holística. Dessa forma, podemos entender o fenômeno do magmatismo de arco como de múltiplas fontes e vários estágios que se complementam (Wilson, 1989).

2.3 Materiais e métodos

A integração de diferentes áreas do conhecimento foi a abordagem escolhida para a resolução do problema geológico investigado nesta tese.

Com isso, diferentes etapas foram seguidas em uma determinada ordem, com vistas a integrar os aspectos gerais com os pontuais, como por exemplo os resultados dos trabalhos de campo e a escolha das amostras destinadas à datação radiométrica e análises isotópicas.

2.3.1 Revisão bibliográfica

A revisão bibliográfica teve por meta cobrir diferentes aspectos do estudo, vinculados basicamente ao conhecimento geológico da área de trabalho e ao estado da arte sobre o assunto.

Entre elementos ligados ao conhecimento da área de estudo citam-se diversos tipos de trabalhos ligados à região, como mapas geológicos, trabalhos acadêmicos, artigos científicos e resumos em anais de eventos. O acompanhamento de trabalhos de mapeamento geológico, de conclusão de curso de graduação e de pós-graduação também foi importante em todo o andamento do estudo, proporcionando uma visão ampla da área.

Entre elementos ligados ao estado da arte sobre o assunto buscou-se artigos científicos das áreas de geologia estrutural, petrologia, geotectônica, geoquímica elementar e isotópica e geocronologia, ligados a gênese e evolução de rochas plutônicas sintectônicas, especificamente as associações do tipo TTG. Reuniões de grupo, com debates de artigos e conversas com orientadores, além de disciplinas procuradas durante o curso também foram fundamentais para o desenvolvimento do arcabouço intelectual e da opinião do autor desta tese no que tange ao assunto de petrologia ígnea.

Com os resultados dos dois tipos de revisão delimitou-se o que seria possível trabalhar na área de estudo, abrangendo assuntos pertinentes à comunidade geológica atual, procurando implantar novos conhecimentos aos até então adquiridos, completar lacunas e propor novos trabalhos e ideias, cumprindo desta forma com a evolução do conhecimento científico.

Além desta revisão, o ponto básico de partida do trabalho foram os dados obtidos até então por Gregory *et al.* (2011), autor da presente tese, que consistem de parte da caracterização de associações magmáticas precoces do Complexo Arroio dos Ratos (CAR), da qual faz início e dá continuidade o estudo da presente tese.

2.3.2 Mapeamento geológico e estrutural

Na área de estudo, o objetivo do mapeamento geológico e estrutural foi identificar diferentes tipos litológicos até então não reconhecidos no CAR, de acordo com o trabalho de Gregory *et al.* (2011), sempre atento as relações de campo,

aspectos petrológicos, estruturais, tectônicos e estratigráficos. Não se teve por objetivo, por exemplo, o mapeamento dos contatos nem de unidades dentro deste complexo.

O controle litológico e estrutural foi fundamental na escolha e coleta das amostras dos diferentes litotipos identificados dentro do CAR. Estas amostras foram destinadas à petrografia, geoquímica elementar e isotópica e geocronologia. Esta tarefa foi extremamente difícil, dado a complexidade litológica e a carência, qualidade e continuidade das exposições, o que é típico do relevo nesta parte do Escudo Sul-rio-grandense. As informações de campo foram obtidas a partir da observação e descrição das litologias e estruturas identificadas, com coleta sistemática de dados estruturais e de amostras orientadas.

Os dados estruturais e orientação de amostras foram medidos com bússola equipada com clinômetro e tratados estatística e geometricamente com estereogramas, utilizando-se o *software* Stereo32. Os pontos de descrição e coleta de amostras foram catalogados com o uso de GPS para a determinação das coordenadas geográficas.

2.3.3 Petrografia e microestruturas

O estudo petrográfico teve por base a descrição de lâminas delgadas em microscópio óptico, levando-se em conta o controle litológico estrutural construído em campo. As amostras foram coletadas orientadas, com o corte paralelo à lineação e perpendicular à foliação. A confecção das lâminas ocorreu nos laboratórios dos Institutos de Geociências da UFRGS (Universidade Federal do Rio Grande do Sul) e da USP (Universidade de São Paulo).

Nesta etapa, procurou-se identificar e caracterizar a composição, as texturas e as microestruturas, visando sistematizar as características composicionais e estruturais de cada grupo de rochas identificado dentro do CAR. Entre técnicas utilizadas citam-se a contagem modal para classificação QAP segundo Streckeisen (1976) e a determinação do teor de anortita do plagioclásio pelo método alfa-normal (Hibbard, 1995). Como base comparativa para o estudo das microestruturas usou-se as revisões de Passchier & Trouw (2005).

O controle das microestruturas foi fundamental para a identificação e caracterização de episódios de recristalização e a sua relação com as tramas tectônicas de meso escala. A identificação de indicadores cinemáticos ajudou na determinação do sentido de cisalhamento nas tramas das rochas. O estudo petrográfico, aliado ao controle litológico estrutural, foi determinante na escolha das amostras destinadas às análises geoquímicas, isotópicas e geocronológicas. Junto com os dados geoquímicos, os resultados da petrografia foram cruciais no entendimento e identificação das relações de contemporaneidade entre magmas básicos e ácidos observadas nos trabalhos de campo.

2.3.4 Litoquímica

Após o controle em meso e micro escala, amostras foram selecionadas para o estudo geoquímico das associações identificadas, visando a determinação da sua composição, série magmática, ambiente geotectônico e semelhança com associações consagradas, como as associações do tipo TTG. Também de fundamental importância foi a identificação de processos de diferenciação, como cristalização fracionada e mistura de magmas, e seu papel na evolução magmática das associações estudadas, corroborando as evidências de campo quanto à ocorrência de magmas básicos contemporâneos aos tonalitos predominantes. O estudo dos elementos traços e terras raras foi essencial para a comparação com as associações do tipo TTG, ou adakíticas, bem como identificar possíveis fontes e processos, o que foi complementado pelo estudo isotópico. O Controle litológico e estrutural, a petrografia e a geoquímica de elementos maiores e traços serviram de base para escolha das amostras para análises isotópicas e geocronológicas.

A amostragem geoquímica acompanhou o controle da campo, coletando as amostras o mais próximo possível do local de laminação petrográfica. Cuidados foram tomados quanto à coleta, no que tange a zonas com contaminação ou heterogeneidades, com muita alteração ou fraturamento, tendo-se o cuidado de coletar apenas lascas frescas e livres de qualquer casca de alteração.

As amostras selecionadas foram pulverizadas e analisadas pelo laboratório AcmeLabs™, no Canadá. As análises quantitativas foram realizadas utilizando-se as técnicas de ICP-ES (Inductively Coupled Plasma Emission Spectrometry) para elementos maiores e ICP-MS (Inductively Coupled Plasma Mass Spectrometry) para

elementos traços. Os resultados das análises geoquímicas foram manejados em *softwares* específicos para a montagem de gráficos (GCDkit 3.0) e comparados com diagramas consagrados da literatura (Rollinson, 1993; Le Maitre, 2002).

2.3.5 Geoquímica Isotópica Rb-Sr e Sm-Nd em rocha total

O estudo isotópico buscou a identificação das fontes e processos petrogenéticos, constituindo-se uma etapa complementar à caracterização estrutural, petrográfica e geoquímica, e fundamental para a investigação da evolução petrológica das rochas estudadas.

As análises de isótopos de Rb-Sr e Sm-Nd foram obtidas no Centro de Pesquisas Geocronológicas (CPGeo), Instituto de Geociências, Universidade de São Paulo. O mesmo pó destinado às análises geoquímicas de elementos maiores e traços foi utilizado para as análises isotópicas, passando por digestão ácida e separação dos elementos de interesse em colunas de troca iônica, seguindo os procedimentos descritos por Sato *et al.* (1995). Não foram adicionados *spikes* e as razões $^{87}Rb/^{86}Sr$ e $^{147}Sm/^{144}Nd$ foram calculadas apartir das análises geoquímicas de elementos traços obtidos em rocha total. As análises isotópicas foram realizadas através de espectrometria de ionização termal no TIMS (Thermal Ionization Mass Spectrometer). Os equipamentos utilizados foram o Thermo Finnigan Triton multi-coletor e Finnigan Mat 262 com coletor simples. As razões isotópicas de $^{87}Sr/^{86}Sr$ foram normalizadas para os valores de $^{86}Sr/^{88}Sr = 0{,}1194$ (Steiger & Jäeger, 1978) e as de $^{143}Nd/^{144}Nd$ para $^{146}Nd/^{144}Nd = 0{,}7219$ (De Paolo, 1981). As condições de operação dos espectrômetros são descritas por Torquato & Kawashita (1994), Sato *et al.* (1995) e Souza (2009).

Os dados gerados foram trabalhados em planilhas de cálculo para a determinação dos parâmetros isotópicos $^{87}Sr/^{86}Sr_{(i)}$, $\varepsilon Nd_{(t)}$ e T_{DM}. Os teores dos elementos Rb, Sr, Sm e Nd foram obtidos das análises geoquímicas e as idades a partir dos dados U-Pb em zircão por LA-MC-ICP-MS. As constantes utilizadas no cálculo foram as referidas por Steiger & Jäeger (1978) para Sr e por De Paolo (1981) para Nd.

2.3.6 Geoquímica Isotópica Pb-Pb em feldspato

As razões dos isótopos de Pb obtidos em felspatos fornecem a razão inicial destes isótopos no magma original, uma vez que o feldspato não absorve urânio durante a cristalização. Com isso, a razão isotópica dentro do cristal permanece constante com o passar do tempo geológico, caso sejam mantidas as condições de sistema fechado para o cristal. Estes dados vem a complementar os dados isotópicos de Sr e Nd e, junto com os demais dados geoquímicos, procuram identificar a caracterizar as fontes geradores das rochas estudadas.

As análises das razões de isótopos de Pb em cristais de K-feldspato foram obtidas por Nu Plasma MC-ICP-MS (Multi-Collector Inductively Coupled Plasma Mass Spectrometer) interligado com um sistema de abrasão a laser New Wave UP213, no laboratório Radiogenic Isotopic Facility (RIF), Universidade de Alberta (UA), Canadá. Os dados foram obtidos em seções polidas com 200 a 250 µm de espessura em modo de varredura, cada análise correspondendo a uma área varrida de 160-800 µm. Os núcleos e as bordas dos cristais foram analisados, desconsiderando-se as áreas fraturadas e com inclusões de minerais. As análises replicadas do padrão NIST612 foram utilizadas para estimar a precisão e acuracidade da ablação por laser usando o mesmo protocolo das amostras. Uma solução de Tl foi simultaneamente aspirada durante a ablação para corrigir o desvio de massa das razões isotópicas de Pb. A intensidade total do sinal de Pb para as análises variou de 0,4 a 1,2 V. A medida das razões isotópicas de Pb apresentam associadas incertezas reportadas em 1σ, que estão abaixo da variação isotópica total registrada nos cristais individuais.

Os dados foram comparados com curvas evolutivas contruídas para os isótopos de Pb, modelamento este denominado por diversos autores como “Plumbotectonics” (*e.g.* Zartman & Haines, 1988).

2.3.7 Geocronologia U-Pb em cristais de zircão por LA-MC-ICPMS

O estudo geocronológico procurou determinar a idade das rochas estudadas, visando mais especificamente a idade de sua cristalização magmática. A escolha das amostras teve por base o longo trabalho de integração dos dados de campo com os petrográficos e geoquímicos. Com isso, a escolha baseou-se em atributos estruturais, petrográficos e geoquímicos determinados nas etapas anteriores.

Cerca de 50 a 100 cristais foram coletados da fração menos magnética e então montados e polidos em resina padrão (“mounts”). Parte das amostras foram preparadas no LGI/UFRGS (Laboratório de Geologia Isotópica/Universidade Federal do Rio Grande do Sul) e detalhes da preparação podem ser encontrados em Chemale *et al.* (2011, 2012). A outra parte das amostras foram preparadas no CPGeo/USP (Centro de Pesquisas Geocronológicas/Universidade de São Paulo), segundo os métodos descritos por Florisbal *et al.* (2012). Todos os cristais datados foram estudados com imagens de BSE (back-scatter electron) e CL (cathodoluminescence) antes das análises.

Os zircões foram analisados em diferentes laboratários usando Nu-Plasma (RIF/UA, Canadá) ou Thermo Finnigan Neptune (LGI/UFRGS e Laboratório de Geocronologia/Universidade de Brasília) MC-ICP-MS (Multi-Collector Inductively Coupled Plasma Mass Spectrometer) acoplado a um sistema de ablação a laser de frequência quintuplicada Nd:YAG (λ=213 nm). Os protocolos analíticos e configurações dos coletores são descritos em detalhe por Kosler *et. al.* (2002), Jackson *et al.* (2004), Simonetti *et al.* (2005) e Chemale *et al.* (2012). Fracionamento de elementos induzido pelo laser ou de massa devido à instrumentação foram corrigidos com referência ao padrão de zircão GJ-1. Duas medidas de análises do padrão GJ-1 foram feitas a cada dez leituras em zircões. O conjunto de dados foram processados *off-line* e reduzidos em uma planilha Excel™. Os erros foram reportados em 1σ, exceto para a amostra TG-01S, que foi reportada em 2σ seguindo os procedimentos laboratoriais internos do RIF/UA. As idades foram calculadas usando as constantes de decaimento referidas por Jaffey *et al.* (1971); ^{238}U – $1{,}55125 \times 10^{-10}$ yr.$^{-1}$ e ^{235}U – $9{,}8485 \times 10^{-10}$ yr.$^{-1}$ e razão $^{238}U/^{235}U$ de 137,88.

As amostras analisadas no LGI/UFRGS foram feitas com *spot* de 25 µm. As condições de operação do laser e descrição detalhada dos métodos analíticos são encontradas em Chemale *et al.* (2011, 2012). As amostras analisadas no RIF/UA foram realizadas com *spot* de 40 µm e os protocolos analíticos e configurações dos coletores são descritas em detalhe por Simonetti *et al.* (2005) e permitem aquisição simultânea das massas de ^{238}U até ^{203}Tl. As condições de operação do laser e a descrição detalhada dos métodos analíticos podem ser encontrados em Florisbal *et al.* (2012). As amostras analisadas no Laboratório de Geocronologia da Universidade de Brasília foram realizadas com *spot* de 30 µm e o fracionamento

induzido pelo laser da razão $^{206}Pb/^{238}U$ foi corrigida usando o método de regressão linear descrito por Kosler *et al.* (2002).

Os gráficos com as concórdias e discórdias para o cálculo das idades foram construídos usando o *software* Isoplot (Ludwig, 1993).

2.4 Análise Integradora

Os principais resultados obtidos com os três artigos publicados em periódicos internacionais foram os seguintes:

O Artigo 1, submetido à revista *Journal of South American Earth Sciences*, versa sobre a determinação de idades radiométricas das rochas estudadas. Foram efetuadas seis datações, divididas entre três associações de tonalitos e dioritos que foram o objeto de estudo do trabalho. As três associações têm idades de cristalização magmática paleoproterozoicas e representam o período meso- a tardi-Riaciano do Paleoproterozoico. Os resultados deste artigo foram fundamentais para o entendimento da evolução temporal do magmatismo do CAR, pois permitiram delimitar não só o tempo como também possibilitar o uso dos parâmetros isotópicos de Sr e Nd, essenciais para avaliação das fontes e processos.

O Artigo 2, submetido à revista *Lithos*, versa sobre a petrogênese das rochas estudadas e foi o principal artigo desta tese, dada a abragência de tipos de dados que envolveu. Junto com os dados de geocronologica, permitiu identificar e avaliar as fontes geradoras das rochas estudadas, bem como entender os processo de evolução crustal envolvidos. Uma das principais conclusões é a identificação de fontes juvenis para a gênese das rochas estudadas. Uma importante interpretação foi deduzida a partir destes dados, no que tange à ocorrência de processos de auto-canibalismo que foram influentes na evolução composicional das rochas estudadas. Também foi fundamental para a discussão das associações TTG com magmatismo básico associado, no que tange ao panorama internacional de discussão a respeito dos aspectos petrogenéticos envolvidos na gênese deste tipo de associação.

O Artigo 3, submetido à revista *Gondwana Research*, versa sobre a determinação da idade ígnea de um anfibolito que corta os paragnaisses do CAR e é interpretado como antigo dique máfico. A idade estareriana obtida é rara no estado

e, junto com o tipo de rocha (anfibolito), é inédita no Escudo Sul-rio-grandense, sendo comparável do enxame de diques máficos da região de Florida, no Uruguai, que cortam o embasamento paleoproterozoico do Cráton Rio de La Plata (Mazzucchelli *et al.*, 1993; Bossi *et al.*, 1995; Halls *et al.*, 2001).

O conjunto dos três artigos permite concluir que o CAR registra um arco magmático continental paleoproterozoico (meso- a tardi-Riaciano), com um período anorogênico no final desta era (Estareriano). A ocorrência de paragnaisses cortados por diques estaterianos remete a uma associação parametamórfica mais antiga que o Complexo Várzea do Capivarita, uma associação de orto e paragnaisses de idade neoproterozoica (Martil *et al.*, submetido), e é alvo de futuros estudos de datação do metarmorfismo e análise de proveniência.

A inevitável comparação com o Complexo Encantadas (CE), uma associação TTG semelhante ao Complexo Arroio dos Ratos que ocorre na porção central do Escudo Sul-rio-grandense (Philipp *et al.*, 2008), permanece em aberto, dados os seguintes fatores: (i) não existem dados isotópicos oficialmente publicados para o CE, o que deixa a comparação em nível de tipos litológicos e composição geoquímica de elementos maiores e traços; (ii) as idades ígneas até então referidas para o CE são mais velhas que as obtidas para o CAR, com idades metamórficas do CE se sobrepondo com a atividade magmática do CAR (Saalmann *et al.*, 2011). Dada a complexa amalgamação de núcleos cratônicos arqueanos durante o Paleoproterozoico, com extensiva formação de crosta continental e faixas móveis, torna-se perigoso uma correlação direta. Embora haja uma evolução média para a aglutinação dos continentes durante o Paleoproterozoico, formando o paleo-mega-continente Atlântica (Rogers, 1996), diversos autores (Brito Neves, 1999; Almeida *et al.*, 2000) relatam o diacronismo com que se deu essa aglutinação, variando em idades e tipos de ambientes envolvidos de um terreno para outro. Soma-se a isso o fato de que durante o Estareriano o CAR registra um ambiente intraplaca, talvez tafrogênico, enquanto idades estaterianas são observadas na porção central do ESrg em granitoides com afinidade de arco magmático continental (Camozzato *et al.*, 2013).

2.5 Referências

Abers, G.A. 2005. Seismic low-velocity layer at the top of subducting slabs: observations, predictions, and systematics. Physics of the Earth and Planetary Interiors, 149(1): 7-29.

Acocella, V. & Funiciello, F. 2010. Kinematic setting and structural control of arc volcanism. *Earth and Planetary Science Letters*, 289(1): 43-53.

Almeida, F.F.M., Brito Neves, B.B. & Dal Ré Carneiro, C. 2000. The origin and evolution of the South American Platform. *Earth-Science Reviews*, 50(1): 77-111.

Barker, E. 1979. *Trondhjemites, dacites, and related rocks*. New York, Elsevier, 659p.

Bitencourt, M.F. 1996. Granitóides sintectônicos da região de Porto Belo, SC: uma abordagem petrológica e estrutural do magmatismo em zonas de cisalhamento. Porto Alegre, 310p. *Tese de doutorado*, Programa de Pós-graduação em Geociências, Instituto de Geociências, Universidade Federal do Rio Grande do Sul.

Bohrson, W.A. & Spera, F.J. 2001. Energy-constrained open-system magmatic processes II: application of energy-constrained assimilation–fractional crystallization (EC-AFC) model to magmatic systems. *Journal of Petrology*, 42(5): 1019-1041.

Bossi, J., Campal, N., Civetta, L., Demarchi, G., Girardi, V.A.V., Mazzucchelli, M. & Molesini, M. 1993. Early Proterozoic dike swarms from western Uruguay: geochemistry, Sr-Nd isotopes and petrogenesis. *Chemical Geology*, 106(3): 263-277.

Brito Neves, B.B. 1999. América do Sul: quatro fusões, quatro fissões e o processo acrescionário andino. *Brazilian Journal of Geology*, 29(3): 379-392.

Camozzato, E., Philipp, R.P. & Chemale Jr., F. 2013. Idades Estaterianas e Calimianas no Domo da Vigia: Complexo Vigia e Porongos, Metagranito Seival e Anfibolito Tupi Silveira, Bagé, RS. *In*: XI Simpósio Nacional de Estudos Tectônicos. *Anais...*(CD). Ouro Preto, MG.

Castillo, P.R., Lonsdale, P.F., Moran, C.L. & Hawkins, J.W. 2009. Geochemistry of mid-Cretaceous Pacific crust being subducted along the Tonga–Kermadec Trench: Implications for the generation of arc lavas. *Lithos*, 112(1): 87-102.

Castillo, P.R. 2012. Adakite petrogenesis. *Lithos*, 134: 304-316.

Castro, A. 2014. The off-crust origin of granite batholiths. *Geoscience Frontiers*, 5(1): 63-75.

Cawood, P.A., Hawkesworth, C.J. & Dhuime, B. 2013. The continental record and the generation of continental crust. *Geological Society of America Bulletin*, 125(1-2): 14-32.

Cembrano, J. & Lara, L. 2009. The link between volcanism and tectonics in the southern volcanic zone of the Chilean Andes: A review. *Tectonophysics*, 471(1): 96-113.

Chemale Jr., F., Kawashita,K., Dossin, I.A., Ávila, J.N., Justino, D., Bertotti, A.L. 2012. U-Pb zircon in situ dating with LA-MC-ICP-MS using a mixed detector configuration. *Anais da Academia Brasileira de Ciências*, 84(2): 275-295.

Chemale Jr., F., Philipp, R.P., Dussin, I.A., Formoso, M.L.L., Kawashita, K., Bertotti, A.L. 2011. Lu-Hf and U-Pb age determinations of Capivarita Anorthosite in the Dom Feliciano Belt, Brazil. *Precambrian Research*, 186: 117-126.

Coldwell, B., Clemens, J. & Petford, N. 2011. Deep crustal melting in the Peruvian Andes: Felsic magma generation during delamination and uplift. *Lithos*, *in press*.

Condie, K.C. 1989. *Plate Tectonics & Crustal Evolution*, Pergamon Press, 476p.

Condie, K.C. 2005. TTGs and adakites: are they both slab melts? *Lithos*, 80: 33-44.

Condie, K.C. & Aster, R.C. 2010. Episodic zircon age spectra of orogenic granitoids: the supercontinent connection and continental growth. *Precambrian Research*, 180(3): 227-236.

Defant, M.J. & Drummond, M.S. 1990. Derivation of some modern arc magmas by melting of Young subducted lithosphere. *Nature*, 347:662-665.

De Souza, Z.S., Martin, H., Peucat, J.J., De Sá, E.F.J. & Macedo, M.H.F. 2007. Calc-alkaline magmatismo at the Archean-Proterozoic transition: the Caicó Complex Basemente (NE Brazil). *Journal of Petrology*, 48(11): 2149-2185.

DePaolo, D.J. 1981. Neodymium isotopes in the Colorado Front Range and crust–mantle evolution in the Proterozoic. *Nature*, 29(1): 193–196.

D'Lemos, R.S., Brown, M. & Strachan, R.A. 1992. Granite magma generation, ascent and emplacement within a transpressional orogen. *Journal of the Geological Society of London*, 149:487-490.

Florisbal, L.M. 2011. Petrogênese de Granitos Sintectônicos em ambiente pós-colisional do Escudo Catarinense: Estudo integrado de Geologia Estrutural, Geoquímica Elemental e Isotópica Sr-Nd-Pb e Geocronologia U-Pb em zircão. São Paulo, 285p. *Tese de Doutorado*, Programa de Pós-graduação em Geociências, Instituto de Geociências, Universidade de São Paulo.

Florisbal, L.M., Janasi, V.A., Bitencourt, M.F., Heaman, L.M. 2012. Space-time relation of post-collisional granitic magmatism in Santa Catarina, southern Brazil: U-Pb LA-MC-ICP-MS zircon geochronology of coeval mafic-felsic magmatism related to the Major Gercino Shear Zone. *Precambrian Research*, 216-219: 132-151.

Gregory, T.R., Bitencourt, M.F. & Nardi, L.V.S. 2011. Caracterização estrutural e petrológica de metatonalitos e metadioritos do Complexo Arroio dos Ratos na sua seção-tipo, região de Quitéria, RS. *Pesquisas em Geociências*, 38(1): 85-108.

Guitreau, M., Blichert-Toft, J., Martin, H., Mojzsis, S.J. & Albarède, F. 2012. Hafnium isotope evidence from Archean granitic rocks for deep-mantle origin of continental crust. *Earth and Planetary Science Letters*, 337: 211-223.

Halls, H.C., Campal, N., Davis, D.W. & Bossi, J. 2001. Magnetic studies and U–Pb geochronology of the Uruguayan dyke swarm, Rio de la Plata craton, Uruguay: paleomagnetic and economic implications. *Journal of South American Earth Sciences*, 14(4): 349-361.

Hasenclever, J., Morgan, J.P., Hort, M. & Rüpke, L.H. 2011. 2D and 3D numerical models on compositionally buoyant diapirs in the mantle wedge. *Earth and Planetary Science Letters*, 311(1): 53-68.

Heuret, A. & Lallemand, S. 2005. Plate motions, slab dynamics and back-arc deformation. *Physics of the Earth and Planetary Interiors*, 149(1): 31-51.

Hibbard, M.J. 1995. *Petrography to petrogenesis*. New Jersey, Prentice Hall, 604p.

Hidalgo, S., Gerbe, M.C., Martin, H., Samaniego, P. & Bourdon, E. 2012. Role of crustal and slab components in the Northern Volcanic Zone of the Andes (Ecuador) constrained by Sr–Nd–O isotopes. *Lithos*, 132: 180-192.

Jackson, S.E., Pearsona, N.J., Griffina, W.L.& Belousova, E.A. 2004. The application of laser ablation-inductively coupled plasma-mass spectrometry to in situ U–Pb zircon geochronology. *Chemical Geology*, 211: 47-69.

Jaffey, A.H., Flynn, K.F., Glendenin, L.E., Bentley, W.C. & Essling, A.M. 1971. Precision measurements of half-lives and specific activities of ^{235}U and ^{238}U. *Physics Review,* C4: 1889–1906.

Jahn, B.M., Glikson, A.Y., Peucat, J.J. & Hickman, A.H. 1981. REE geochemistry and isotopic data of Archean silicic volcanics and granitoids from the Pilbara Block, Western Australia: implications for the early crustal evolution. *Geochimica et Cosmochimica Acta*, 45: 1633-1652.

Kosler J., Fonneland, H., Sylvester, P., Tubrett, M., Pedersen, R.B., 2002. U-Pb dating of detrital zircons for sediment provenance studies – a comparison of laser ablation ICPMS and SIMS techniques. *Chemical Geology*, 182: 605-618.

Le Maitre, R.W. 2002. *Igneous Rocks: A Classification and Glossary of Terms. Recommendations of the International Union of Geological Sciences, Subcommission on the Systematics of Igneous Rocks*. Cambridge University Press.

Lister, G. & Forster, M. 2009. Tectonic mode switches and the nature of orogenesis. *Lithos*, 113(1): 274-291.

Ludwig, K.R. 1993. New isoplot version 2.2. Berkeley Geochronology Center, February.

Machado, A., Chemale Jr, F., Conceição, R.V., Kawaskita, K., Morata, D., Oteíza, O. & Van Schmus, W.R. 2005. Modeling of subduction components in the genesis of the Meso-Cenozoic igneous rocks from the South Shetland Arc, Antarctica. *Lithos*, :82(3): 435-453.

Marschall, H.R. & Schumacher, J.C. 2012. Arc magmas sourced from mélange diapirs in subduction zones. *Nature Geoscience*, 5(12): 862-867.

Martil, M.M.D., Bitencourt, M.F., Armstrong, R., Nardi, L.V.S., Chemale Jr., F. Geochronology of orthogneisses from the Várzea do Capivarita Complex thrust pile and implications for the timing of continental collision in southernmost Brazil. *Precambrian Research* (*submitted*).

Martin, H. 1999. Adakitic magmas: modern analogues of Archaean granitoids. *Lithos*. 46: 411-429.

Martin, H., Smithies, R.H., Rapp, R., Moyen, J.F. & Champion, D. 2005. An overview of adakite, tonalite-trondhjemite-granodiorite (TTG), and sanukitoid: relationships and some implications for crustal evolution. *Lithos*, 79:1-24.

Martin, H., Moyen, J.F., Guitreau, M., Blichert-Toft, J. & Le Pennec, J.L. 2014. Why Archaean TTG cannot be generated by MORB melting in subduction zones. *Lithos*, 198: 1-13.

Mazzucchelli, M., Rivalenti, G., Piccirillo, E.M., Girardi, V.A.V., Civetta, L. & Petrini, R. 1995. Petrology of the Proterozoic mafic dyke swarms of Uruguay and constraints on their mantle source composition. *Precambrian Research*, 74(3): 177-194.

Moores, E.M. & Twiss, R.J. 1995. *Tectonics*. Freeman, New York, 415p.

Moyen, J.F. 2009. High Sr/Y and La/Yb ratios: the meaning of the “adakitic signature”. *Lithos*, 112(3): 556-574.

Moyen, J.F., & Martin, H. 2012. Forty years of TTG research. *Lithos*, 148: 312-336.

Nardi, L.V.S. & Bitencourt, M.F.A.S. 2007. Magmatismo granítico e evolução crustal no sul do Brasil. *In*: Iannuzzi, R. & Frantz, J.C. (Ed.). *50 Anos de Geologia. Instituto de Geociências. Contribuições.* Porto Alegre, Editora Comunicação e Identidade, CIGO e IG-UFRGS, p. 125-141.

Naqvi, S.M. & Rana Prathap, J.G. 2007. Geochemistry of adakites from Neoarchean active continental margin of Shimoga schist belt, Western Dharwar Craton, India: Implications for the genesis of TTG. *Precambrian Research*, 156: 32-54.

Papazachos, B.C. & Panagiotopoulos, D.G. 1993. Normal faults associated with volcanic activity arc. *Tectonophysics*, 220(1): 301-308.

Passchier, C.W. & Trouw, R.A. 2005. *Microtectonics*. Berlin, Springer, 366p, 2ed.

Paterson, S.R., Tobisch, O.T. & Vernon, R.H. 1991. Emplacement and deformation of granitoids during volcanic arc construction in the Foothills terrane, central Sierra Nevada, California. *Tectonophysics*, 191(1): 89-110.

Peacock, S.M., Keken, P.E.V., Holloway, S.D., Hacker, B.R., Abers, G.A. & Fergason, R.L. 2005. Thermal structure of the Costa Rica–Nicaragua subduction zone. *Physics of the Earth and Planetary Interiors*, 149(1): 187-200.

Peccerillo, A., Dallai, L., Frezzotti, M.L. & Kempton, P.D. 2004. Sr–Nd–Pb–O isotopic evidence for decreasing crustal contamination with ongoing magma evolution at Alicudi volcano (Aeolian arc, Italy): implications for style of magma-crust interaction and for mantle source compositions. *Lithos*, 78(1): 217-233.

Phillip, R.P., Lusa, M. & Nardi, L.V.S. 2008. Petrology of dioritic, tonalitic and trondhjemitic gneisses from Encantadas Complex, Santana da Boa Vista, southernmost Brazil: paleoproterozoic continental-arc magmatism. *Anais da Academia Brasileira de Ciências*, 80(4): 1-14.

Ramos, V.A. 2010. The tectonic regime along the Andes: Present-day and Mesozoic regimes. *Geological Journal*, 45 (1): 2-25.

Rapp, R.P., Shimizu, N., Norman, M.D. & Applegate, G.S. 1999. Reaction between slab-derived melts and peridotite in the mantle wedge: experimental constraints at 3.8 GPa. *Chemical Geology*, 160(4): 335-356.

Rapp, R.P., Watson, E.B. & Miller, C.F. 1991. Partial melting of amphibolites/eclogite and the origin of Archean trondhjemites and tonalites. *Precambrian Research*, 51: 1-25.

Reichardt, H. & Weinberg, R.F. 2012. The dike swarm of the Karakoram shear zone, Ladakh, NW India: Linking granite source to batholith. *Geological Society of America Bulletin*, 124(1-2): 89-103.

Rogers, J.J. 1996. A history of continents in the past three billion years. *The journal of geology*, 104: 91-107.

Rollinson, H.R. 1993. *Using geochemical data: evaluation, presentation, interpretation*. Singapore, Pearson Education, 352p.

Rollinson, H.R. 2007. *Early Earth systems: a geochemical approach*. Blackwell Publishing, Oxford, UK, 296p.

Rollinson, H.R. & Martin, H. 2005. Geodynamic controls on adakite, TTG and sanukitoid genesis: implications for models of crust formation. Introduction to the Special Issue. *Lithos*, 79: ix-xii.

Saalmann, K., Gerdes, A., Lahaye, Y., Hartmann, L.A., Remus, M.V.D. & Läufer, A. 2011. Multiple accretion at the eastern margin of the Rio de la Plata craton: the prolonged Brasiliano orogeny in southernmost Brazil. *International Journal of Earth Sciences*, 100 (2-3): 355-378.

Saint-Blanquat, M., Horsman, E., Habert, G., Morgan, S., Vanderhaeghe, O., Law, R., Tikoff, B. 2011. Multiscale magmatic cyclicity, duration of pluton construction, and the paradoxical relationship between tectonism and plutonism in continental arcs. *Tectonophysics*. 500: 20-33.

Samsonov, A.V., Bogina, M.M., Bibikova, E.V., Petrova, A.Y. & Shchipanski, A.A. 2005. The relationship between adakitic, calc-alkaline volcanic rocks and TTGs: implications for the tectonic setting of the Karelian greenstone belts, Baltic Shield. *Lithos*, 79: 83-106.

Sato, K., Tassinari, C.C.G., Kawashita, K., Petronilho, L. 1995. O método geocronológico Sm-Nd no IG/USP e suas aplicações. *Anais da Academia Brasileira de Ciências*, 67: 315-336.

Sawyer, E.W., Cesare, B. & Brown, M. 2011. When the continental crust melts. *Elements*, 7(4): 229-234.

Schiano, P., Clocchiatti, R., Shimizu, N., Maury, R.C., Jochum, K.P. & Hofmann, A.W. 1995. Hydrous, silica-rich melts in the sub-arc mantle and their relationship with erupted arc lavas. *Nature*, 377(6550): 595-600.

Simonetti, A., Heaman, L.M., Hartlaub, R.P., Creaser, R.A., MacHattie, T.G.& Böhm, C. 2005. U-Pb zircon dating by laser ablation-MC-ICP-MS using a new multiple ion counting Faraday collector array. *Journal of Analytical Atomic Spectrometry*, 20: 677-686.

Smithies, R.H. 2000. The Archean tonalite-trondhjemite-granodiorite (TTG) series is not an analogue of Cenozoic adakite. *Earth and Planetary Science Letters*, 182: 115-125.

Sorensen, S.S. & Grossman, J.N. 1989. Enrichment of trace elements in garnet amphibolites from a paleo-subduction zone: Catalina Schist, southern California. *Geochimica et Cosmochimica Acta*, 53(12): 3155-3177.

Souza, S.L. 2009. Métodos radiométricos Rb-Sr e Sm-Nd no CPGeo Igc-USP. *In:* Simpósio 45 anos de Geocronologia no Brasil, 2009, São Paulo. *Boletim de Resumos Expandidos*: 137-139.

Spera, F.J. & Bohrson, W.A. 2001. Energy-constrained open-system magmatic processes I: general model and energy-constrained assimilation and fractional crystallization (EC-AFC) formulation. *Journal of Petrology*, 42(5): 999-1018.

Springer, W. & Seck, H.A. 1997. Partial fusion of basic granulites at 5 to 15 kbar: implications for the origin of TTG magmas. *Contributions to Mineralogy and Petrology*, 127: 30-45.

Steiger, R.H. & Jager, E. 1978. Subcommission on geochronology: Convention on the use of decay constants in geo- and cosmo-chronology. *Earth and Planetary Science Letters*, 36: 359-362.

Streckeisen, A.L. 1976. To each plutonic rock, its proper name. *Earth Sciences Reviews*, 12: 1-33.

Symington, N.J., Weinberg, R.F., Hasalová, P., Wolfram, L.C., Raveggi, M. & Armstrong, R.A. 2014. Multiple intrusions and remelting-remobilization events in a

magmatic arc: The St. Peter Suite, South Australia. *Geological Society of America Bulletin*, B30975-1.

Thomson, S.T. 2002. Late Cenozoic geomorphic and tectonic evolution of the Patagonian Andes between latitudes 42°S and 46°S: an appraisal based on fission-track results from the transpressional intra-arc Liquiñe-Ofqui fault zone. *Geological Society of America Bulletin*. 114 (9): 1159–1173.

Torquato, J.R. & Kawashita, K., 1994 . Geologia Nuclear V - O método Rb/Sr. *Revista de Geologia*, 46p.

Vernon, R.H., Collins, W.J., Cook, N.D.J. 2012. Metamorphism and deformation of mafic and felsic rocks in a magma transfer zone, Stewart Island, New Zealand. *Journal of Metamorphic Geology*. 30 (5): 473-488.

Wilson, M. 1989. *Igneous Petrogenesis*. Londres, Chapman & Hall, 466p.

Zartman, R.E. & Haines, S.M. 1988. The plumbotectonic model for Pb isotopic systematics among major terrestrial reservoirs – a case for bi-directional transport. *Geochimica et Cosmochimica Acta*, 52(6): 1327-1339.

3. Artigos publicados em periódicos internacionais

3.1 Artigo 1 submetido à revista Journal of South American Earth Sciences

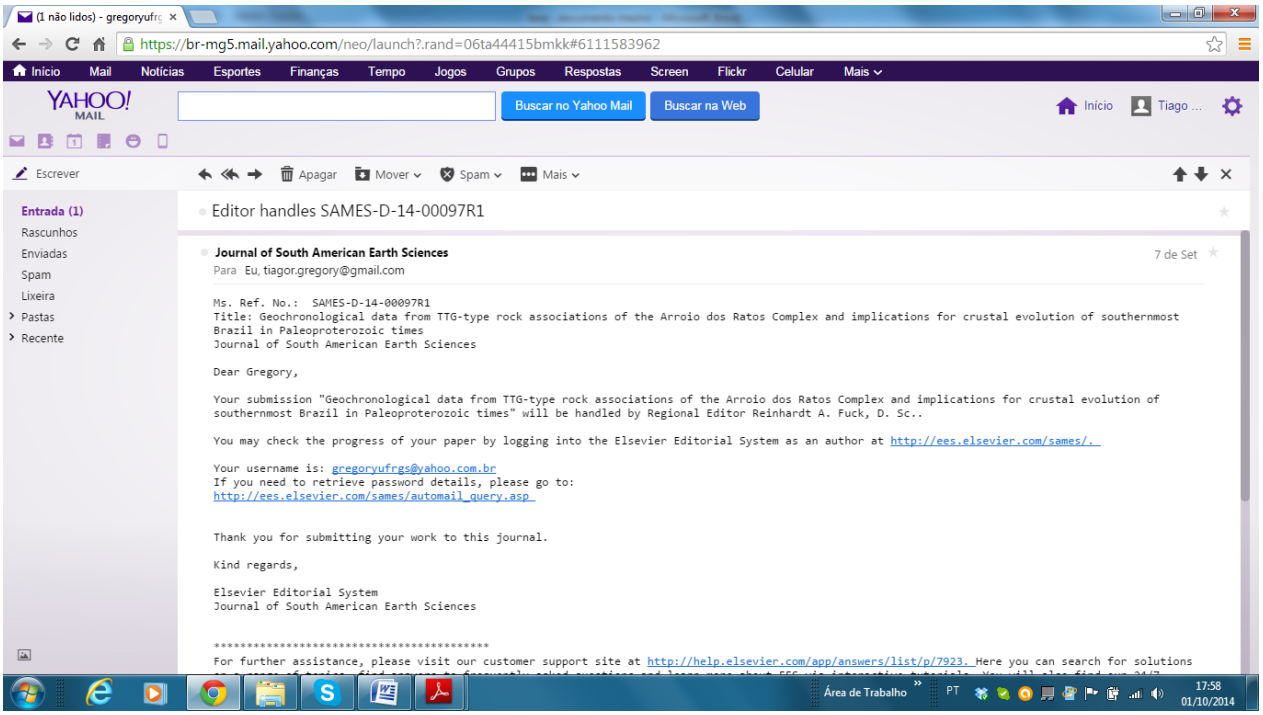

Geochronological data from TTG-type rock associations of the Arroio dos Ratos Complex and implications for crustal evolution of southernmost Brazil in Paleoproterozoic times

Tiago Rafael Gregory[a,*], Maria de Fátima Bitencourt[a], Lauro Valentim Stoll Nardi[a], Luana Moreira Florisbal[b] & Farid Chemale Jr[c]

[a] Instituto de Geociências, Universidade Federal do Rio Grande do Sul, Av. Bento Gonçalves, 9500, Porto Alegre, CEP 91501-970, RS, Brazil

[b] Companhia de Pesquisa de Recursos Minerais, São Paulo, Rua Costa, 55, CEP 01304-010, SP, Brazil

[c] Instituto de Geociências, Universidade de Brasília, Campus Universitário Darcy Ribeiro, Brasília, DF, CEP 70904-970, Brazil

* Corresponding author. Tel.: +15 51 9725 1566

E-mail address: gregoryufrgs@yahoo.com.br (T.R. Gregory)

Keywords

TTG-type associations; Continental arc magmatism; Zircon U-Pb LA-MC-ICP-MS; Paleoproterozoic magmatism in Sul-rio-grandense Shield; Syntectonic magmatism.

Highlights

In southern Brazil, tonalitic/dioritic rock associations of Paleoproterozoic age were identified, around 2,070 and 2,150 Ma.

The Paleoproterozoic associations identified in southern Brazil have continental magmatic arc affinity, analogue to TTG-type ones, and show significant coeval mafic/basic magmatism.

The Paleoproterozoic TTG-type associations identified in southern Brazil have strong deformation registered in metatonalites that are intruded by less deformed tonalites of nearly the same age.

Abstract

U-Pb isotope analyses by LA-MC-ICPMS (Laser Ablation – Multi Collector – Inductively Coupled Plasma Mass Spectrometry) in zircon crystals from metatonalites, tonalites and granodiorite gneiss from the Arroio dos Ratos Complex (ARC) early magmatism in southernmost Brazil are presented. The ARC is located in the eastern portion of the Sul-rio-grandense Shield, occurring as septa and roof pendants on granitoids emplaced along the Southern Brazilian Shear Belt (SBSB). The SBSB corresponds to a translithospheric structure composed of several anastomosed shear zones of dominantly transcurrent kinematics whose syntectonic magmatism, of Neoproterozoic age, is characteristic of post-collisional environments. The studied rocks comprise TTG-type associations with coeval mafic magmatism, deformed and metamorphosed within a ductile shear zone. Zircons obtained from six samples are interpreted as igneous given that the crystals are subhedral to euhedral,

bipyramidal, with concentric zonation, have ratios Th/U between 0.13 and 0.81 and have restricted evidence of overgrowth. The oldest Association 1 (A1) has structures compatible with recrystallization under conditions of high temperature and an igneous age of 2,148 ± 33 Ma, obtained in a metatonalite. The rocks of Association 2 (A2) have similar compositions, although with a more significant coeval mafic fraction. They are intrusive into A1 and also show high-temperature recrystallization features. However, they are less deformed and partly preserve their primary, igneous fabrics. The igneous ages obtained from two A2 tonalites are 2,150 ± 28 Ma and 2,136 ± 27 Ma. Association 3 (A3) is represented by tonalitic to granodioritic gneisses whose structure, composition and metamorphic features are similar to those of A1 rocks, except for the absence of coeval mafic magmas in the former. Local features resulting from partial melting are present in A3 rocks. Three samples from A3 were dated. A tonalitic gneiss gives igneous age of 2,099 ± 10 Ma and two granodioritic gneisses give igneous ages of 2,081 ± 7 Ma and 2,077 ± 13 Ma. Restricted to A1, inheritance is represented by one subhedral, zoned, gently rounded zircon crystal interpreted as igneous, of 2,732 ± 40 Ma ($^{207}Pb/^{206}Pb$ age), with discordance of 9% and $^{232}Th/^{238}U$ratio of 1.17. A single Neoproteozoic metamorphic date value was obtained from the rim of a zircon crystal of Paleoproterozoic core. The age of 635 ± 6 Ma ($^{207}Pb/^{206}Pb$ age), with Th/U ratio < 0.1 and 1% discordance, is interpreted as compatible with adjacent SBSB magmatism. The three associations are interpreted to represent the record of successive magmatic pulses that mark the evolution of a Paleoproterozoic continental magmatic arc. In the study area, these magmatic arc associations represent relict areas partly reworked and relatively well-preserved from Neoproterozoic tectono-magmatic post-collisional events during the construction of the Southern Brazilian Shear Belt.

1. Introduction

Associations of TTG-type (tonalite, trondhjemite, granodiorite) record magmatic events which mark important cycles of adding juvenile material to the crust, contributing to its growth from the Archean to the present day (Barker, 1979; Condie, 2005). Debate over the genesis and evolution of these associations has been heated over time with questions about the occurrence or not of modern type geotectonic environments in the Archean Eon, source and mode of extraction of parental magmas, as melting of subducted plate or of metasomatized mantle wedge (Martin *et al.*, 2005), or even of portions of the mafic lower crust (Condie, 2005). A genetic connection between TTG and magmatic arcs with subduction of oceanic crust is widely proposed (Barker, 1979; Jahn *et al.*, 1981; Defant & Drummond, 1990; Springer & Seck, 1997; Martin *et al.*, 2005), although some authors point out other possibilities, such as partial melting of basic granulite in the lower crust (Rapp *et al.*, 1991) or of deep roots of oceanic plateaus (Condie, 2005).

Although little referred to, the rocks of TTG-type associations are often deformed and associated with basic or mafic rocks, as stated by Barker (1979). In certain cases, a banded structure is present and interpreted to reflect the heterogeneities of the original plutonic system (McGregor, 1979). The preferred alignment of these structures due to shear zones with which they are commonly associated, leads to the use of the term gneissic for their characterization. TTG-type associations include biotite and/or amphibole as mafic phases, and more rarely garnet is identified as an accessory mineral. The Na_2O/K_2O ratios are greater than 1, with Al_2O_3 typically > 15% at 70% of SiO_2 and REE patterns moderate to strongly fractionated, with HREE depletion in relation to LREE (Barker, 1979; Condie, 2005), due to the presence of garnet in the residue of partial melting. This has led to the interpretation of great depths for the formation of these magmas (Barker, 1979; Jahn *et al.*, 1980; Defant & Drummond, 1990; Rapp *et al.*, 1991; Springer & Seck, 1997; Condie, 2005; Martin *et al.*, 2005).

As it is common in Precambrian terranes, the emplacement of younger syntectonic granitoids in host rocks that have in many cases similar composition and structure, makes it difficult to distinguish between different units. Fieldwork, with careful observations and systematic collection of samples, integrating data from structural geology, petrography and geochemistry, have been successfully employed in the recognition of different units within a terrane of foliated/banded granitoids. The addition of geochronological data is fundamental to the elucidation of diachronism among some rock sequences often grouped into complexes.

In southernmost Brazil, rock associations lying East of the main, NE-trending transcurrent structures have been previously assigned to Neoproterozoic arc magmatism (Fernandes *et al*., 1992, among others). A TTG-type association was identified in this part of the Sul-rio-grandense Shield (SrgS), southern Brazil, by Gregory *et al.* (2011) as part of the Arroio dos Ratos Complex (ARC). The present study focuses on the age determation of the ARC rock types representative of its early magmatic phases. This is a TTG-type association of coeval felsic and mafic rocks, deformed and recrystallized as emplaced within an active shear zone (Gregory *et al.*, 2011). Detailed geological mapping, systematic sampling and lithological-structural studies permit an assessment to be made of the nature of the magmatism within this complex, revealing a Paleoproterozoic substrate surrounded by granitoids correlated to the Southern Brazilian Shear Belt (SBSB), of Neoproterozoic age.

2. Geological setting

The study area is situated in the southern portion of the Mantiqueira Province (Almeida *et al.*, 1981), which is an extensive Neoproterozoic mobile belt. This mobile belt records the collision between Kalahari and Rio de la Plata cratons that has eventually led to the amalgamation of West Gondwana supercontinent.

The eastern part of this Mantiqueira Province segment features a wide shear belt comprised of several anastomosing shear zones that extend from the state of Santa Catarina (south Brazil) to Uruguay (Fig. 1). In southern Brazil, this set of translithospheric structures is designated the Southern Brazilian Shear Belt (SBSB) and its discontinuities are thought to have conditioned Neoproterozoic post-collisional magmatism (Bitencourt & Nardi, 1993; 2000; Florisbal *et al.*, 2012) under transcurrent kinematics between 650 and 580 Ma.

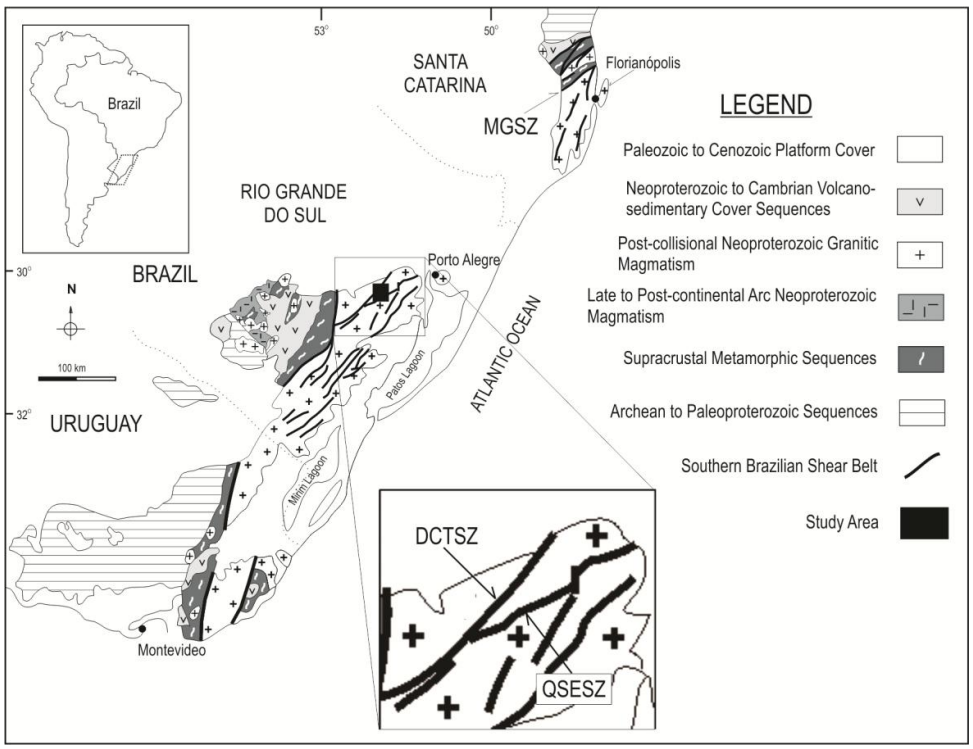

Figure 1 – Main geotectonic units from southern Brazil and Uruguay, with localization of the study area (modified from Nardi & Bitencourt, 2007). MGSZ –Major Gercino Shear Zone; DCTSZ – Dorsal de Canguçu Transcurrent Shear Zone; QSESZ – Quitéria-Serra do Erval Shear Zone.

To the west, a supracrustal metamorphic belt separates the SBSB from Neoproterozoic rock sequences attributed to mature continental magmatic arc environment (Garavaglia *et al.*, 2002; 2006) of 704 ± 13 Ma (U-Pb in zircon – Babinski *et al.*, 1996) that are partially hidden under Cambrian to Neoproterozoic volcanosedimentary cover sequences. Further to the west and southwest, Archaean and Paleoproterozoic associations are found within the remnants of the Rio de la Plata Craton, as pointed out by Hartmann *et al.* (2000) (Fig. 1). Paleoproterozoic, TTG-type associations are also referred by Saalmann *et al.* (2011) and Camozzato *et al.* (2013) as forming the basement of the supracrutal metamorphic rocks in the state of Rio Grande do Sul (Fig. 1).

In the study area and neighbouring regions, the basement for the SBSB granitoids is represented by the Varzea do Capivarita Complex (as defined by Martil *et al.*, 2011), comprised of a multi-scale interleaving of ortho- and paragneisses metamorphosed at *ca.* 650 Ma, where the igneous protoliths represent a mature magmatic arc association of *ca.* 790 Ma (Martil *et al.*, submitted), and *ca.* 640 Ma syntectonic syenite magmatism (Bitencourt *et al.*, 2011). This unit is interpreted as a thrust pile by Martil *et al.*(submitted for publication) and signals the main collisional episode at 650 Ma in southern Brazil.

The rocks presently studied correspond to a different type of pre-SBSB association, represented by the Arroio dos Ratos Complex (ARC). This is a TTG-type association with coeval mafic magmatism, as defined by Gregory *et al.* (2011), bearing a continental magmatic arc geochemical signature. These rocks are recognized as preserved segments, partly reworked by ductile shear zones of the SBSB, whose original relations are recognizable in low-strain zones.

In the study area (Fig. 2), the ARC is limited by two shear zones (Fig. 2 and inset of Fig. 1) along which Neoproterozoic post-collisional granites are positioned. The Dorsal de Canguçu (Fernandes & Koester, 1999) and Quitéria-Serra do Erval shear zones (Knijnik *et al.*, 2013) have their

minimum interval of activity (658 to 605 Ma) limited by the magmatic age of their syntectonic granites, determined by Frantz *et al.* (2003), Koester *et al.* (2008), and Knijnik *et al.* (2012). Later reactivation of these shear zones, possibly under lower-temperature and shallower conditions, are marked by quartz-mylonites and phyllonites in discontinuous ridges (Fig. 2) currently under investigation, whose movement ages are not yet determined precisely.

To the southeast of these structures (Fig. 2) several undeformed plutonic, hypabyssal and volcanic rock sequences signal the late magmatic phases of post-collisional setting with a large volume of extensional, alkaline magmatism at *ca.* 580 Ma, as pointed out by Sommer *et al.* (2013).

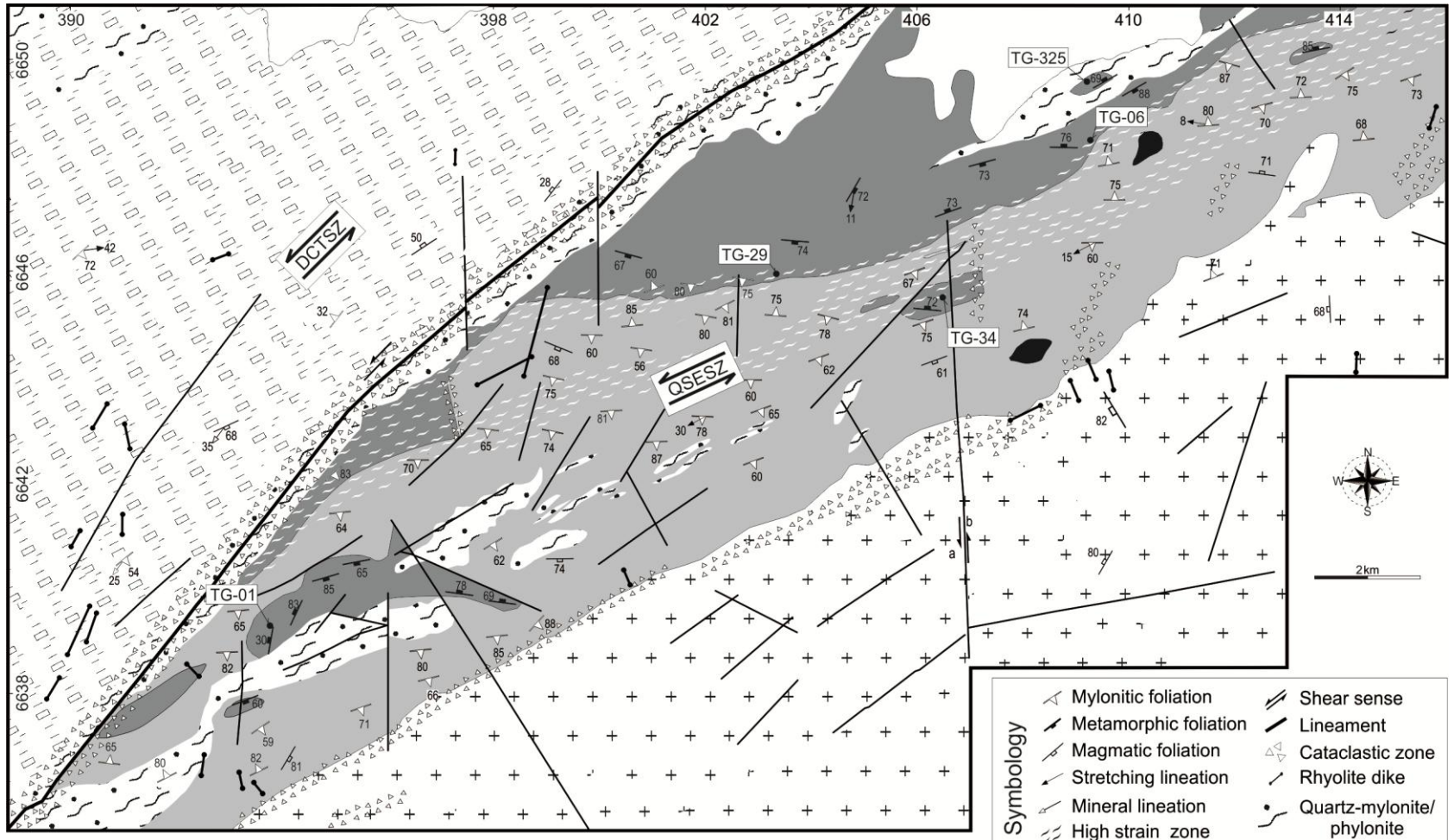

LEGEND

- Paleozoic Sedimentary Cover
- Late Transcurrent Plutonic and Hypabyssal Rocks ~580 Ma
- Quitéria-Serra do Erval Syntranscurrent Granitoids ~630 Ma
- Dorsal de Canguçu Syntranscurrent Granitoids 658-605 Ma
- High-grade Parametamorphic Rocks
- Arroio dos Ratos Complex

Figure 2 – Geological map of Quitéria-Serra do Erval region (modified from Gregory *et al.*, 2011), with location of dated samples points. DCTSZ – Dorsal de Canguçu Transcurrent Shear Zone; QSESZ – Quitéria-Serra do Erval Shear Zone.

3. Geology and Petrology of the Arroio dos Ratos Complex

Two structurally discordant tonalitic-dioritic associations were identified by Gregory *et al.* (2011) at the ARC type-section, based mainly on field and petrographic criteria. The oldest association (A1) comprises garnet-biotite metatonalites with anastomosed foliation marked by the orientation of biotite and lenticular quartz-feldspathic aggregates, quartz ribbons and medium- to coarse-grained, recrystallized plagioclase. An irregular banding is occasionally developed parallel to the main fabric, enhanced by deformed trondhjemitic veins. In such places, early isoclinal folding of the veins (F1) is observed, and fold axes and axial planes are parallel to the stretching lineation and foliation plane, respectively. A high temperature crenulation cleavage is observed in areas of tight foliation folding, with disruption of hinges and flow parallel to the axial planes. The granoblastic texture is observable in hand specimen, and microstructures of plagioclase, such as interlobate contacts, indicate high temperature recrystallization processes (600° C), according to Passchier & Trouw (2005, p. 62). The metatonalites contain dark enclaves of fine texture and variable composition (basic to acidic), with higher mafic content than their host, most of them interpreted as sheared synplutonic dikes (Fig. 3a). The A1 host rocks are found only as variable-size xenoliths in the metatonalites. They comprise tonalitic gneisses, calc-silicate and metavolcanosedimentary rocks. According to Gregory *et al.* (2011), the original, pre-F2 geometry of the foliation in A1 rock types would have been gently-dipping towards WSW, and top-to-east shear sense.

The A2 Association is composed of tonalites and diorites intrusive into A1 rock types (Figs. 3a and 3b). The contacts are either sharp or diffuse, and these rocks also display high-temperature recrystallization features, but they are less deformed, and partially preserve their primary structure. The A2 foliation is magmatic, marked by the alignment of micas and feldspars, with local solid-state deformation marked by elongate quartz aggregates and plagioclase porphyroclasts. The foliation strikes generally EW, with steep dips to the south. The stretching lineation is not well developed and plunges at moderate to low angles to WSW.

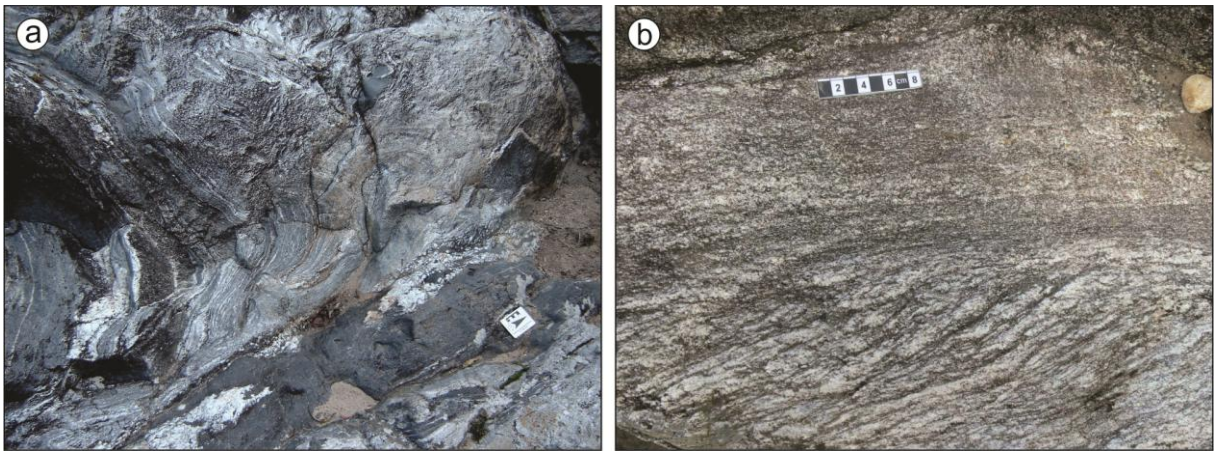

Figure 3 – Field aspects of A1 and A2 associations. (a) A1 (top left) is represented by foliated metatonalites with mafic enclaves affected by open folds of southward-dipping axial plane (left on the photo). A2 mafic/basic varieties are more massive, interspersed with their contemporary felsic terms (bottom right), positioned along an F2 fold axial plane. (b) Discordant intrusive relation of A2 (above) in A1 (below) rocks. Note the diffuse contact between the rocks of the two associations, suggestive of low contrast in temperature at the time of A2 intrusion.

The geochemical study of A1 rocks (Gregory *et al.*, 2011) demonstrates its derivation from silica-supersaturated, subalkaline, metaluminous to peraluminous igneous protholiths related to medium- and high-potassium calc-alkaline series magmatism. The behavior of trace- and rare-earth elements indicates a mature continental arc setting, comparable to the TTG-type associations reviewed by Condie (2005) and Martin *et al.* (2005). Geochemical patterns also show that differentiation processes have mostly followed mineral fractionation trends involving plagioclase, amphibole and biotite in different proportions. Element mobilization due to metamorphic processes is not evident, and the rocks preserve their original composition despite their well-developed granoblastic texture.

The A3 lithological association is composed of tonalitic to granodioritic gneisses whose composition and structure are similar to those in other lithological types of the ARC. However, these rocks are distinguished by their well-developed metamorphic banding (Fig. 4a) as well as by the apparent lack of coeval mafic material. The rocks are fine-to medium-grained and the foliation is characterized by elongate quartz-feldspathic aggregates, recrystallized quartz ribbons and aligned biotite flakes. The banded pattern is given by elongate quartz-feldspathic aggregates, and in certain cases accompanied by coarser grained leucocratic injections parallel to the foliation. Mafic-rich varieties have a more strongly developed banded structure (Fig. 4b). The foliation and the banded pattern feature tight folds, with the formation of a second, axial-planar foliation, and the pre-existing structure rotation indicates dextral sense of shear, also determined in S-C structures. Partial melting features are locally present along the C-planes.

Microstructures formed under high temperature conditions are ubiquitous, but a lower temperature episode tends to obliterate them to different degrees. Even so, the interlobate feldspar crystal contacts indicating thermal conditions similar to those determined for the A1 rocks can be observed.

Preliminary geochemical data from A2 and A3 rocks indicate that they are similar to the A1 rocks and suggest a common origin and evolution, with A3 showing the most differentiated varieties.

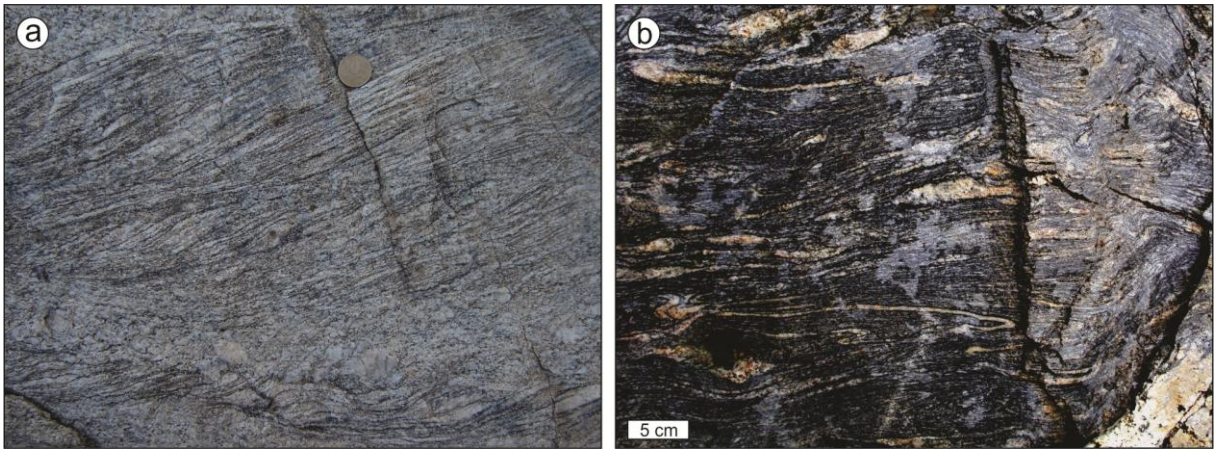

Figure 4 – Field aspect of A3 rocks. (a) Granodioritic orthogneiss with dextral displacement of the main banding by a less penetrative foliation. (b) Strongly-developed banded structure, typical of highly-deformed, mafic-rich tonalitic varieties.

A lower temperature deformation episode affects all three rock associations described in the Arroio dos Ratos Complex. It is marked by fine-grained mosaics of recrystallized quartz, and core-mantle structures in feldspars, where mantles comprise subgrains and new grains. Bookshelf-type, antithetic fractures of feldspar crystals are common, as well as intense hydrothermal alteration of

plagioclase to white micas. Brittle-ductile behavior of quartz and plagioclase indicates temperature conditions equivalent to upper greenschist facies (400-600° C – Passchier & Trouw, 2005, p. 62). This episode is possibly correlated to the tectono-thermal event that generated the SBSB. In areas where this deformation reworks the planar structures of the ARC rocks the main structures are discrete, brittle-ductile shear bands of sinistral shear sense developed over the main foliation. Within high-strain zones of the shear belt, the well-developed, sinistral mylonitic foliation obliterates former contacts and original structures of the ARC. Temperatures within the shear zones are intermittently raised due to the emplacement of syntectonic granitoids (Fig. 2).

4. Geochronology

4.1 Pre-existing data

Pre-existing geochronological data for the study area are ambiguous, with Neoproterozoic and Paleoproterozoic ages (Tab. 1). Because the area of occurrence of the Arroio dos Ratos unit (as in Fernandes *et al.*, 1988) is larger than presently admitted, it is most likely that some of the age data previously obtained represent in fact magmatic ages of intrusive granites, now separated from the ARC in individual plutons. The Neoproterozoic ages of these granitic plutons (Fig. 2) are established either by geochronological data (Knijnik *et al.*, 2012; Centeno, 2012) or by stratigraphic constraints of known units (Fontana *et al.*, 2012). The published data shown in Table 1 do not rule out the possibility of Neoproterozoic rocks within the Arroio dos Ratos Complex, since precise location of dated sample is not always presented. Additionally, its structure is complex enough to allow for tectonic slices of different ages to have passed unnoticed. Therefore, a wide variety of ARC rocks were analysed in different structural situations, so as to increase the chances of unraveling the complete history of this unit.

Table 1 – Pre-existing isotope data for the ARC area as defined by Fernandes *et al.* (1988). 1 = magmatic age; 2 = metamorphic age; 3 = crustal residence; 4 = orogenic event (resetting).

REFERENCE	METHOD	ROCK TYPES	AGE (interpretation)
Silva *et al.* (1999)	Zircon U-Pb SHRIMP	granodioritic gneiss	1,573±39 Ma (1)
			631±13 Ma (2)
	Sm/Nd TDM		2,062 Ma (3)
Leite e*t al.* (2000)	Zircon U-Pb SHRIMP	granodiorite	2,078±13 Ma (1)
			1 to 0.59 Ga (4)
Koester *et al*. (2008)	Zircon U-Pb LA-ICP-MS	granodioritic gneiss	650.1±4.7 Ma (1)

4.2 Analytical procedures

About 50 to 100 crystals were collected from the least magnetic zircon fraction of samples TG-01M (A1) and TG-06A (A3) and then mounted and polished in a standard epoxy mount. All the samples were prepared by conventional procedures at LGI/UFRGS (Laboratório de Geologia Isotópica/Universidade Federal do Rio Grande do Sul) and the details of zircon separation can be found in Chemale *et al.* (2011, 2012). Zircons from another group of samples (TG-01S = A2; TG-34A = A2; TG-29A and TG-325A = A3) were separated at CPGeo (Centro de Pesquisas Geocronológicas), University of São Paulo, and a detailed description of the method can be found in Florisbal *et al.* (2012). All dated crystals were studied by back-scatter electron (BSE) and cathodoluminescence (CL) microscope images before LA-MC-ICP-MS analyses.

The zircons were analyzed at different laboratories using a Nu-Plasma MC-ICP-MS coupled to a frequency quintupled (λ=213 nm) Nd:YAG laser ablation system. Analytical protocols and collectors configurations are described in detail by Kosler *et al.* (2002), Jackson *et al.* (2004), Simonetti *et al.* (2005) and Chemale *et al.* (2012). Laser-induced elemental fractional and instrumental mass discrimination were corrected by the reference zircon standard (GJ-1). Two measurements of GJ-1 standard analyses were done to every ten zircon spots. The raw data were processed off-line and reduced using an Excel worksheet. Errors reported in 1σ, except for sample TG-01S that is reported in 2σ, following the internal laboratory standards from University of Alberta. The ages were calculated using the decay constants reported by Jaffey *et al.* (1971); ^{238}U – $1.55125x10^{-10}$ $yr.^{-1}$ and ^{235}U – $9.8485x10^{-10}$ $yr.^{-1}$ and a $^{238}U/^{235}U$ ratio of 137.88. All the U-Pb plots were constructed using Isoplot (Ludwig, 1993).

Samples TG-01M and TG-06A were analyzed at LGI/UFRGS. U-Pb data were acquired with spot size of 25 µm. Laser operating conditions and detailed description of analytical method can be found in Chemale *et al.* (2011, 2012). Sample TG-01S was analyzed at RIF/UA (Radiogenic Isotope Facility, University of Alberta, Canada). U-Pb data were acquired on single zircon crystal with spot size of 40 µm. The analytical protocol and collector configuration is described in detail by Simonetti *et al.* (2005) and allows simultaneous acquisition of masses from ^{238}U to ^{203}Tl. Laser operating conditions and detailed description of analytical method can be found in Florisbal *et al.* (2012). Samples TG-34A, TG-29A and TG-325A were analyzed at Laboratório de Geocronologia, University of Brasília. Analyses were performed using spot size of 30 µm and laser induced fractionation of the $^{206}Pb/^{238}U$ ratio was corrected using the linear regression method (Kosler *et al.*, 2002).

4.3 Samples and results

Six representative samples of the CAR magmatism were selected for geochronological studies. Sample TG-01M is a foliated garnet-biotite metatonalite from A1, samples TG-01S and TG-34A are foliated biotite tonalites from A2 and TG-06A, TG-29A and TG-325A are metagranodiorites (TG-06A and TG-29A) and banded metatonalites (TG-325A) from A3. Sample locations are shown in figure 2 and table 2.

Table 2 – UTM coordinates of the analyzed samples (fuse: 22J; datum: Córrego Alegre).

Sample	Unit	Litology	UTM (m) E	UTM (m) N
TG-01M	A1	metatonalite	393,952	6,639,228
TG-01S	A2	tonalite	393,952	6,639,228
TG-34A	A2	tonalite	406,486	6,645,503
TG-06A	A3	granodioritic gneiss	409,336	6,648,414
TG-29A	A3	granodioritic gneiss	403,340	6,645,948
TG-325A	A3	tonalitic gneiss	409,220	6,649,495

The studied zircon populations are very similar and present many common characteristics, as illustrated in figures 5 and 6. Crystal sizes vary between 70 and 200 µm, with aspect ratio of 1:2 to 1:4. Most of the crystals are subhedral to euhedral, prismatic, in general with preserved bypiramids. Subrounded and more rarely rounded crystals are also found (*eg.* TG-01M and 34A). Inclusions are very scarce and fractures are not frequent. Concentric zoning patterns are always identified. Overgrowths are restricted to thin (< 15 µm) dark or bright rims that can be identified at crystal

borders, sometimes outlining its morphology. The subrounded shape of many crystals is due to this kind of rim, as illustrated in some of the crystals of TG-01S and 34A. No ages were obtained from these rims because they are narrower than the 25 to 40 µm LA-MC-ICP-MS spot sizes. Although rare, some irregular zoning patterns are also identified. Some metamict zircons were identified only in samples TG-29A and TG-34A.

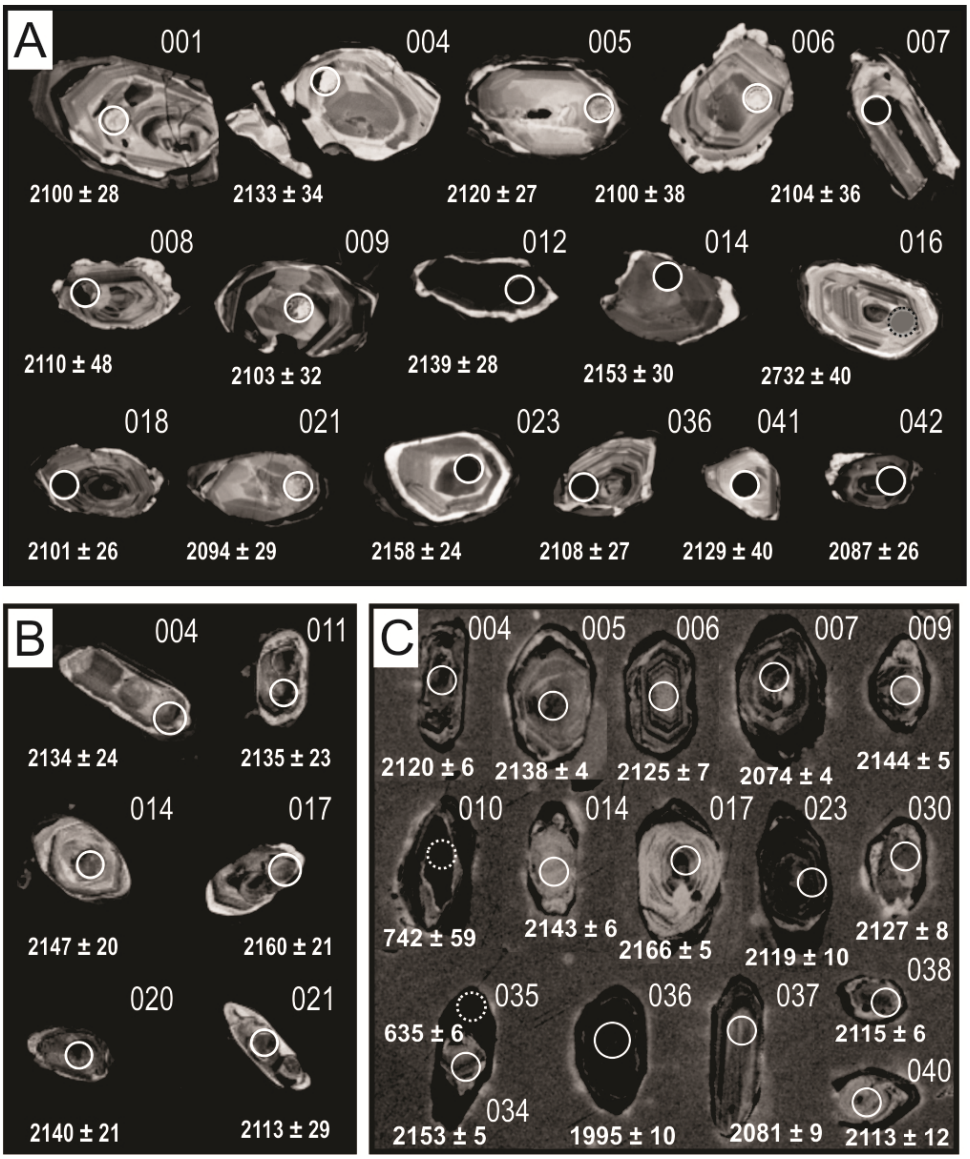

Figure 5 – Cathodoluminescence (CL) images of zircon grains from A1 and A2 samples, with location of spots (circles). (a) TG-01M – metatonalite from A1 (spot = 25 µm). (b) TG-01S – tonalite from A2 (spot = 40 µm). (c) TG-34A – tonalite from A2 (spot = 30 µm). Empty circle, with continuous outline – igneous age; empty circle with dashed white outline – metamorphic ages; filled circle, with dashed black outline – inherited age. $^{207}Pb/^{206}Pb$ ages (Ma).

The U-Pb ages obtained in all the samples give upper intercept discordia ages with low associated discordance (< 14-10%) (Tab.3).

All the obtained ages are Paleoproterozoic. They are interpreted as crystallization ages on the basis of crystal morphology and zoning patterns, both compatible with magmatic crystals (Fig. 5 and 6), with Th/U ratios of 0.13 to 0.81 (Tab. 3). The similarity of zircon morphologies, with no distinct cores or truncated zoning patterns, the presence of rare rounded crystals and the single, narrow,

Paleoproterozoic age interval identified in all samples does not point to the presence of inherited crystals. Only one zircon crystal found in sample TG-01M provides a $^{207}Pb/^{206}Pb$ Archean age of 2,732 ± 40 Ma (Fig. 5a and Tab. 3). This grain is slightly rounded and has Th/U ratio of 1.17, compatible with magmatic sources (Rubatto, 2002). In sample TG-34A two distinct Neoproterozoic ages were identified: a $^{207}Pb/^{206}Pb$ date of 742 ± 59 Ma of a metamict core (Fig. 5c) and a $^{207}Pb/^{206}Pb$ date of 635 ± 6 Ma for a rim of a Paleoproterozoic core (Fig. 5c). The Neoproterozoic data have low associated error and are highly concordant, with Th/U ratios varying from < 0.01 to 0.06 that suggest metamorphic origin. Sample TG-34A is the one presenting the most scattered data set in comparison to other samples, but its concordant Neoproterozoic ages may represent either a complex Pb-loss scenario or even the possibility of mixed spot analyses, like merging core and rim regions of a grain. However, the 635 ± 6 Ma age value is correlated to the Southern Brazilian Shear Belt activity (*e.g.* Florisbal *et al.*, 2012; Knijnik *et al.*, 2012) that is largely known as the structure which overprints the ARC rock associations and controls the emplacement of nearby Neoproterozoic syntectonic granites. The signicance of the 742 ± 59 Ma age is open to further interpretation.

The great majority of the results obtained in this study set a Paleoproterozoic age (Meso- to late-Rhyacian) for the ARC magmatism (Th/U > 0.1).The oldest association, A1, has magmatic crystallization at 2,148 ± 33 Ma (Fig. 7a). The A2 rocks, intrusive into A1, have crystallization ages of 2,150 ± 28 Ma and 2,136 ± 27 Ma (Figs. 7b and 7c). The A3 rocks have crystallization ages of 2,099 ± 10 Ma (Fig. 7d), 2,081 ± 7 Ma (Fig. 7e) and 2,077 ± 13 Ma (Fig. 7f).

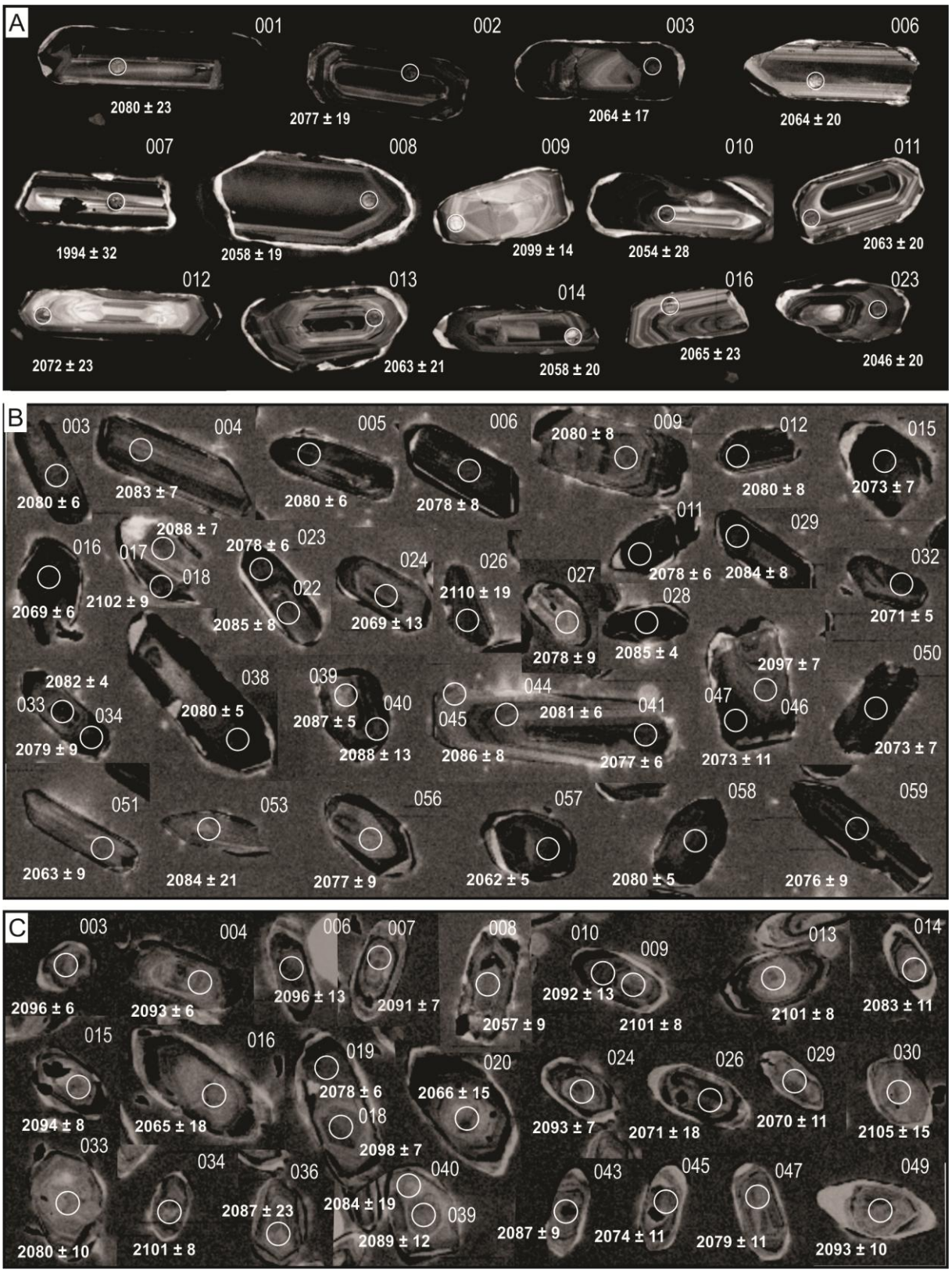

Figure 6 – Cathodoluminescence (CL) images of zircon grains from A3 samples, with location of spots (circles). (a) TG-06A – granodioritic gneiss from A3 (spot = 25 µm). (b) TG-29A – granodioritic gneiss from A3 (spot = 30 µm). (c) TG-325A – tonalitic gneiss from A3 (spot = 30 µm). Empty circle, with continuous outline – igneous age. $^{207}Pb/^{206}Pb$ ages (Ma).

Table 3 – LA-MC-ICP-MS U-Pb data used for age calculation for the Arroio dos Ratos Complex studied rocks.

sample	Spot	Isotopic Ratio							Age and error (Ma)							Th/U
spot	size	$^{207}Pb/^{235}U$	error (%)	$^{206}Pb/^{238}U$	error (%)	rho	$^{207}Pb/^{206}Pb$	error (%)	$^{206}Pb/^{238}U$	error	$^{207}Pb/^{235}U$	error	$^{207}Pb/^{206}Pb$	error	% Disc	
TG-01M			1σ		1σ			1σ		1σ		1σ		1σ		
001	25µm	6.50727	1.62303	0.36254	0.91649	0.565	0.13018	1.33950	1994	18	2047	33	2100	28	5.05	0.65
004	25µm	7.01202	1.75787	0.38339	0.72178	0.411	0.13265	1.60285	2092	15	2113	37	2133	34	1.93	0.29
005	25µm	6.71150	1.46228	0.36980	0.72562	0.496	0.13163	1.26954	2028	15	2074	30	2120	27	4.31	0.47
006	25µm	6.45246	2.01629	0.35962	0.91130	0.452	0.13013	1.79860	1980	18	2039	41	2100	38	5.68	0.53
007	25µm	6.45145	2.26523	0.35877	1.50971	0.666	0.13042	1.68881	1976	30	2039	46	2104	36	6.05	0.34
008	25µm	5.79101	2.49811	0.32089	1.07386	0.430	0.13089	2.25553	1794	19	1945	49	2110	48	14.97	0.30
009	25µm	6.26316	1.67874	0.34850	0.69073	0.411	0.13034	1.53006	1927	13	2013	34	2103	32	8.33	0.81
012	25µm	6.62315	1.42704	0.36104	0.53365	0.374	0.13305	1.32350	1987	11	2062	29	2139	28	7.08	0.45
014	25µm	6.92586	2.01850	0.37438	1.46009	0.723	0.13417	1.39374	2050	30	2102	42	2153	30	4.80	0.61
016*	25µm	12.2485	1.90166	0.47052	1.21274	0.638	0.18880	1.46477	2486	30	2624	50	2732	40	9.00	1.17
018	25µm	6.02913	1.62779	0.33571	1.03853	0.638	0.13025	1.25346	1866	19	1980	32	2101	26	11.20	0.48
021	25µm	6.17234	1.72594	0.34520	1.02438	0.594	0.12968	1.38907	1912	20	2001	35	2094	29	8.70	0.42
023	25µm	7.17440	1.40022	0.38666	0.85295	0.609	0.13457	1.11045	2107	18	2133	30	2158	24	2.37	0.46
036	25µm	6.68226	1.45264	0.37060	0.64723	0.446	0.13077	1.30049	2032	13	2070	30	2108	27	3.61	0.36
041	25µm	6.75620	2.13843	0.37028	1.06230	0.497	0.13234	1.85590	2031	22	2080	44	2129	40	4.63	0.60
042	25µm	6.28401	1.72208	0.35279	1.16570	0.677	0.12919	1.26756	1948	23	2016	35	2087	26	6.66	0.63
TG-01S			2σ		2σ			2σ		2σ		2σ		2σ		
004r	40µm	6.92687	3.92414	0.37858	3.67954	0.938	0.13270	1.36398	2070	65	2102	34	2134	24	3.53	nd
011r	40µm	6.27346	3.68521	0.34264	3.44968	0.936	0.13279	1.29528	1899	57	2015	32	2135	23	12.74	nd
014c	40µm	6.81718	4.37014	0.36983	4.22356	0.967	0.13369	1.12200	2029	73	2088	38	2147	20	6.43	nd
017r	40µm	6.56544	3.95998	0.35353	3.77620	0.954	0.13469	1.18791	1951	63	2055	34	2160	21	11.18	nd
020c	40µm	6.30936	4.05303	0.34365	3.86731	0.954	0.13316	1.20907	1904	63	2020	35	2140	21	12.71	nd
021r	40µm	6.25076	4.06831	0.34567	3.72610	0.916	0.13115	1.63172	1914	61	2012	35	2113	29	10.91	nd
TG-34A			1σ		1σ			1σ		1σ		1σ		1σ		
004	30µm	7.86419	0.89483	0.43331	0.82166	0.907	0.13163	0.35438	2321	16	2216	8	2120	6	-9.47	0.35
005	30µm	7.30356	0.75920	0.39821	0.71864	0.937	0.13302	0.24483	2161	13	2149	7	2138	4	-1.05	0.64
006	30µm	6.99151	0.65407	0.38402	0.50526	0.838	0.13204	0.41536	2095	9	2110	6	2125	7	1.43	0.60
007	30µm	6.30473	0.65562	0.35648	0.60567	0.902	0.12827	0.25100	1965	10	2019	6	2074	4	5.25	0.40
009	30µm	6.97244	0.73457	0.37880	0.67645	0.904	0.13350	0.28636	2071	12	2108	7	2144	5	3.44	0.40
010	30µm	1.09066	2.99901	0.12357	1.12878	0.611	0.06401	2.77847	751	8	749	16	742	59	-1.21	0.06
014	30µm	6.67642	1.05234	0.36296	0.98645	0.932	0.13341	0.36652	1996	17	2070	9	2143	6	6.86	0.56
017c	30µm	7.15971	0.61060	0.38413	0.53457	0.829	0.13518	0.29509	2096	10	2132	5	2166	5	3.27	0.33
023c	30µm	5.94858	1.13903	0.32789	1.00094	0.869	0.13158	0.54361	1828	16	1968	10	2119	10	13.73	0.42
030	30µm	7.11379	0.80410	0.39047	0.64451	0.876	0.13213	0.48082	2125	12	2126	7	2127	8	0.07	0.57
034c	30µm	7.02279	1.20211	0.37966	1.16771	0.970	0.13416	0.28550	2075	21	2114	11	2153	5	3.64	0.33
035r	30µm	0.85917	0.68530	0.10237	0.61648	0.873	0.06087	0.29930	628	4	630	3	635	6	0.99	<0.01
036	30µm	5.48891	0.87019	0.32461	0.68280	0.882	0.12264	0.53946	1812	11	1899	7	1995	10	9.16	0.37
037	30µm	6.67577	1.55463	0.37604	1.46045	0.937	0.12876	0.53288	2058	26	2069	14	2081	9	1.12	0.30
038	30µm	6.88979	0.79080	0.38063	0.71656	0.889	0.13128	0.33453	2079	13	2097	7	2115	6	1.70	0.36
040	30µm	6.33866	0.95947	0.35057	0.67565	0.821	0.13114	0.68123	1937	11	2024	8	2113	12	8.33	0.53
TG-06A			1σ		1σ			1σ		1σ		1σ		1σ		
001	25µm	6.62227	1.28712	0.37335	0.66398	0.516	0.12864	1.10263	2045	14	2062	27	2080	23	1.65	0.50
002	25µm	6.79852	1.07289	0.38390	0.53840	0.502	0.12844	0.92802	2094	11	2086	22	2077	19	-0.86	0.32
003	25µm	6.32481	0.97680	0.35970	0.50691	0.519	0.12753	0.83497	1981	10	2022	20	2064	17	4.04	0.21
006	25µm	6.78607	1.08230	0.38594	0.45737	0.423	0.12753	0.98090	2104	10	2084	23	2064	20	-1.93	0.26
007	25µm	5.12531	1.67466	0.30333	0.42733	0.255	0.12255	1.61922	1708	7	1840	31	1994	32	14.34	0.37
008	25µm	6.76893	1.10711	0.38630	0.62645	0.566	0.12709	0.91283	2106	13	2082	23	2058	19	-2.31	0.26
009	25µm	6.62781	0.91432	0.36954	0.64688	0.707	0.13008	0.64616	2027	13	2063	19	2099	14	3.42	0.32
010	25µm	6.44779	1.56634	0.36881	0.77646	0.496	0.12680	1.36034	2024	16	2039	32	2054	28	1.47	0.35
011	25µm	6.19886	1.07186	0.35269	0.48403	0.452	0.12747	0.95635	1947	9	2004	21	2063	20	5.62	0.24
012	25µm	6.43165	1.25712	0.36416	0.55686	0.443	0.12809	1.12706	2002	11	2037	26	2072	23	3.38	0.27
013	25µm	6.29181	1.11424	0.35810	0.47078	0.423	0.12743	1.00990	1973	9	2017	22	2063	21	4.34	0.32
014	25µm	6.33919	1.09974	0.36180	0.54223	0.493	0.12708	0.95678	1991	11	2024	22	2058	20	3.27	0.32
016	25µm	6.39884	1.46453	0.36382	0.94171	0.643	0.12756	1.12162	2000	19	2032	30	2065	23	3.12	0.22
023	25µm	6.26554	1.03713	0.36005	0.33302	0.321	0.12621	0.98220	1982	7	2014	21	2046	20	3.10	0.24
TG-29A			1σ		1σ			1σ		1σ		1σ		1σ		
003	30µm	6.57417	0.74884	0.37052	0.65843	0.853	0.12869	0.35670	2032	11	2056	7	2080	6	2.32	0.26
004	30µm	6.70374	0.81859	0.37710	0.72810	0.870	0.12893	0.37410	2063	13	2073	7	2083	7	0.99	0.30
005	30µm	6.60786	0.84371	0.37253	0.77694	0.909	0.12865	0.32896	2041	14	2060	7	2080	6	1.84	0.22
006	30µm	6.65553	0.74078	0.37548	0.59650	0.878	0.12856	0.43926	2055	10	2067	7	2078	8	1.12	0.25
009	30µm	6.56663	0.77971	0.37004	0.64239	0.786	0.12870	0.44192	2030	11	2055	7	2080	8	2.44	0.28
011	30µm	6.83782	0.62158	0.38577	0.50292	0.734	0.12856	0.36528	2103	9	2091	6	2078	6	-1.20	0.17
012	30µm	6.75964	0.72973	0.38109	0.57143	0.855	0.12864	0.45384	2081	10	2080	6	2080	8	-0.09	0.16
015	30µm	6.43464	0.63756	0.36419	0.51177	0.730	0.12814	0.38022	2002	9	2037	6	2073	7	3.41	0.24
016	30µm	6.56349	0.94643	0.37227	0.88408	0.927	0.12787	0.33782	2040	15	2054	8	2069	6	1.39	0.14
017c	30µm	6.41043	0.79003	0.35964	0.67406	0.824	0.12928	0.41206	1980	11	2034	7	2088	7	5.16	0.43
018r	30µm	6.59742	0.88729	0.36717	0.71166	0.901	0.13032	0.52992	2016	12	2059	8	2102	9	4.10	0.32
022c	30µm	6.89586	0.71688	0.38755	0.55428	0.710	0.12905	0.45463	2111	10	2098	6	2085	8	-1.27	0.44
023r	30µm	6.72832	0.74061	0.37957	0.66675	0.879	0.12856	0.32241	2074	12	2076	7	2078	6	0.20	0.23
024	30µm	6.83008	0.96220	0.38743	0.64866	0.820	0.12786	0.71069	2111	12	2090	9	2069	13	-2.04	0.31
026	30µm	7.05352	1.45974	0.39086	0.96926	0.643	0.13088	1.09151	2127	18	2118	13	2110	19	-0.80	0.24
027	30µm	6.75402	1.12084	0.38114	0.99278	0.876	0.12852	0.52026	2082	18	2080	10	2078	9	-0.18	0.33
028	30µm	6.90657	0.79127	0.38807	0.74914	0.938	0.12908	0.25475	2114	14	2100	7	2085	4	-1.36	0.16
029	30µm	6.84456	0.66840	0.38482	0.50729	0.823	0.12900	0.43523	2099	9	2092	6	2084	8	-0.69	0.18
032	30µm	6.20184	0.59846	0.35135	0.51718	0.809	0.12802	0.30112	1941	9	2005	5	2071	5	6.27	0.13

Table 3 – (*continued*)

sample	Spot	Isotopic Ratio							Age and error (Ma)							Th/U
spot	size	$^{207}Pb/^{235}U$	error (%)	$^{206}Pb/^{238}U$	error (%)	rho	$^{207}Pb/^{206}Pb$	error (%)	$^{206}Pb/^{238}U$	error	$^{207}Pb/^{235}U$	error	$^{207}Pb/^{206}Pb$	error	% Disc	
033c	30µm	6.40247	0.58801	0.36053	0.54502	0.899	0.12880	0.22070	1985	9	2033	5	2082	4	4.66	0.33
034r	30µm	6.72651	0.70342	0.37932	0.50754	0.634	0.12861	0.48705	2073	9	2076	6	2079	9	0.29	0.14
038r	30µm	6.37286	0.65407	0.35915	0.58922	0.871	0.12869	0.28394	1978	10	2029	6	2080	5	4.91	0.19
039c	30µm	5.96608	0.58765	0.33499	0.50098	0.788	0.12917	0.30718	1863	8	1971	5	2087	5	10.74	0.39
040r	30µm	6.47721	0.90059	0.36341	0.50250	0.465	0.12927	0.74736	1998	9	2043	8	2088	13	4.30	0.23
041c	30µm	6.37226	0.76307	0.35970	0.69181	0.943	0.12848	0.32199	1981	12	2028	7	2077	6	4.65	0.21
044c	30µm	6.00304	0.67046	0.33806	0.58748	0.840	0.12879	0.32308	1877	10	1976	6	2081	6	9.81	0.29
045r	30µm	6.37855	0.93038	0.35824	0.80078	0.842	0.12913	0.47367	1974	14	2029	8	2086	8	5.39	0.30
046c	30µm	6.37228	0.81867	0.35575	0.70444	0.835	0.12991	0.41711	1962	12	2028	7	2097	7	6.43	0.28
047r	30µm	6.31601	0.96545	0.35742	0.71699	0.853	0.12816	0.64654	1970	12	2021	8	2073	11	4.97	0.17
050	30µm	6.43699	0.78850	0.36435	0.69162	0.853	0.12813	0.37867	2003	12	2037	7	2073	7	3.36	0.17
051	30µm	5.99003	1.06674	0.34095	0.94853	0.879	0.12742	0.48809	1891	16	1974	9	2063	9	8.31	0.21
053	30µm	6.23626	1.47544	0.35067	0.83995	0.771	0.12898	1.21301	1938	14	2010	13	2084	21	7.02	0.35
056	30µm	5.96952	0.80818	0.33712	0.63898	0.748	0.12842	0.49483	1873	10	1971	7	2077	9	9.81	0.30
057	30µm	6.04422	0.71601	0.34418	0.64825	0.883	0.12736	0.30405	1907	11	1982	6	2062	5	7.52	0.24
058	30µm	6.68612	0.72201	0.37677	0.65812	0.891	0.12870	0.29694	2061	12	2071	6	2080	5	0.92	0.32
059	30µm	6.75688	0.93095	0.38160	0.76990	0.907	0.12842	0.52337	2084	14	2080	8	2076	9	-0.35	0.35
TG-325A			1σ		1σ			1σ		1σ		1σ		1σ		
003	30µm	6.48329	0.91487	0.36210	0.83868	0.906	0.12986	0.36552	1992	14	2044	8	2096	6	4.96	0.28
004	30µm	6.49789	0.70378	0.36348	0.62606	0.862	0.12965	0.32149	1999	11	2046	6	2093	6	4.52	0.24
006	30µm	6.74915	0.89977	0.37689	0.53468	0.738	0.12988	0.72367	2062	9	2079	8	2096	13	1.65	0.33
007	30µm	6.14629	1.42472	0.34428	1.35946	0.952	0.12948	0.42625	1907	22	1997	12	2091	7	8.79	0.32
008	30µm	5.81583	1.19767	0.33215	1.08030	0.895	0.12699	0.51708	1849	17	1949	10	2057	9	10.11	0.30
009c	30µm	6.83816	0.78264	0.38075	0.62443	0.754	0.13026	0.47181	2080	11	2091	7	2101	8	1.03	0.29
010r	30µm	6.47286	0.95074	0.36229	0.59333	0.757	0.12958	0.74288	1993	10	2042	8	2092	13	4.74	0.22
013	30µm	6.70467	0.81375	0.37339	0.66412	0.781	0.13023	0.47025	2045	12	2073	7	2101	8	2.65	0.29
014	30µm	6.66125	1.05262	0.37471	0.82965	0.765	0.12893	0.64784	2052	15	2067	9	2083	11	1.53	0.32
015	30µm	6.63678	0.72878	0.37104	0.56580	0.717	0.12973	0.45933	2034	10	2064	6	2094	8	2.87	0.33
016c	30µm	5.83730	1.24354	0.33190	0.72704	0.774	0.12756	1.00885	1848	12	1952	11	2065	18	10.51	0.26
018c	30µm	6.63369	0.71035	0.37013	0.57197	0.752	0.12999	0.42124	2030	10	2064	6	2098	7	3.23	0.36
019r	30µm	6.33931	0.68899	0.35766	0.59229	0.821	0.12855	0.35200	1971	10	2024	6	2078	6	5.15	0.24
020c	30µm	6.28356	1.04285	0.35690	0.62602	0.762	0.12769	0.83405	1967	11	2016	9	2066	15	4.79	0.29
024	30µm	6.70827	0.68753	0.37537	0.55689	0.753	0.12961	0.40320	2055	10	2074	6	2093	7	1.82	0.30
026	30µm	6.59313	1.25609	0.37349	0.71913	0.769	0.12803	1.02986	2046	13	2058	11	2071	18	1.22	0.33
029	30µm	6.83651	1.00594	0.38757	0.79535	0.765	0.12793	0.61589	2112	14	2090	9	2070	11	-2.02	0.30
030	30µm	6.80990	1.44099	0.37845	1.16769	0.926	0.13051	0.84437	2069	21	2087	13	2105	15	1.70	0.34
033	30µm	5.88063	1.11952	0.33143	0.96060	0.845	0.12868	0.57494	1845	15	1958	10	2080	10	11.29	0.30
034	30µm	6.60839	0.91442	0.36813	0.80809	0.868	0.13019	0.42796	2021	14	2060	8	2101	8	3.81	0.29
036	30µm	6.64181	1.53690	0.37282	0.76485	0.713	0.12921	1.33306	2043	13	2065	14	2087	23	2.14	0.26
039c	30µm	6.54199	1.03706	0.36693	0.78614	0.730	0.12931	0.67637	2015	14	2052	9	2089	12	3.52	0.34
040r	30µm	6.49744	1.32287	0.36533	0.75185	0.760	0.12899	1.08844	2007	13	2046	12	2084	19	3.69	0.25
043	30µm	6.35092	0.87537	0.35655	0.71542	0.788	0.12919	0.50444	1966	12	2026	8	2087	9	5.80	0.32
045c	30µm	6.22638	1.15642	0.35204	0.97900	0.834	0.12827	0.61553	1944	16	2008	10	2074	11	6.27	0.30
047	30µm	6.22000	1.23894	0.35070	1.06143	0.846	0.12863	0.63902	1938	18	2007	11	2079	11	6.80	0.26
049c	30µm	6.67240	0.90489	0.37321	0.72023	0.765	0.12966	0.54780	2045	13	2069	8	2093	10	2.34	0.29

All Pb ratios corrected for common Pb. * is inheritance. % Disc is discordance. C = core and R = rim.

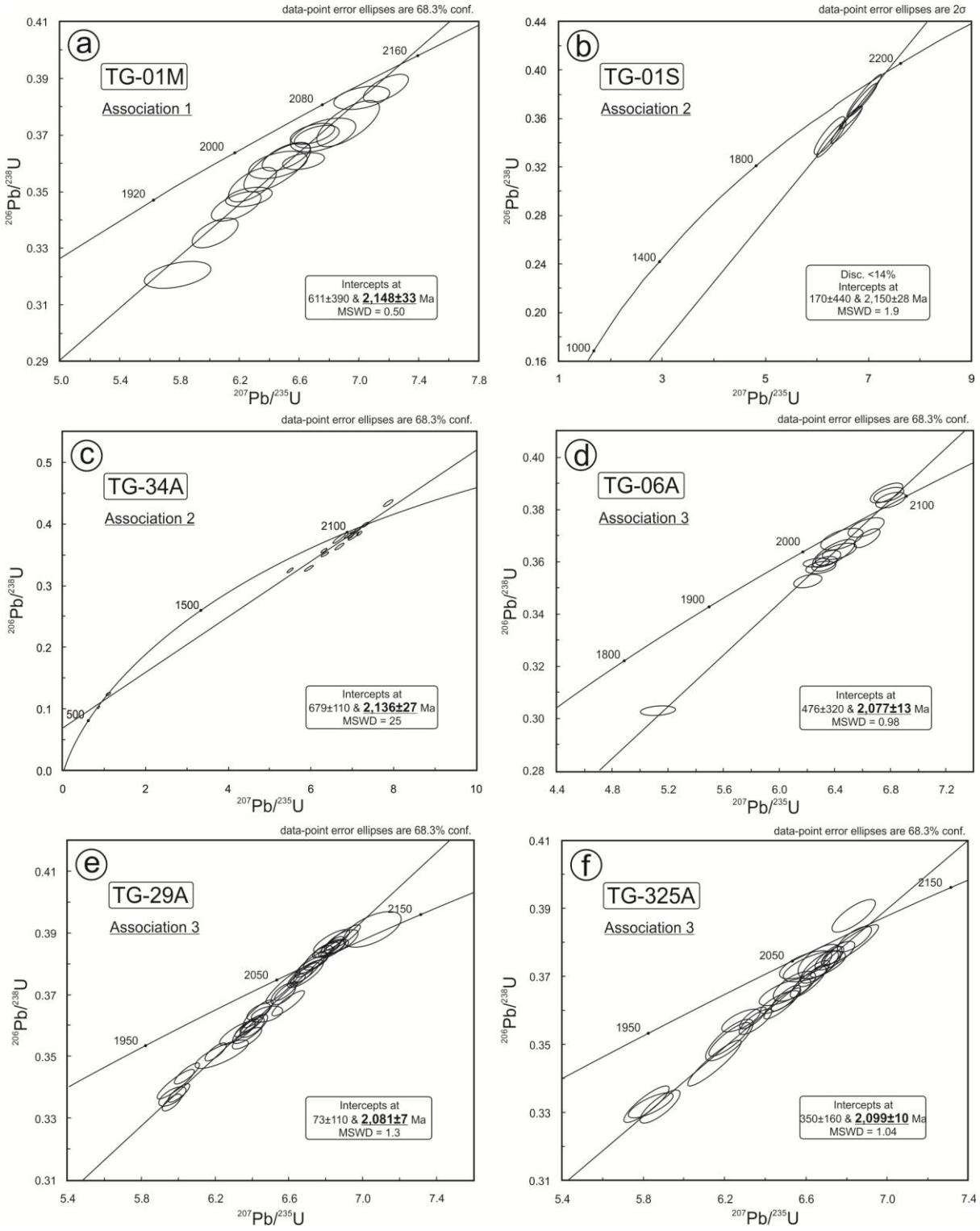

Figure 7 – Concordia diagrams for zircons of the Arroio dos Ratos Complex. (a) Sample TG-01M – metatonalite from Association 1. (b) Sample TG-01S – tonalite from Association 2. (c) Sample TG-34A – tonalite from Association 2. (d) Sample TG-06A – metagranodiorite from Association 3. (e) Sample TG-29A – metagranodiorite from Association 3. (f) Sample TG-325A – metatonalite from Association 3. All upper intercepts are igneous age. Only in sample TG-34A (7c) the lower intercept corresponds to a metamorphic age value.

5. Discussion and Conclusions

The ages determined from all three lithological associations within the Arroio dos Ratos Complex are interpreted to be igneous on the basis of crystal morphology, core-border textural relations and Th/U rations grater than 0.1.

The present results lead to the interpretation of the Arroio dos Ratos Complex magmatism as Paleoproterozoic. The oldest age values are found in A1 (2,148 ± 33 Ma) and A2 (2,150 ± 28 Ma and 2,136 ± 27 Ma) tonalites. The tonalites and granodiorites from A3 are younger (2,099 ± 10 Ma, 2,081 ± 7 Ma and 2,077 ± 13), but their similarity in composition leads to their interpretation as a more evolved part of the same magmatic arc, which is in accordance with the wide range of duration currently accepted for other subduction systems, like the Andes (Wilson, 1989).

The intimate spatial association of different lithological types found in the ARC, as paragneisses, orthogneisses and metamorphosed plutonic rocks of varied composition leads to speculation over their significance, as they may represent successive magmatic-deformational pulses within this ancient arc (meso to late-Rhyacian) that were juxtaposed by later deformation events. The strong imprint of a moderately-dipping, dextral shear zone, especially in A3 rocks, must result from an important deformational event under temperatures high enough to cause partial-melting, as described in these rocks. However, the age of such an event is still unknown, and will possibly be revealed in future studies, by determining the age of these syntectonic neosomes.

The record of Neoproterozoic magmatic arc environments in the Sul-rio-grandense Shield is found in its western portion (Fig. 1) where juvenile accretion is described in the Vila Nova Belt from 750 to 680 Ma (Babinski *et al.*, 1996; Garavaglia *et al.*, 2006; Hartmann *et al.*, 2011). Neoproterozoic arc magmatism is found in the central portion of the SrgS as well, where Martil *et al.* (submitted to publication) describe high-grade orthogneisses (former volcanic rocks) with 790 Ma igneous age (U-Pb zircon) interleaved with paragneisses in the Varzea do Capivarita Complex. However, the presence of Neoproterozoic magmatic arc environments in the eastern portion of the SrgS has long been subject of debate. While Fernandes *et al.* (1992, 1995) interpret the Neoproterozoic magmatism in this granitic belt as the roots of an Andean-type magmatic arc, Bitencourt and Nardi (1993) propose that the arc assemblages should be sought in the orthogneisses that form the basement of the Southern Brazilian Shear Belt.

The results from this study do not point to the existence of a Neoproterozoic magmatic arc in this region. They do indicate the presence of a Paleoproterozoic continental arc magmatism which covered a minimum time interval of *ca*. 70 Ma (2,150 to 2,077), considering the central age values obtained. Therefore, the studied magmatic associations are considered to represent the basement for the Neoproterozoic post-collisional granitic magmatism focused by the SBSB, in agreement with the proposition made by Bitencourt and Nardi (1993).

The intrusive relationships observed in the field indicate the relative ages of the A1 and A2 associations, but the large overlapping uncertainties in the individual ages calculated for the samples do not allow for any precise age difference to be calculated. In spite of the features indicative of different deformation intensity recorded in the rocks of these two associations, the diffuse contacts observed in xenoliths suggest that the host rocks (A1) were still warm when the intrusion of A2 magmas occurred. The complex interleaving of magmas in time and space, with local strain field variation, has been demonstrated by several authors (*e.g.* Annen, 2011; Saint-Blanquat *et al.*, 2011; Menand *et al.*, 2011; Miller *et al.*, 2011; Vernon *et al.*, 2012, Florisbal *et al.*, 2012) as the record of multi-scale events responsible for the construction of plutons and batholiths in magmatic arcs or transpressive settings.

The relations between the ARC rocks and the Neoproterozoic syntectonic granitoids conditioned by the Southern Brazilian Shear Belt may be summarized as follows:

(i) More than megaxenoliths and septa, the Paleoproterozoic ARC rocks represent roof pendants, or *in situ* wall rocks, for the Neoproterozoic syntectonic granites (NSG);

(ii) In high strain zones of the Quitéria-Serra do Erval Shear Zone, where the NSG are frequently emplaced (Fig. 2), the original structure of the ARC rocks is extremely transposed, but this is mitigated when going towards less-deformed areas of the complex, where its cratonic nature is preserved; in low-strain zones, the Neoproterozoic imprint is recognized as discrete, sinistral, brittle-ductile shear bands developed over the dextral shearing structures of the ARC;

(iii) The age of the dextral shearing and partial melting observed in the ARC rocks is yet undetermined; it may be either late Paleoproterozoic or it could be correlated to the Neoproterozoic dextral shearing present in neighbouring areas, such as reported by Martil *et al.* (submitted).

Acknowledgments

We are grateful to prof. Márcio Martins Pimentel for his help with obtaining part of the isotope data. We also acknowledge two JSAES anonymous reviewers for their help in improving the manuscript. This work had partial financial support from the National Research Council (CNPq) to M.F. Bitencourt (Universal Project n. 471266/2010-8) and from the Rio Grande do Sul State Research Foundation (FAPERGS) to L. Nardi (Proc. n. 10.16039), as well as a PhD research grant from CNPq to T.R. Gregory.

References

Albarède, F. & Beard, B. 2004. Analytical methods for non-traditional isotopes. *Reviews in mineralogy and geochemistry*, *55*(1): 113-152.

Almeida, F.F.M., Hasui, Y., Brito Neves, B.B. & Fuck, R.A. 1981. Brazilian structural provinces: an introduction. *Earth-Science Reviews*,*17*(1): 1-29.

Annen, C. 2011. Implications of incremental emplacement of magma bodies for magma differentiation, thermal aureole dimensions and plutonism-volcanism relationships. *Tectonophysics*, 500: 3-10.

Babinski, M., Chemale Jr., F., Hartmann, L.A., Van Schmus, W.R. & Silva, L.C. 1996. Juvenile accretion at 750-700 Ma in southern Brazil. *Geology*, 24(5):439-442.

Barker, E. 1979. *Trondhjemites, dacites, and related rocks*. New York, Elsevier, 659p.

Bitencourt, M.F., De Toni, G.B., Florisbal, L.M., Martil, M.M.D., Niessing, M., Gregory, T.R., Nardi, L.V.S., Heaman, L.M., Dufrane, S.A. 2011. Structural geology and U-Pb age of unusual Neoproterozoic syn-collisional syenite-tonalite association from southernmost Brazil. *In:* Seventh Hutton Symposium on Granites and Related Rocks, 2011, Avila. *Abstracts Book*. Avila: Universidad de Salamanca, v.u.p. 21-21.

Bitencourt, M.F. & Nardi, L.V.S. 1993. Late- to Post-collisional Brasiliano Magmatism in Southernmost Brazil. *Anais da Academia Brasileria de Ciências*, 65: 3-16.

Bitencourt, M.F. & Nardi, L.V.S. 2000. Tectonic setting and sources of magmatism related to the southern Brazilian shear belt. *Revista Brasileira de Geociências*, 30(1): 186-189.

Camozzato, E., Philipp, R.P. & Chemale Jr., F. 2013. Idades Estaterianas e Calimianas no Domo da Vigia: Complexo Vigia e Porongos, Metagranito Seival e Anfibolito Tupi Silveira, Bagé, RS. *In*: XI Simpósio Nacional de Estudos Tectônicos. *Anais...*(CD). Ouro Preto, MG.

Centeno, A., Nardi, L.V.S., Bitencourt, M.F., 2012. Os granitóides sintectônicos pós-colisionais Sanga do Areal, intrusivos no Complexo Arroio dos Ratos, na região de Quitéria, RS. Dissertação de mestrado. Porto Alegre: IGEO/UFRGS. [66 f.] il.

Chemale Jr., F., Kawashita,K., Dossin, I.A., Ávila, J.N., Justino, D., Bertotti, A.L. 2012. U-Pb zircon in situ dating with LA-MC-ICP-MS using a mixed detector configuration. *Anais da Academia Brasileira de Ciências*, 84(2): 275-295.

Chemale Jr., F., Philipp, R.P., Dussin, I.A., Formoso, M.L.L., Kawashita, K., Bertotti, A.L. 2011. Lu-Hf and U-Pb age determinations of Capivarita Anorthosite in the Dom Feliciano Belt, Brazil. *Precambrian Research*, 186: 117-126.

Condie, K.C. 2005. TTGs and adakites: are they both slab melts? *Lithos*, 80: 33-44.

Defant, M.J. & Drummond, M.S. 1990. Derivation of some modern arc magmas by melting of Young subducted lithosphere. *Nature*, 347:662-665.

Fernandes, L.A.D. & Koester, E. 1999. The Neoproterozoic Dorsal de Canguçú strike-slip shear zone: its nature and role in the tectonic evolution of southern Brazil. *Journal of African Earth Sciences*,1: 3-24.

Fernandes, L.A.D., Menegat, R., Costa, A.F.U., Koester, E., Porcher, C.C., Tommasi, A., Kraemer, G., Ramgrab, G.E. & Camozzato, E. 1995. Evolução tectônica do Cinturão Dom Feliciano no Escudo Sul-rio-grandense: Parte 1 – Uma contribuição a partir do registro geológico. *Revista Brasileira de Geociências*, 25(4): 351-374.

Fernandes, L.A.D., Tommasi, A. & Porcher, C.C. 1992. Deformation patterns in the southern Brazilian branch of the Dom Feliciano Belt: A reappraisal. *Journal of South American Earth Sciences*, 5(1): 77-96.

Fernandes, L.A.D., Tommasi, A., Porcher, C.C., Vieira Jr., N., Marques-Toigo, M., Guerra-Sommer, M., Piccoli, A.E. 1988. *Mapa geológico de parte das folhas de Quitéria (SH 22-Y-B-I-4) e Várzea do Capivarita (SH 22-Y-B-I-3), RS*. Porto Alegre, UFRGS, Série Mapas, 1 v., 1 mapa preto e branco, escala 1:50.000.

Florisbal, L.M.F., Janasi, V.A., Bitencourt, M.F., Heaman, L.M. 2012. Space-time relation of post-collisional granitic magmatism in Santa Catarina, southern Brazil: U-Pb LA-MC-ICP-MS zircon geochronology of coeval mafic-felsic magmatism related to the Major Gercino Shear Zone. *Precambrian Research*, 216-219: 132-151.

Fontana, E., Nardi, L.V.S., Bitencourt, M.F., Knijnik, D.B. 2012. Caracterização geoquímica e petrogenética dos Granitoides Arroio Divisa, região de Quitéria, Rio Grande do Sul. *GeologiaUSP*, 12(3): 33-56.

Frantz J.C., McNaughton N.J., Marques J.C., Hartmann L.A., Botelho, N.F., Caravaca, G. 2003. SHRIMP U-Pb zircon ages of granitoids from southernmost Brazil: constraints on the temporal evolution of the Dorsal de Canguçu Transcurrent Shear zone and the eastern Dom Feliciano Belt. *In:*IV South American symposium of isotope geology. *Short papers…*(p. 174–177). Salvador, Brazil.

Garavaglia, L., Bitencourt, M.F. & Nardi, L.V.S. 2002. Cumulatic Diorites Related to Post-collisional, Brasiliano/Pan-African Mafic Magmatism in the Vila Nova Belt, Southern Brazil. *Gondwana Research*, 5:519-534.

Garavaglia, L., Koester, E., Bitencourt, M.F. & Nardi, L.V.S. 2006. Isotopic Signature of Late magmatic Arc to Post-collisonal Magmatism in the Vila Nova Belt, Southern Brazil. *In*: South-American Symposium on Isotope Geology, 5, 2006, Punta del Este. *Short Papers...*(p. 101-104).Punta del Este, Universidad de la Republica.

Gregory, T.R., Bitencourt, M.F. & Nardi, L.V.S. 2011. Caracterização estrutural e petrológica de metatonalitos e metadioritos do Complexo Arroio dos Ratos na sua seção-tipo, região de Quitéria, RS. *Pesquisas em Geociências*, 38(1): 85-108.

Hartmann, L.A., Leite, J.A.D., Silva, L.C., Remus, M.V.D., McNaughton, N.J., Groves, D.I., Fletcher, I.R., Santos, J.O.S. & Vasconcellos, M.A.Z. 2000. Advances in SHRIMP geochronology and their impact on understanding the tectonic and metallogenic evolution of southern Brazil. *Australian Journal of Earth Sciences*, 47:829-844.

Hartmann, L.A., Philipp, R.P., Santos, J.O.S. & McNaughton, N.J. 2011. Time frame of 753-680 Ma juvenile accretion during the São Gabriel orogeny, southern Brazilian Shield. *Gondwana Research*, 19: 84-99.

Jackson, S.E., Pearsona, N.J., Griffina, W.L.& Belousova, E.A. 2004. The application of laser ablation-inductively coupled plasma-mass spectrometry to in situ U–Pb zircon geochronology. *Chemical Geology*, 211: 47-69.

Jaffey, A.H., Flynn, K.F., Glendenin, L.E., Bentley, W.C. & Essling, A.M. 1971. Precision measurements of half-lives and specific activities of ^{235}U and ^{238}U. *Physics Review*, C4: 1889–1906.

Jahn, B.M., Glikson, A.Y., Peucat, J.J. & Hickman, A.H. 1981. REE geochemistry and isotopic data of Archean silicic volcanics and granitoids from the Pilbara Block, Western Australia: implications for the early crustal evolution. *Geochimica et Cosmochimica Acta*, 45: 1633-1652.

Knijnik, D.B., Bitencourt, M.F., Gregory, T.R. 2013. A Zona de Cisalhamento Quitéria-Serra do Erval e o magmatismo sintectônico precoce do Cinturão de Cisalhamento Sul-brasileiro. *In*: XI Simpósio Nacional de Estudos Tectônicos. *Anais...*(CD) Ouro Preto, MG.

Knijnik, D.B., Bitencourt, M.F., Nardi, L.V.S., Pinto, V.M., Fontana, E. 2012. Caracterização Geoquímica do Granodiorito Cruzeiro do Sul: magmatismo shoshonítico pós-colisional neoproterozoico em zona de transcorrência, região de Quitéria, RS. *Geologia USP*, 12(1): 17-38.

Koester, E., Chemale Jr., F., Porcher, C.C., Bertotti, A.L. & Fernandes, L.A.D. 2008. U-Pb ages of granitoids from Eastern Sul-riograndense Shield. *In*: VI South American Symposium on Isotope Geology. *Anais…*(p. 95). San Carlos de Bariloche, Argentina.

Kosler J., Fonneland, H., Sylvester, P., Tubrett, M., Pedersen, R.B., 2002. U-Pb dating of detrital zircons for sediment provenance studies – a comparison of laser ablation ICPMS and SIMS techniques. *Chemical Geology*, 182: 605-618.

Leite, J.A.D., Hartmann, L.A., Fernandes, L.A.D., McNaughton, N.J., Soliani Jr, E., Koester, E., Santos, J.O.S. & Vasconcellos, M.A.Z. 2000. Zircon U-Pb SHRIMP dating of gneissic basement of the Dom Feliciano Belt, southernmost Brazil. *Journal of South American Earth Sciences*, 13: 739-750.

Ludwig, K.R. 1993. New isoplot version 2.2. Berkeley Geochronology Center, February.

Martil, M.M.D., Bitencourt, M.F. & Nardi, L.V.S. 2011. Caracterização estrutural e petrológica do magmatismo pré-colisional do Escudo Sul-rio-grandense: os ortognaisses do Complexo Metamórfico Várzea do Capivarita. *Pesquisas em Geociências*, 38(2): 181-201.

Martil, M.M.D., Bitencourt, M.F., Armstrong, R., Nardi, L.V.S., Chemale Jr., F. Geochronology of orthogneisses from the Várzea do Capivarita Complex thrust pile and implications for the timing of continental collision in southernmost Brazil. Precambrian Research (*submitted*).

Martin, H., Smithies, R.H., Rapp, R., Moyen, J.F. & Champion, D. 2005. An overview of adakite, tonalite-trondhjemite-granodiorite (TTG), and sanukitoid: relationships and some implications for crustal evolution. *Lithos*, 79:1-24.

McGregor, V.R. 1979. Archean gray gneisses and the origino f the continental crust: evidence the Godthab region, West Greenland. *In*: Barker, E. (Ed.). *Trondhjemites, dacites, and related rocks*. New York, Elsevier, p. 169-204.

Menand, T., Saint-Blanquat, M.& Annen, C. 2011. Emplacement of magma pulses and growth of magma bodies. *Tectonophysics*. 500: 1-2.

Miller, C.F., Furbish, D.J., Walker, B.A., Claiborne, L.L., Koteas, G.C., Bleick, H.A.& Miller, J.S. 2011. Growth of plutons by incremental emplacement of sheets in crystal-rich host: evidence from Miocene intrusions of the Colorado River region, Nevada, USA. *Tectonophysics*. 500: 65-77.

Nardi, L.V.S. & Bitencourt, M.F. 2007. Magmatismo granítico e evolução crustal no sul do Brasil. *In*: Iannuzzi, R. & Frantz, J.C. (Ed.). *50 Anos de Geologia. Instituto de Geociências. Contribuições.* Porto Alegre, Editora Comunicação e Identidade, CIGO e IG-UFRGS, p. 125-141.

Passchier, C.W. & Trouw, R.A. 2005. *Microtectonics*. Berlin, Springer, 366p, 2ed.

Rapp, R.P., Watson, E.B. & Miller, C.F. 1991. Partial melting of amphibolites/eclogite and the origin of Archean trondhjemites and tonalites. *Precambrian Research*, 51: 1-25.

Rubatto, D. 2002. Zircon trace element geochemistry: partitioning with garnet and the link between U–Pb ages and metamorphism. *Chemical Geology*, 184(1): 123-138.

Saint-Blanquat, M., Horsman, E., Habert, G., Morgan, S., Vanderhaeghe, O., Law, R.& Tikoff, B. 2011. Multiscale magmatic cyclicity, duration of pluton construction, and the paradoxical relationship between tectonism and plutonism in continental arcs. *Tectonophysics*. 500: 20-33.

Saalmann, K., Gerdes, A., Lahaye, Y., Hartmann, L.A., Remus, M.V.D. & Läufer, A. 2011. Multiple accretion at the eastern margin of the Rio de la Plata craton: the prolonged Brasiliano orogeny in southernmost Brazil. *International Journal of Earth Sciences*, 100 (2-3): 355-378.

Silva, L.C., Hartmann, L.A., McNaughton, N.J. & Fletcher, I.R. 1999. SHRIMP U/Pb Zircon Dating of Neoproterozoic Granitic Magmatism and Collision in the Pelotas Batholith, Southernmost Brazil. *International Geology Review*, 41: 531-551.

Simonetti, A., Heaman, L.M., Hartlaub, R.P., Creaser, R.A., MacHattie, T.G.& Böhm, C. 2005. U-Pb zircon dating by laser ablation-MC-ICP-MS using a new multiple ion counting Faraday collector array. *Journal of Analytical Atomic Spectrometry*, 20: 677-686.

Sommer, C.A., Philipp, R.P., Lima, E.F., Basei, M.S., Oliveira, D.S. & Filho, J.N. 2013. Geoquímica e geocronologia das rochas riolíticas associadas ao Batólito Pelotas, porção oriental do Escudo Sul-rio-grandense: dados preliminares. *In:* XIV Congresso Brasileiro de Geoquímica. *Anais…*(CD). Diamantina-MG.

Springer, W. & Seck, H.A. 1997. Partial fusion of basic granulites at 5 to 15 kbar: implications for the origin of TTG magmas. *Contributions to Mineralogy and Petrology*, 127: 30-45.

Vernon, R.H., Collins, W.J.& Cook, N.D.J. 2012. Metamorphism and deformation of mafic and felsic rocks in a magma transfer zone, Stewart Island, New Zealand. *Journal of Metamorphic Geology*, 30(5): 473-488.

Wilson, M. 1989. *Igneous Petrogenesis*. Londres, Chapman & Hall, 466p.

3.2 Artigo 2 submetido à revista Lithos

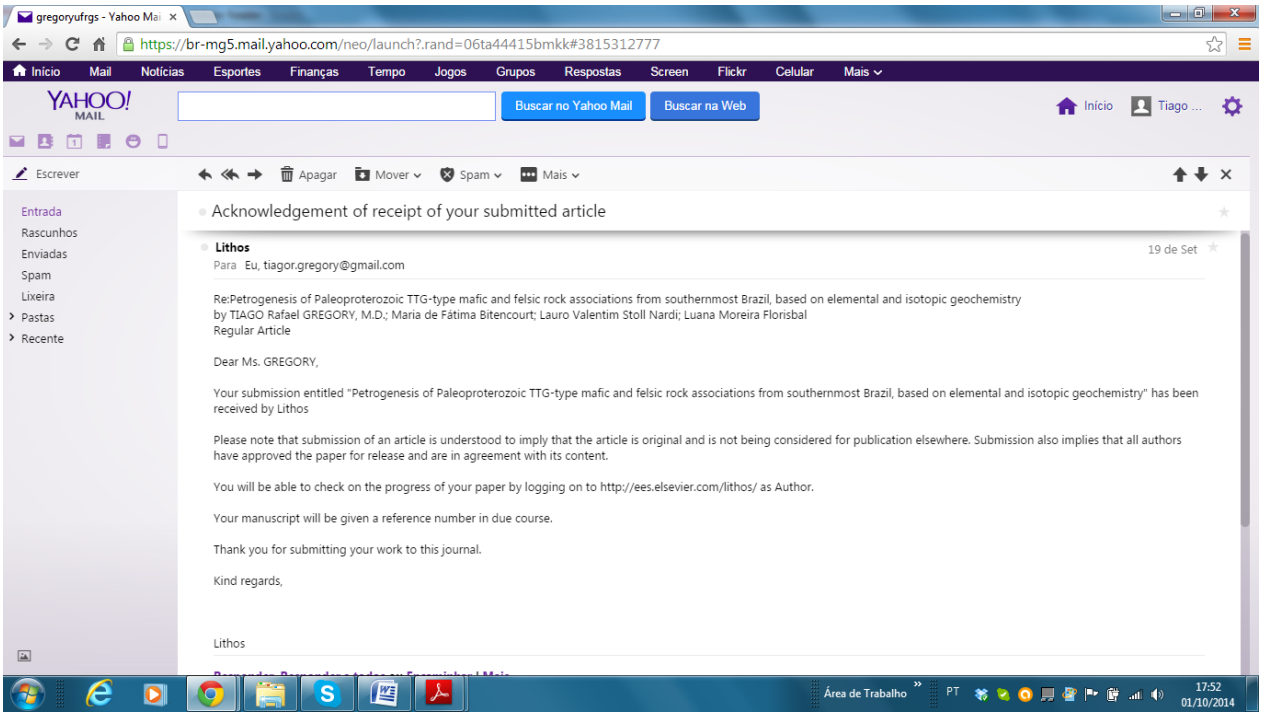

Petrogenesis of Paleoproterozoic TTG-type mafic and felsic rock associations from southernmost Brazil, based on elemental and isotopic geochemistry

Tiago Rafael Gregory[a,*], Maria de Fátima Bitencourt[a], Lauro Valentim Stoll Nardi[a] & Luana Moreira Florisbal[b]

[a] Instituto de Geociências, Universidade Federal do Rio Grande do Sul, Porto Alegre RS 91501-970, Brazil

[b] Instituto de Geociências, Universidade de São Paulo, São Paulo SP 05508-080, Brazil

* Corresponding author. Tel.: +15 51 9725 1566

E-mail address: gregoryufrgs@yahoo.com.br (T.R. Gregory)

Keywords

TTG-type associations; Continental arc magmatism; Sr-Nd-Pb isotopes; Paleoproterozoic magmatism in southern Brazil.

Highlights

In southernmost Brazil, Paleoproterozoic TTG-type rock associations are described together with coeval mafic/basic magmas as part of the Arroio dos Ratos Complex.

Sr-Nd-Pb isotopic data indicate juvenile provenance for two of the three studied associations.

Although the TTG signature is suggestive of melting of the subducted plate, the present data suggest extraction from E-MORB type enriched mantle for the genesis of the studied rocks.

Abstract

In southern Brazil, three associations of tonalites and granodiorites that are geochemically similar to tonalite-trondhjemite-granodiorite (TTG) or adakitic associations have been identified as originating from the Arroio dos Ratos Complex (ARC) Paleoproterozoic magmatism. The metatonalites of Association 1 (A1; 2,148 ± 33 Ma) have a fabric that is compatible with strong solid-state deformation. The tonalites and granodiorites of Association 2 (A2; 2,150 ± 28 Ma) are intrusive in A1 and have a similar composition, but are less deformed and their primary structures are partly preserved. Both associations display contemporary relations with basic to intermediate magmas. Association 3 (A3; 2,077 ± 13 Ma) is represented by tonalitic to granodioritic gneisses, without any associated basic to intermediate magmatism, and its main characteristic is the banding that resulted from strong solid-state deformation. Partial melting features are locally present in A3. The geochemical compositions of the three associations are similar and indicate sources related to a continental magmatic arc environment. The $^{87}Sr/^{86}Sr_{(i)}$ ratios (between 0.701 and 0.703), positive $\varepsilon Nd_{(t)}$ values (+1.45 to +5.19), and T_{DM} ages close to the crystallization ages indicate juvenile sources for the A1 and A2 associations. The A3 rocks have an $^{87}Sr/^{86}Sr_{(i)}$ ratio of 0.715, an $\varepsilon Nd_{(t)}$ value of

+0.47 and a T_{DM} age that is close to the crystallization age, indicating a source composition similar to that of the other associations, though richer in Rb, but its origin remains under discussion. The Pb isotopic ratios of A1 and A2 are similar and compatible with the evolution of the mantle and orogen ($^{208}Pb/^{204}Pb$ = 37.3-37.6; $^{207}Pb/^{204}Pb$ = 15.62-15.65; $^{206}Pb/^{204}Pb$ = 18.0-18.2). The Pb isotopic ratios of A3 differ from A1 and A2, indicating a source that was poorer in Th ($^{208}Pb/^{204}Pb$ = 37.1; $^{207}Pb/^{204}Pb$ = 15.64; $^{206}Pb/^{204}Pb$ = 18.5). The geochemistry of associations A1 and A2 suggest a juvenile source with contamination by crustal material. However, the Sr-Nd-Pb isotopic signature of this crustal material is similar to the source material that originates these associations and that may be the crust generated in the magmatic arc, which is compatible with the geochronological results. The dataset points to the occurrence of self-cannibalism processes in the generation of the ARC rocks. Although subduction plate melting processes are commonly accepted mechanisms for the generation of TTG or adakitic associations, the major and trace element geochemical data and the isotopic data obtained in this study suggest that melting of metasomatized mantle (E-MORB type) as the source for the generation of the ARC rocks. In this case, the generation of rock associations with typical adakitic characteristics *(i.e.*, the depletion of heavy rare earth elements) may have arisen from the melting of a garnet-lherzolite-type mantle, which is also indicated by the contemporary relationships with basic to intermediate magmas. The three associations display microstructures that indicate two episodes of recrystallization, one of a higher temperature and one of a lower temperature. The age of the high-temperature structure remains under discussion and may be attributed to a Paleoproterozoic metamorphic event. The low-temperature structure is compatible with the temperature conditions observed in adjacent areas, in the host rocks of the Neoproterozoic post-collisional granitoids that have been emplaced along the Southern Brazilian Shear Belt (SBSB). Zircon crystals with a Paleoproterozoic igneous core exhibit a metamorphic overgrowth at 635 ± 6 Ma, compatible with the crystallization ages of the SBSB granitoids.

1. Introduction

Associations of the tonalite-trondhjemite-granodiorite (TTG) type are important constituents of magmatic arcs, demonstrating the importance of subduction zones for crustal growth and plate tectonics as the driving force of petrogenetic processes.

The debate concerning the genesis of plutonic (called TTG) or volcanic (called adakite) associations and their crustal evolutions follows the discussion of the petrogenetic processes acting in subduction zones, with special reference to melting taking place in the basaltic portion of a subducted plate or in the lithospheric mantle of the overlying plate (Barker, 1979; Jahn *et al.*, 1981; Defant & Drummond, 1990; Rapp *et al.*, 1991; Martin, 1993; Springer & Seck, 1997; Martin, 1999; Moyen *et al.*, 2001; Condie, 2005; Martin *et al.*, 2005; Moyen & Martin, 2012). The results from experimental petrology (Rapp *et al.*, 1991; Springer & Seck, 1997), the lack of associated basaltic rocks (Defant & Drummond, 1990; Jahn *et al.*, 1981), and the occurrence of adakitic veins and inclusions in peridotites (Sorensen & Grossman, 1989; Schiano *et al.*, 1995) have led several authors to interpret these associations as originating from melting of the basaltic portion of the subducted oceanic plate, which would leave a garnet-rich residue that would account for the depletion in heavy rare earth elements (REEs) typical of these associations. However, Castillo (2012) has noted that the great importance given to differences in a few geochemical parameters (La/Yb and Sr/Yb) to the detriment of the great similarity in numerous other parameters, such as the so-called classic calc-alkaline arc magmatism (melting of mantle wedge; Martin, 1999), renders the use of the terms TTG and adakite extremely fragile because of their genetic connotations. Condie (2005) has also noted that different environments can generate such a signature and that geochemical data should not be used alone for reconstructions of ancient geotectonic environments. Alternatively, occurrences of glass inclusions in olivines and

adakitic veins in peridotites can be interpreted as the record of mantle metasomatism rather than the passage of melts through the mantle because experimental results demonstrate that a large melt/rock ratio (2:1) is required for a plate melt to not completely react with the peridotitic mantle (Rapp *et al.*, 1999). In addition, Ramos (2010) has demonstrated the role of tectonics in the generation of a greater or smaller volume of basaltic rocks during magmatic feeding in the crust under extensional or contractional regime, respectively.

Although the models of plate melting *versus* mantle melting for the genesis of TTG or adakitic associations are not yet well resolved, the integration of major and trace element geochemical data with isotopic data has been instrumental in furthering the discussion of the evolution of magmatic arc rocks (Peccerillo *et al.*, 2004; Machado *et al.*, 2005; Castillo *et al.*, 2009; Hidalgo *et al.*, 2012). Such data often point towards a secondary role, either as contaminant or metasomatizer agent, played by fluids or melts derived from the subducted plate or from the sediments it carries. Similarly, the integration of various knowledge fields has revealed the efficacy of a holistic approach for the investigation of ancient plutonic associations, especially when accompanied by tectonic deformation (D'Lemos, 1992; Bitencourt, 1996; Nardi & Bitencourt, 2007; Florisbal, 2012a, b), integrating structural geology, petrography, geochemistry, and isotopic and geochronological data. With this approach, arc magmatism can be understood as a phenomenon that results from multiple sources, at various stages, that complement each other.

This study aims to investigate the sources and evolutionary processes of the Paleoproterozoic magmatism from the Arroio dos Ratos Complex (ARC), a TTG-type association with a contemporary basic magmatism, located in southern Brazil. To this end, structural geology, petrography, major and trace-element geochemistry, and Sr-Nd-Pb isotope geochemistry data from the three associations identified in this complex are presented. The determination of the spatio-temporal relationships of magmatic sources was achieved by integrating these results with the U-Pb zircon geochronological data previously obtained for these associations (Gregory *et al.*, submitted for publication).

2. Geological setting

The study area is situated in the southern portion of the Mantiqueira Province (Almeida *et al.*, 1981), which corresponds to an extensive Neoproterozoic mobile belt. This mobile belt registers the collision between Kalahari and Rio de la Plata cratons that has eventually led to the amalgamation of West Gondwana supercontinent.

The eastern part of this Mantiqueira Province segment features a wide shear belt comprised of several, anastomosing shear zones, that extends from the state of Santa Catarina (south Brazil) to Uruguay (Fig. 1). In southern Brazil, this set of translithospheric structures is designated Southern Brazilian Shear Belt (SBSB) and its discontinuities are thought to have conditioned Neoproterozoic post-collisional magmatism (Bitencourt & Nardi, 1993; 2000; Florisbal *et al.*, 2012b) under transcurrent kinematics between 650 and 580 Ma.

To the west, a supracrustal metamorphic belt separates the SBSB from Neoproterozoic rock sequences attributed to mature continental magmatic arc environment (Garavaglia *et al.*, 2002; 2006) of 704 ± 13 Ma (U-Pb in zircon – Babinski *et al.*, 1996) that are partially hidden under Cambrian to Neoproterozoic volcanosedimentary cover sequences. Further to the west and southwest, Archaean and Paleoproterozoic associations are found within the remnants of the Rio de la Plata Craton, as pointed out by Hartmann *et al.* (2000) (Fig. 1). Paleoproterozoic, TTG-type associations are also referred by Saalmann *et al.* (2011) and Camozzato *et al.* (2013) as forming the basement of the supracrutal metamorphic rocks in the shield areas of Rio Grande do Sul (Fig. 1).

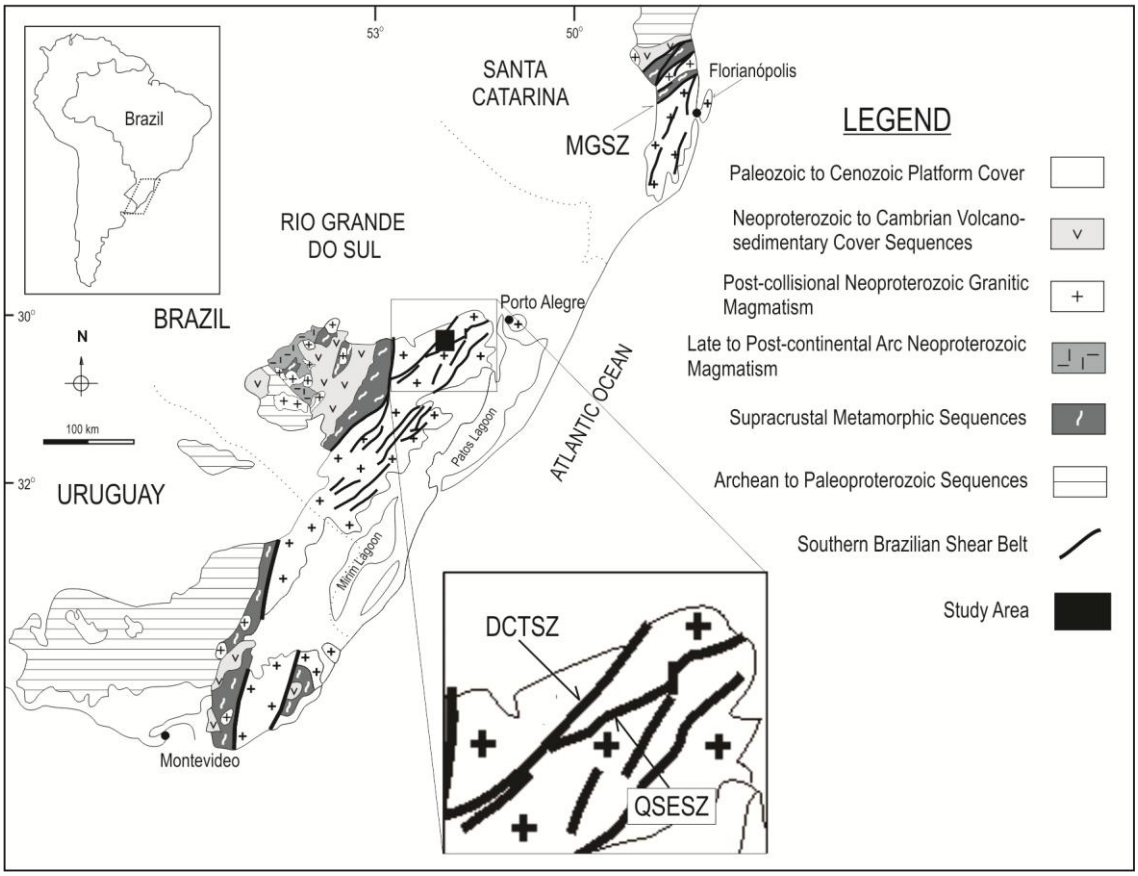

Figure 1 – Main geotectonic units from southern Brazil and Uruguay, with location of the study area (modified from Nardi & Bitencourt, 2007). MGSZ – Major Gercino Shear Zone; DCTSZ – Dorsal de Canguçu Transcurrent Shear Zone; QSESZ – Quitéria-Serra do Erval Shear Zone.

In the study area and neighbouring regions, the country rock for the SBSB granitoids are represented by the Várzea do Capivarita Complex (as defined by Martil *et al.*, 2011), comprised of a multi-scale interleaving of ortho- and paragneisses metamorphosed at *ca.* 650 Ma, where the igneous protoliths represent a mature magmatic arc association of ca. 790 Ma (Martil *et al.*, submitted), and *ca.* 640 Ma syntectonic syenite magmatism (Bitencourt *et al.*, 2011). This unit is interpreted as a thrust pile by Martil *et al.* (submitted for publication) and signals the main collisional episode at 650 Ma in southern Brazil.

The rocks presently studied correspond to a different type of pre-SBSB association, represented by the Arroio dos Ratos Complex (ARC). This is a Paleoproterozoic (2,077 ± 13 Ga to 2,150 ± 28 Ma, Gregory *et al.*, submitted for publication) TTG-type association with coeval mafic magmatism, as defined by Gregory *et al.* (2011), bearing a continental magmatic arc geochemical signature. These rocks are recognized as preserved segments, partly reworked by ductile shear zones of the SBSB, whose original relations are preserved in low-strain zones.

In the study area (Fig. 2), the ARC is limited by two shear zones (Fig. 2 and inset of Fig. 1) along which Neoproterozoic post-collisional granites are positioned. The Dorsal de Canguçu (Fernandes & Koester, 1999) and Quitéria-Serra do Erval shear zones (Knijnik *et al.*, 2013) have their minimum interval of activity (658 to 605 Ma) limited by the magmatic age of their syntectonic granites, as determined by Frantz *et al.* (2003), Koester *et al.* (2008), and Knijnik *et al.* (2012). Later reactivation of these shear zones, possibly under lower-temperature and shallower conditions, are

marked by quartz-mylonites and phyllonites in discontinuous ridges (Fig. 2) currently under investigation, whose movement ages are not yet determined precisely.

To the southeast of these structures (Fig. 2) several undeformed plutonic, hypabyssal and volcanic rock sequences signal the late magmatic phases of post-collisional setting with a large volume of extensional, alkaline magmatism at ca. 580 Ma, as pointed out by Sommer *et al.* (2013).

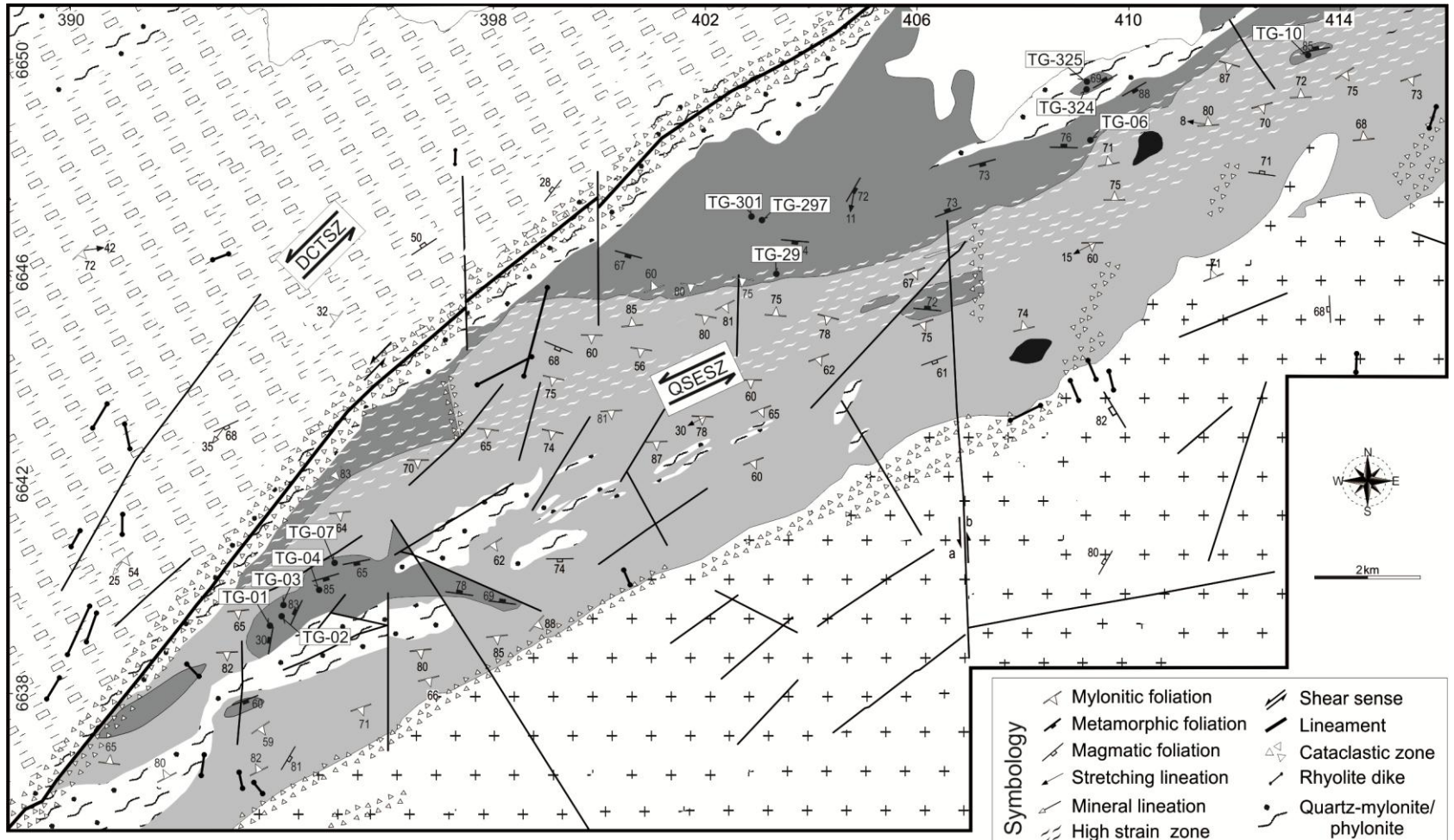

LEGEND

- Paleozoic Sedimentary Cover
- Quitéria-Serra do Erval Syntranscurrent Granitoids ~630 Ma
- High-grade Parametamorphic Rocks
- Late Transcurrent Plutonic and Hypabyssal Rocks ~580 Ma
- Dorsal de Canguçu Syntranscurrent Granitoids 658-605 Ma
- Arroio dos Ratos Complex

Figure 2 – Geological map of Quitéria-Serra do Erval region (modified from Gregory *et al.*, 2011), with location of analyzed sample points. DCTSZ – Dorsal de Canguçu Transcurrent Shear Zone; QSESZ – Quitéria-Serra do Erval Shear Zone.

3. Analytical procedures

3.1. Major and trace elements

The geochemical study of representative samples of ARC A2 and A3 rock associations was based on quantitative analysis of major and trace elements in 14 samples of A2 and 6 samples of A3. The analyses were performed at AcmeLabs™, Canada, using the techniques of ICP-ES (Inductively Coupled Plasma Emission Spectrometry) for major elements and ICP-MS (Inductively Coupled Plasma Mass Spectrometry) for trace and rare earth elements.

3.2. Sr and Nd isotopes

Rb-Sr and Sm-Nd isotope analyses were obtained at Centro de Pesquisas Geocronológicas (CPGeo), Instituto de Geociências, Universidade de São Paulo. The same powders used for whole-rock elemental analyses were taken into solution by acid digestion, and the elements of interest were separated in ion-exchange columns following the procedures described in Sato *et al.* (1995). No spikes were added; $^{87}Rb/^{86}Sr$ and $^{147}Sm/^{144}Nd$ ratios were calculated from whole-rock analyses obtained by ICP-MS. The isotope analyses were done by thermal ionization mass spectrometry (TIMS) in a VG354 spectrometer equipped witha single Faraday detector.

3.3. Pb isotopes

Pb isotope ratio analyses of K-feldspar crystals were obtained by using a Nu Plasma Multi-Collector Inductively Coupled Plasma Mass Spectrometer (LA-MC-ICP-MS), interfaced with a NewWave UP213 laser ablation system at the Radiogenic Isotopic Facility (RIF), University of Alberta, Canada. Data were obtained on 200 to 250 mm-thick polished sections in raster mode; each analysis corresponds to a 160-800 mm raster area. Crystal cores and rims were analyzed, ensuring that altered or cracked areas and mineral inclusions were avoided. Replicate analyses of the standard NIST612 were used to estimate the precision and accuracy of the laser ablation using the same protocol as the samples. A Tl solution was simultaneously aspirated during ablation to correct for mass bias of Pb isotope ratios. Total Pb signal intensities for the analyses varied from 0.4 to 1.2 V. The measured Pb isotope ratios show associated 1σ uncertainties that are below the total isotopic variation recorded in individual crystals.

4. ARC Geology

4.1. Geology and structures

Two structurally discordant tonalitic-dioritic associations were identified by Gregory *et al.* (2011) at the ARC type-section, based mainly on field and petrographic criteria (Fig. 3a, b, c). The oldest association (A1) comprises garnet-biotite metatonalites with anastomosed foliation marked by the orientation of biotite and lenticular quartz-feldspathic aggregates, quartz ribbons and medium- to coarse-grained, recrystallized plagioclase. An irregular banding is occasionally developed parallel to

the main fabric, enhanced by deformed trondhjemitic veins. In such places, early isoclinal folding of the veins (F1) is observed, and fold axes and axial planes are paralell to the stretching lineation and foliation plane, respectively. A high temperature crenulation cleavage is observed in areas of tight foliation folding, with disruption of hinges and flow parallel to the axial planes.

These metatonalites contain enclaves of fine-textured rocks with variable composition (basic to acidic), with a high content of mafic minerals, interpreted as sheared syn-plutonic dykes because of their partially preserved tabular geometry (Fig. 3b). The A1 basement is represented by tonalitic gneisses, calc silicate and metavolcanosedimentary rocks that occur as xenoliths in the metatonalites. With the reconstitution of the late folds (F2) that affected the A1 rocks, the geometry of its foliation would have been subhorizontal or gently dipping to the WSW, with top-to-E movement.

Association 2 (A2) is intrusive in A1 and contains the same types of xenoliths, represented by calc silicate rocks, tonalitic gneisses, metavolcanics, and pelitic schists. The contacts with A1 are either sharp or diffuse, suggesting a low temperature contrast at the time of intrusion of the A2 magmas, despite their distinct foliation morphology (Fig. 3a, b, c). The ages of the two associations are within error range, 2,148 ± 33 Ma for A1 and 2,150 ± 28 for A2 (Gregory *et al.*, submitted for pulication).

The biotite tonalites and granodiorites of A2 have a hypidiomorphic inequigranular medium-to-coarse texture, and are primarily characterized by their magmatic foliation, marked by the shape orientation of tbiotite and feldspar, in addition to quartz and elongate quartz-feldspar aggregates. A2 locally displays a weak-to-moderate solid-state deformation, marked by the stretching of quartz, feldspars, and felsic aggregates, developing a planar fabric that is parallel to its primary foliation. Even in these zones, the stretching lineation is not well marked, and the preservation of the primary geometry is often observed. In other areas, the foliation is very incipient and the rock is massive. Variations in grain size are frequent, as well as variations in the content of mafic minerals. Trondhjemitic or late-leucogranodioritic injections are common and occur parallel to the foliation or at an angle, imparting a very heterogeneous aspect to the rock.

The felsic rocks of A2 contain dark-colored, centimetric to metric enclaves that are elongated and oriented with its foliation. They are represented by mafic rocks, such as fine-grained diorites and quartz-diorites with a hypidiomorphic texture and with amphibole predominating over biotite. The foliation is incipient, marked by amphibole and biotite orientation, parallel or sub-parallel to the host tonalites. The rock is sometimes massive. The contacts between tonalites and enclaves are either sharp or diffuse, with interfingering and mechanical capture of crystals from the tonalite, attesting to its contemporaneity (Fig. 3b, c, d, e). The mafic rocks are present in the form of narrow and elongate zones which, combined with the evidence for mutual intrusion with the A2 tonalites and the formation of hybrid rocks near the contacts (Fig. 3f), suggests that they are disrupted synplutonic dykes. This characterization attests to the participation of less differentiated magmas derived from the mantle in the magmatic evolution of A2, as noted by Gregory *et al.* (2011) for A1.

While the foliation orientations of A1 display a large dispersion (Fig. 4a), the A2 foliation is regular and relatively constant, with an approximately flat or slightly anastomosed geometry. It strikes mostly E-W, and dips at high angles mainly to the S (Fig. 4b). The stretching lineation, rarely observed, exhibits low-to-medium plunging to the W and SW. The dispersion observed in the orientation of A1 main foliation (Fig. 4a) most likely results from the effect of F2 folds. A2 foliation orientations are compatible with the axial plane of these folds, as observed in the field (Fig. 3b).

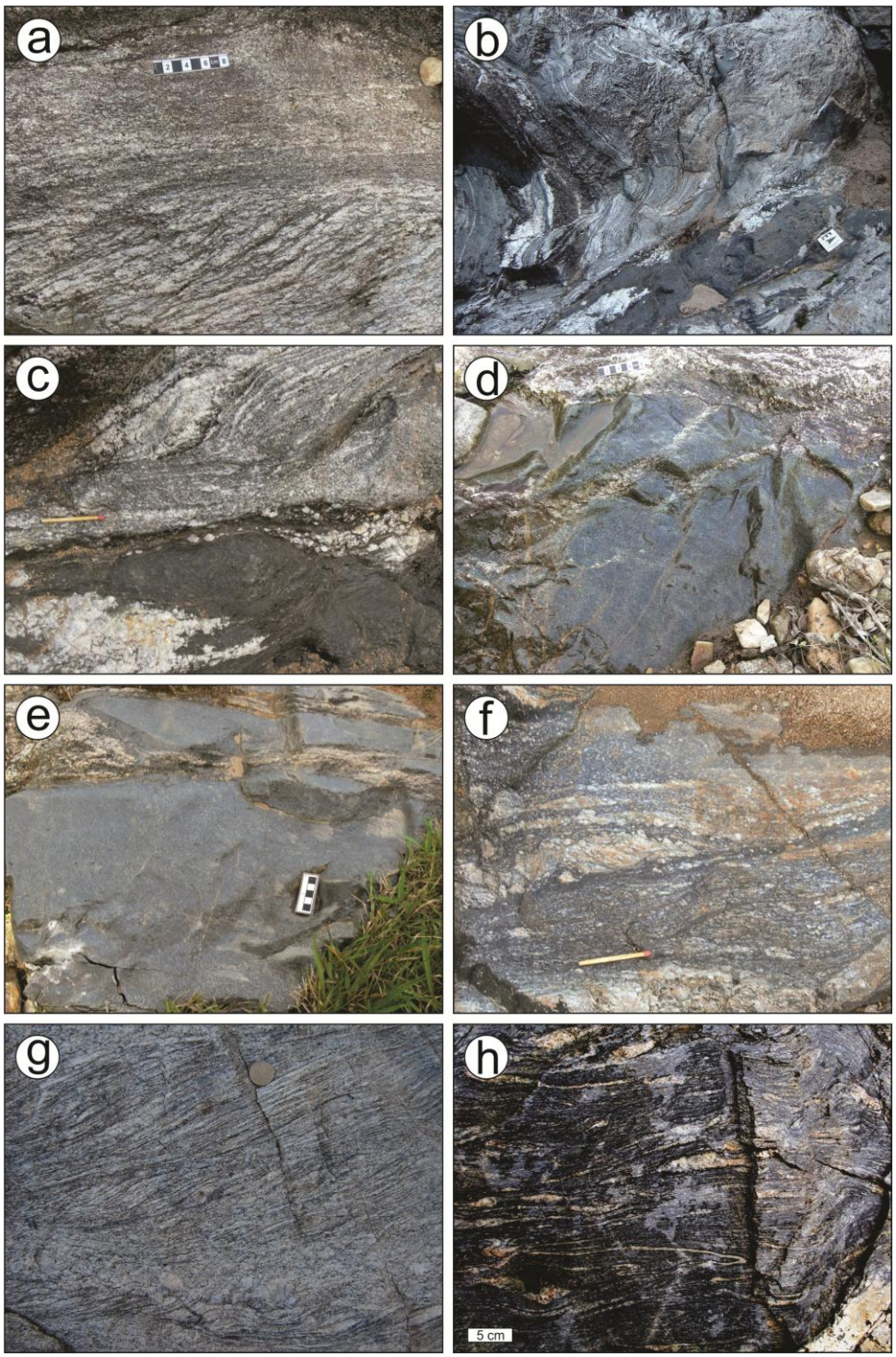

Figure 3 – Lithological and structural aspects of A1, A2, and A3 rock associations. (a) A2 tonalite (top), slightly foliated, in discordant contact with the A1 metatonalite (bottom). Note the slightly diffuse contact and morphological discordance of the foliations. (b) Contact relation between A1 and A2. At the top of the photograph, A1 foliated metatonalites and mafic enclaves are affected by an open fold with S-dipping axial plane (to the left in the photo). At the bottom right, more massive, mafic/basic A2 rocks are interspersed with coeval felsic varieties (at the contact and at the lower right corner of the photo), positioned along the axial plane of the fold affecting A1. (c) Detail of figure 3b – A1 (top) intruded by A2 rocks (bottom). At the contact, the A2 tonalites are observed (center of photo), interspersed with mafic rocks (bottom). Note mechanical capturing of feldspar crystals from the leucotonalites by the A2 mafic magma. (d) Massive aspect of A2 mafic rocks. Note injections connected to the A2 tonalites (top). (e) Another detail of the A2 mafic rocks. Note the parallel injections from A2 (top) that irregularly enter, and sometimes disappear into, the mafic rock, with diffuse contacts. (f) Detail of hybrid rocks formed near along narrow interaction zones between the felsic and mafic rocks of A2. (g) A3 granodioritic gneiss; a discrete cleavage displaces the gneissic banding with dextral shear sense and is locally invaded by liquid from partial melting. (h) Typicallly well-developed banding of mafic-rich, tonalitic varieties of A3.

Association 3 (A3) is represented by tonalitic and granodioritic gneisses and its main characteristics are a well-developed metamorphic-deformational banding and a granoblastic texture. The field relationship of A3 with the A1 and A2 rocks is undetermined, but its connection with the ARC is indicated by the petrographic, structural, and geochemical data presented herein and by geochronological studies (Gregory *et al.*, submitted). No contemporary mafic rocks were identified in the A3 association.

The A3 rocks are fine-to-medium grained and exhibit foliation marked by elongate quartz-feldspar aggregates, strips of recrystallized quartz, and aligned biotite flakes. The banded pattern is created by very elongate quartz-feldspar aggregates and, in some cases, is enhanced by coarser-grained trondhjemitic injections oriented parallel to the foliation (Fig. 3g, h). The more mafic-rich rocks (tonalitic gneisses) have a better developed banded structure (Fig. 3h). The foliation and banding show tight folds with an axial plane foliation, and the rotation of the pre-existing structure indicates a dextral sense of shear for the S-C structure. Partial melting features are locally observed and the resulting liquids are channeled into the C planes (Fig. 3g). The distribution pattern of A3 foliations is similar to the one shown for A1 (Fig. 4c).

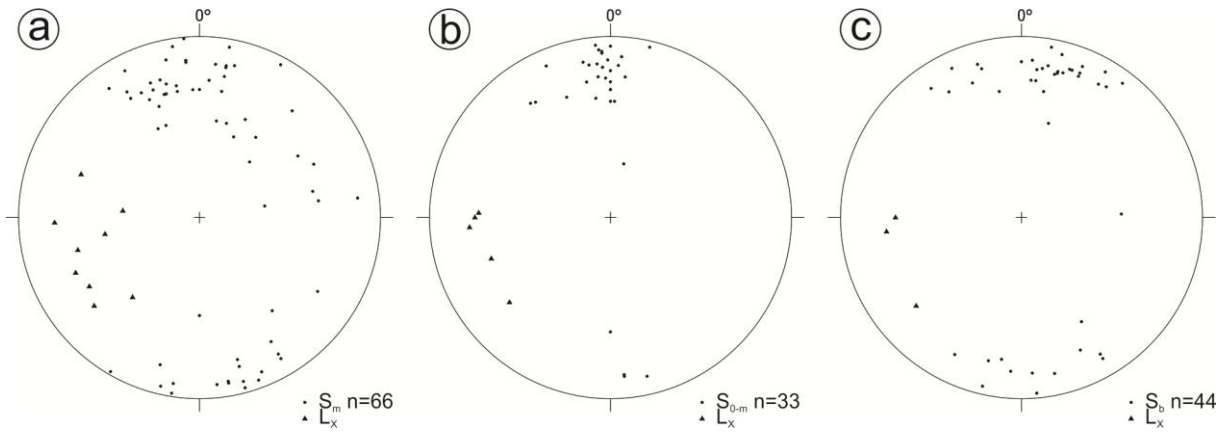

Figure 4 – Stereographic equiarea projection (lower hemisphere) for the structural elements of associations A1, A2, and A3 of the ARC. (a) A1: metamorphic foliation (S_m) and stretching lineation (L_X). (b) A2: igneous and metamorphic foliation (S_0//S_m) and stretching lineation (L_X). (c) A3: metamorphic foliation/banding (S_b) and stretching lineation (L_X).

4.2. Petrography

The granoblastic texture of A1 metatonalites is observable in hand sample, and plagioclase (An_{27-33}) microstructures, such as interlobed contacts, indicate high temperature recrystallization processes (>600°C) according to Passchier & Trouw (2005, p. 62). In these rocks, the occurrence of preserved crystal faces is very rare and anhedral or amoeboid shapes predominate. Garnet, apatite, and zircon are accessory phases. In the A1 mafic rocks, plagioclase (An_{40-45}) is usually subhedral, but triple junctions are frequent and contacts are often lobate to wavy, indicating recrystallization under thermal conditions similar to the metatonalites. The mafic phase is represented by common hornblende and biotite. Amphibole predominates in the less-differentiated mafic rocks and biotite in the more evolved rocks. The accessory mineralogy is represented by opaque minerals, allanite, titanite, and apatite.

In the tonalites and granodiorites of A2 plagioclase (An_{27-33}) igneous microstructures, such as subhedral crystals and albite twinning, are partially preserved. This greater preservation of primary structures is the main microstructural difference between the A2 and A1 metatonalites. The high-temperature solid-state deformation microstructures described for A1 by Gregory *et al.* (2011) also

occur in A2. Such structures comprise large recrystallized plagioclase crystals, new plagioclase grains formed at the margins of old grains, sinuous, slightly lobate plagioclase-plagioclase and plagioclase-quartz contacts, and well-developed chessboard subgrain pattern in quartz. (Kruhl, 1996) (Fig. 5a, b, c). Zircon, apatite, opaque minerals and very rarely garnet are the accessory phases. Lower temperature microstructures are also observed, such as kinking of twins, wedge twinning, wavy extinction, and fractures. Quartz is mainly recrystallized to a mosaic of fine grains that obliterates the old microstructures, such as the chessboard pattern. A hydrothermal episode is characterized by alterations to white mica and chlorite in the plagioclase and by the formation of chlorite interspersed with biotite, which are also observed in the other associations.

The A2 mafic rocks have dioritic to quartz-dioritic composition. Their content of mafic minerals is high (40-50%), always represented by greater amounts of amphibole (common hornblende) than biotite. Plagioclase (An_{33-46}) is subhedral to anhedral, with preserved albite twinning. The microstructures identified in plagioclase and quartz are the same high- and low-temperature microstructures identified in the A2 tonalites. Accessory minerals include apatite and opaque minerals.

In the tonalitic and granodioritic gneisses of A3, granoblastic texture is widespread. The tonalitic rocks are richer in mafic minerals (>15%) than the granodioritic rocks (<10%), with occurrence hornblende and biotite in the former and only biotite in the latter. The identified microstructures are similar to those of A1, according to features such as the interlobate granoblastic texture between plagioclase and quartz crystals, and chessboard pattern in quartz, which is best developed in A3 (Fig. 5d, e, f). Garnet is a very common accessory mineral, as well as zircon and monazite. The low temperature evidence observed in A1 and A2 are also present in A3, with intense obliteration of the high-temperature microstructures. There is a strong alteration of plagioclase, with rare preservation of growth twinning, sericitization, and the formation of wedge twinning.

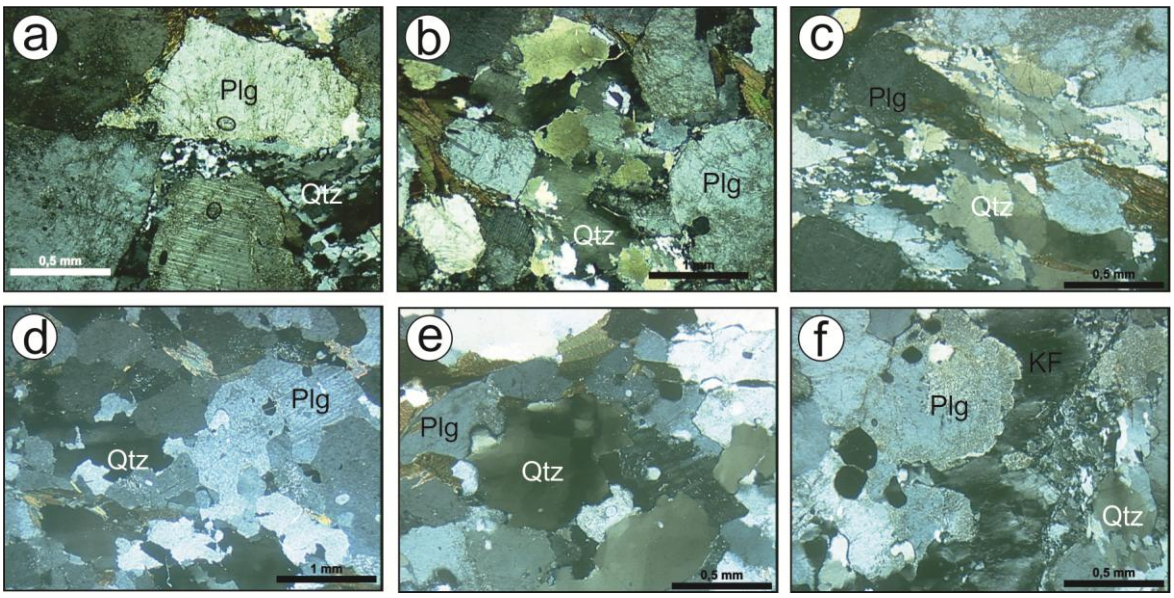

Figure 5 – Microstructural aspects of the studied rocks. (a) Association 2 – Subhedral plagioclase crystals with straight to wavy borders and triple junctions. Old quartz crystals with chessboard patterns (bottom right) with superimposed recrystallization to a fine irregular mosaic. (b) Association 2 – Subhedral plagioclase crystals with straight or wavy borders and triple junctions, in contact with old quartz crystals with chessboard pattern that is overlaid by new grains of *ca*. 0.3 mm. A fine-textured mosaic is observed at the bottom of the photo. (c) Association 2 – Detail of low-temperature, very fine mosaic (pictured left) developed over old, elongate quartz grains with high-temperature microstructures (chessboard pattern and larger crystals with triple junctions and more regular boundaries, pictured to the right of the photo). (d) Association 3 – Plagioclase crystals with irregular edges and lobate-to-interlobate contacts between themselves and with quartz, often with triple junctions. The quartz is generally monocrystalline, with chessboard pattern. (e) Association 3 – Chessboard pattern

developed in quartz and irregular contacts that are lobate-to-interlobate, and sometimes straight, between plagioclase and quartz crystals, characterizing the typical interlobate and polygonal granoblastic texture of the tonalitic gneisses. (f) Association 3 – low-temperature features developed in granodioritic gneisses. Old feldspar and plagioclase crystals of interlobate granoblastic textures are superimposed by wavy extinction; marginal grainsize reduction and the formation of a very fine-grained mosaic in the quartz crystals. Legend: Plg – plagioclase; Qtz – quartz; KF – K-feldspar.

4.3.Major and trace element geochemistry

The geochemical data of ARC rocks are shown in Table 1. For comparison purposes, representative samples of the A1 Association (from Gregory *et al.*, 2011) were also plotted in geochemical diagrams. As seen in the diagrams for major elements (%wt), with SiO_2 as differentiation index (Fig. 6), all associations show a common evolution, given their linear patterns of differentiation, similar to those of basic magmas that evolve to acid liquids by fractional crystallization of ferromagnesian minerals and plagioclase. The K_2O/Na_2O ratio is usually <1, independent of the degree of differentiation, which defines their sodic character.

In the TAS diagram (Cox *et al.*, 1979) for plutonic rocks, all the samples are identified with the silica supersaturated subalkaline series (Fig. 7a). In the diagram K_2O *vs* SiO_2 proposed by Le Maitre (2002) A2 and A3 rocks are similar to the subalkaline associations of medium to high potassium content (Fig. 7b). The calc-alkaline character is indicated in the diagrams of Jensen (1976) (Fig. 7c), Irvine & Baragar (1971) (Fig. 7d) and FeO^T/MgO of Miyashiro (1974) (Fig. 7e). A2 mafic rocks are located near the boundary between the calc-alkaline and tholeiitic fields, which is due to their high Fe/Mg ratio, suggestive of a transitional character. Their high Al_2O_3 contents (>16%wt), on the other hand, confirms their calc-alkaline affinity.

The A2 as well as A1 mafic rocks are metaluminous, while the felsic are peraluminous as shown in the diagram A/NK *vs* A/CNK suggested by Maniar & Piccoli (1989) (Fig. 7f). A3 is predominantly peraluminous.

According to the classification proposed by Frost *et al.* (2001), which takes into account the $FeO^T/(FeO^T+MgO)$ ratio and a modified alkali index (Na_2O+K_2O-CaO), the ARC felsic rocks (A1, A2 and A3) are classified as magnesian granitoids, plotting within the field of cordilleran granites, which belong to calcic and calc-alkaline series.

A2 and A3 rocks show enrichment in incompatible elements such as Rb, Ba, and Sr along with the differentiation. Sr shows a larger dispersion probably caused by fractionation of plagioclase at different stages of differentiation. Low-mobility elements, as Nb, Zr, Y, and Ta, show increasing dispersion with the differentiation. Nb tends to be enriched in some of the least differentiated rocks. Rare earth elements (REE) have contrasting behavior for LREE and HREE, with enrichment of the former (La, Ce, Pr, Nd) and depletion of the heavy ones (Er, Tm, Yb, Lu) with increasing differentiation. Y behaves like Yb, given the chemical similarity of both cations. Negative anomalies of Nb are displayed in E-MORB normalized spidergrams (Sun & McDonough, 1989), and are taken as typical of magmas produced by partial melting of mantle sources affected by subduction of oceanic crust (Fig. 8a, b). The mafic rocks of A2 have geochemical patterns very similar to their equivalents from A1, though more enriched for most elements, and with less intense Nb negative anomalies (Fig. 8a). Comparing the felsic varieties of the three associations, it a very similar pattern emerges, with larger variation of more compatible elements, including HREE, and sharper Ti negative anomalies (Fig. 8b).

Table 1 – Major (%wt) and trace (ppm) elements data from A2 and A3 rocks of the Arroio dos Ratos Complex.

group	Association 2														Association 3					
unit	Fine-grained mafic rocks				Medium- to coarse-grained felsic rocks										tonalitic and granodioritic gnaisses					
sample	TG-2L	TG-02M	TG-02N	TG-02G	TG-03I	TG-01S	TG-301B	TG-01W	TG-04B	TG-01U	TG-01V	TG-02O	TG-07E	TG-297A	TG-10A	TG-325A	TG-324A	TG-325B	TG-29A	TG-06A
SiO_2	49.89	51.33	51.63	55.03	66.67	67.7	68.14	68.18	68.87	70.13	70.57	70.64	71.7	72.04	66.24	68.15	68.76	71.01	72.9	75.6
Al_2O_3	17.54	17.27	17.57	16.71	16.92	15.07	15.66	14.75	14.91	15.01	14.76	15.13	14.83	13.89	16.46	15.35	15.15	15.07	13.07	11.85
$Fe_2O_3^T$	11.9	11.45	11.38	10.58	3.39	3.57	4.5	5.92	4.18	4.25	3.33	2.91	2.46	2.47	3.83	5.4	3.73	3.37	2.68	2.05
MnO	0.181	0.15	0.17	0.173	0.05	0.056	0.04	0.1	0.068	0.05	0.03	0.04	0.03	0.02	0.055	0.08	0.05	0.07	0.04	0.03
MgO	4.86	4.26	3.57	3.6	1.32	1.07	1.53	1.37	1.63	0.96	0.86	0.8	0.95	0.74	1.88	1.2	1.08	0.62	0.16	0.15
CaO	9.36	8.99	8.51	8.15	2.58	2.08	1.64	2.98	2.66	2.62	1.9	2.48	2.08	0.53	3.52	2.69	2.8	2.23	1.21	0.85
Na_2O	2.13	2.77	2.99	1.55	4.29	3.11	4.06	3.13	3.79	4.04	3.68	3.8	4.34	3.55	4.74	3.97	4.48	4.42	2.83	2.75
K_2O	1.83	1.05	1.25	0.98	3.23	3.62	2.19	1.73	2.31	1.67	3.29	2.6	2.51	4.9	1.68	1.9	2.45	2.1	4.76	3.73
TiO_2	1.633	1.31	1.31	1.254	0.32	0.471	0.45	0.47	0.512	0.41	0.28	0.29	0.22	0.22	0.414	0.45	0.32	0.24	0.18	0.182
P_2O_5	0.32	0.35	0.35	0.38	0.15	0.11	0.13	0.16	0.27	0.1	0.18	0.07	0.07	0.16	0.16	0.11	0.08	0.07	0.14	0.1
LOI	1.34	0.8	1	1.1	1	1.02	1.5	1.1	1.61	0.7	1	1.1	0.7	1.3	1.35	0.6	1	0.7	1.8	1.52
Total	101	99.79	99.77	99.52	99.86	97.86	99.87	99.88	100.8	99.91	99.85	99.83	99.88	99.84	100.3	99.86	99.85	99.9	99.75	98.81
Sc	31	30	28	28	6	9	11	19	9	7	3	7	4	4	7	10	5	5	4	3
Be	1	4	2	2	<1	1	2	<1	2	2	2	2	2	<1	6	3	3	5	4	2
V	162	140	119	142	19	33	45	16	53	<8	<8	22	9	11	56	9	11	<8	<8	< 5
Ba	418	221	414	223	393	822	425	267	334	242	665	799	499	1000	554	468	697	459	1053	1060
Sr	441	346.8	378.5	287	345.7	257	224.9	214.5	290	241.9	269.2	348.3	295.9	157.7	555	239.2	289.3	243.2	152.5	147
Y	30	36.8	43.1	36	13.5	8	21.1	54.5	6	11.1	8.8	38.7	4.6	10	3	22.9	14.5	16.7	36.5	25
Zr	146	169.8	208.8	186	32.1	139	129.1	189.9	118	145.4	114.7	88.9	116.7	109	118	217	135.7	118.6	234.4	245
Cr	160			150		< 20			50						30	<14	27	<14	34	< 20
Co	35	30.5	28.6	28	6	10	10.7	10.3	10	7.7	6.1	6.4	3.5	4.4	8	10.4	7.8	5.4	1.7	< 1
Ni	20	<20	<20	< 20	<20	< 20	32	<20	< 20	<20	<20	<20	<20	<20	20	<20	<20	<20	<20	< 20
Cu	20	28.6	38.9	20	10.7	< 10	28.5	12.9	20	20.9	15.7	28.7	17.2	24	30	18.7	10.4	24.9	19.4	< 10
Zn	120	54	59	150	59	70	63	85	240	73	106	138	46	37	80	92	57	54	27	< 30
Ga	22	22.4	22.7	24	21.6	21	22.6	20.2	22	21.3	18.6	18	17.7	16.7	20	20.5	19.3	18.6	17.5	17
Ge	2			2		2			1						< 1					1
As	< 5	<0.5	<0.5	< 5	<0.5	< 5	1.9	<0.5	< 5	<0.5	0.7	<0.5	<0.5	2.3	< 5	<0.5	<0.5	<0.5	1.5	< 5
Rb	82	37	43.8	46	112.1	144	109.5	106.3	119	92.7	117.1	86	80.3	166.5	84	114.7	70.6	74.8	137.5	101
Nb	12	14.5	16.4	12	10.4	9	10.9	9	11	10.2	9.9	5.3	6.1	6	4	7.8	5.2	5.5	5.7	6
Mo	< 2	0.8	1.1	< 2	0.3	< 2	0.8	0.3	< 2	0.4	0.1	0.4	0.2	0.5	< 2	0.4	0.1	0.3	3	< 2
Ag	0.9	<0.1	<0.1	< 0.5	<0.1	2.2	<0.1	<0.1	< 0.5	<0.1	0.1	0.1	<0.1	<0.1	< 0.5	<0.1	<0.1	<0.1	<0.1	< 0.5
In	< 0.2			< 0.2		< 0.2			< 0.2						< 0.2					< 0.2
Sn	5	4	3	5	3	9	3	6	5	5	6	3	2	3	2	3	4	2	2	3
Sb	1.2	<0.1	<0.1	< 0.5	<0.1	1.8	<0.1	<0.1	5.9	<0.1	<0.1	<0.1	<0.1	<0.1	< 0.5	<0.1	<0.1	<0.1	<0.1	0.6
Cs	5.3	4.3	5.8	6.7	6.9	6.3	5.1	8.6	7.4	6.1	5	4.4	2.2	2.3	13.5	8.4	2	3.5	1.8	1.5
La	15	21	26.3	24.9	63	18.6	25.6	20.7	34.1	13	13.6	23.4	23.8	26.8	24.8	30.9	21	19.2	70.8	65.3
Ce	34.4	41.7	51.6	58.1	113.5	37.6	46.9	40.7	71.2	24	23.7	42.2	39.9	45.9	48.6	55.4	37.3	33.4	150	136
Pr	4.9	6.18	7.23	7.12	14.02	4.59	5.71	6.15	7.48	2.89	2.95	5.31	4.57	6.07	5.49	7.39	4.72	4.24	17.2	17.5
Nd	19	29	35.1	30	51.9	15.3	21.8	27.4	26.4	10.8	10.5	19.6	15.9	24.1	18	29.6	17.5	16.9	61.8	56.6
Sm	4.6	6.42	7.21	6.6	8.95	2.9	4.53	9.24	4.6	2.38	2.44	4.79	2.71	4.2	3.1	6.04	3.65	3.14	11.07	9.6
Eu	1.6	1.87	2.04	1.98	1.03	1.3	0.99	1.15	0.98	0.87	0.88	1.18	0.74	0.92	0.87	1.1	0.8	0.71	0.97	0.9
Gd	4.9	6.88	8.05	7.1	6.63	2.3	4.34	10.91	3.8	2.26	2.22	5.12	1.83	3.57	2.4	5.32	3.2	2.67	9.4	6.4
Tb	0.9	0.99	1.17	1.2	0.71	0.3	0.59	1.76	0.5	0.34	0.32	0.89	0.22	0.44	0.3	0.73	0.45	0.38	1.1	0.9
Dy	5.5	7.6	8.1	7.3	3.38	1.7	3.83	12.01	2.2	2.18	1.61	6.41	1.05	2.24	1.6	4.36	2.49	2.5	6.95	4.6
Ho	1.1	1.24	1.44	1.4	0.46	0.3	0.62	1.91	0.3	0.39	0.22	1.2	0.13	0.31	0.3	0.77	0.44	0.57	1.29	0.9
Er	3.2	4.38	5.29	4.3	1.21	0.9	1.94	6.26	0.8	1.09	0.75	4.48	0.32	0.89	0.8	2.52	1.35	2.01	4.06	2.9
Tm	0.49	0.47	0.61	0.65	0.11	0.13	0.27	0.62	0.1	0.12	0.08	0.49	0.03	0.09	0.11	0.3	0.19	0.26	0.61	0.48
Yb	3.1	3.54	4.88	4.2	0.85	0.8	1.89	4.46	0.5	0.87	0.78	3.5	0.28	0.61	0.6	2.16	1.59	2.27	4.43	3
Lu	0.44	0.5	0.59	0.62	0.1	0.11	0.23	0.51	0.07	0.09	0.08	0.44	0.02	0.08	0.09	0.27	0.18	0.28	0.61	0.45
Hf	3.8	5	5.4	5	1	4.5	4.1	6.1	3.2	4.9	3.5	2.6	3.1	3.3	3.3	6.2	4.4	3.7	7.6	7.8
Ta	0.7	0.7	0.9	1.1	1.2	0.9	1.2	0.6	1.6	0.9	0.8	0.5	0.4	0.5	0.4	0.5	0.4	0.6	0.3	0.4
W	1	<0.5	0.7	3	<0.5	< 1	1	<0.5	2	1.2	<0.5	1.2	<0.5	1.2	2	0.7	<0.5	<0.5	0.7	< 1
Tl	0.5	<0.1	<0.1	0.3	0.2	1.1	0.3	0.5	0.7	0.4	0.1	0.1	0.1	<0.1	0.8	0.4	0.1	0.2	<0.1	0.5
Pb	6	2.5	2.7	6	8.3	21	4.1	4.4	64	4.6	46.7	6.6	3.8	9.4	12	3.6	3.3	4	4.4	12
Bi	< 0.4	<0.1	<0.1	< 0.4	<0.1	< 0.4	0.4	<0.1	< 0.4	<0.1	0.1	<0.1	<0.1	<0.1	< 0.4	0.1	<0.1	<0.1	0.2	< 0.4
Th	1.3	1.5	2.1	2.7	26.6	4.7	6.4	3	9.5	2.3	2.3	7.5	5.4	8.2	2.7	7.5	7.1	5.7	16.4	19.3
U	0.6	0.8	0.6	1.4	4	2.1	5.5	0.9	2.1	1.3	1.1	2	1.4	4.7	0.4	2.7	2.8	1.7	2.1	1.9

The diagrams of rare earth elements normalized to chondritic values of Boynton (1984) for the mafic (Fig. 8c) and felsic rocks (Fig. 8d) of A2 show distinct patterns. The mafic ones have regular patterns, slightly fractionated, with a slight negative Eu anomaly and low HREE depletion (Fig. 8c). The felsic varieties have more irregular patterns, with large dispersion of HREE and a sharper, negative or positive, Eu anomaly (Fig. 8d). Compared to A1, the A2 and A3 felsic rocks show much larger dispersion, particularly for HREE. The same behavior is observed in relation to A2 mafic rocks. Mafic rocks from both A1 and A2 show parallel patterns with higher REE contents and more intense Eu anomalies, positive or negative, in the A2 rocks. The patterns of A2 mafic rocks with Ce_N values from 40 to 80, Yb_N from 10 to 20, are similar to those of island-arc or active-continental-margin magmatism, and the higher content of all REE in A2 relative to A1 can be explained by smaller melt fractions of the mantle source. The relatively low fractionation of LREE to HREE of mafic rocks

suggests the absence of garnet in the source. The A3 felsic rocks feature a similar pattern of A2 felsic rocks, although on average they are less enriched in REE.

Along with the A1, the A2 and A3 felsic rocks plot in the upper part of the volcanic-arc granitoid field (Pearce 1996) which suggests a mature continental arc (Fig. 9a, b, c, d). Given the higher Rb and Y+Nb content, some samples enter the post-collisional magmatism field (Fig. 9a).

As discussed by Gregory *et al.* (2011) for the A1, the A2 and A3 geochemical data are also comparable to Proterozoic TTG-type associations (tonalite, trondhjemite, granodiorite), as revised by Condie (2005) (Tab. 2). Most of the A2 and A3 data lies within the proposed intervals that define TTG. In all associations (A1, A2 and A3), the Al_2O_3 and Sr contents show some values lower than those referred by Condie (2005), which is ascribed to intense plagioclase fractionation (Tab. 1 and 2, Fig. 6 and 8d). A2 and A3 rocks also show, in relation to typical TTG values, a larger variation of HREE and Y, La_N/Yb_N and K_2O/Na_2O ratios, which indicates that magmatic differentiation was probably accomplished through more than one process in order to produce such large dispersion of compositional parameters.

As for A1, geochemical data of A2 and A3 rocks are comparable to modern adakites studied by Defant & Drummond (1990), which are considered by Martin (1986, 1999) and Moyen & Martin (2012) as analogues of Archaean TTG Associations, although there are still debates about such analogy (Condie, 2005). The felsic terms of A1, A2 and A3 occupy a transitional position between the fields of adakites and calc-alkaline- or classical-island-arc magmatism (Fig. 10a, b), which are interpreted as melting of subducted slab or mantle wedge, respectively. The A2 and A3 show greater variation in both fields, as pointed out previously for REE patterns (Fig. 8d). In relation to adakites the A2 and A3 rocks are depleted in Sr and show higher K_2O/Na_2O ratios (Tab. 2, Fig. 10b).

Compared with E-MORB patterns (Fig. 8a, b) the mafic and felsic ARC rocks show similar patterns, with felsic varieties showing LILE enrichment and the greatest negative anomalies in Nb, Sr, P, Zr, and Ti, and strong depletion in HREE (Dy, Yb, Lu) and Y. The high partition coefficients of HREE and Y in garnet, particularly in dacitic compositions, indicate the presence of this mineral as a residual phase in the source. That leads to suggest a mantle wedge metasomatized by subduction-related fluids, composed mainly of garnet lherzolite, as the source of the ARC magmas. Condie (2005) and Martin *et al.* (2005), amongst other authors, have suggested that TTG and adakite associations may be produced by melting of the oceanic plate with a garnet eclogite residue. However, the abundance of mafic rocks in the ARC, as well as their pattern against E-MORB, support the idea that a mantle wedge modified by subduction fluids was the source of ARC. The enrichment in incompatible elements and strong depletion in HREE (values <1) point to a crustal contaminant in the evolution of ARC magmatism.

A2 mafic rocks are diorites and quartz-diorites related to medium-K calc-alkaline series. The trace element composition, including the REE patterns, are also similar to those of basic rocks from active continental margins or mature magmatic arcs. Low La/Nb ratios, Nb, Ta and Ti negative anomalies illustrated in spidergrams (Fig. 8a, b) are an additional evidence of mantle sources modified by subduction-related processes. Mafic rocks from A2 show low-fractionated REE patterns similar to those of classical magmatism at island-arc or active-continental-margins (Wilson, 1989). In relation to the previous A1 magmatism, A2 mafic rocks show higher Fe/Mg ratios that can be related to a less oxidized mantle source. The less pronounced Nb, Ta and Ti anomalies, as well as the higher HFS and RE element content of A2 relative to A1 can be explained by lower melt fractions of similar sources. The subtle difference between A1 e A2 mafic rocks can be observed in the geotectonic settings discriminant diagrams for mafic rocks (Fig. 11a, b).

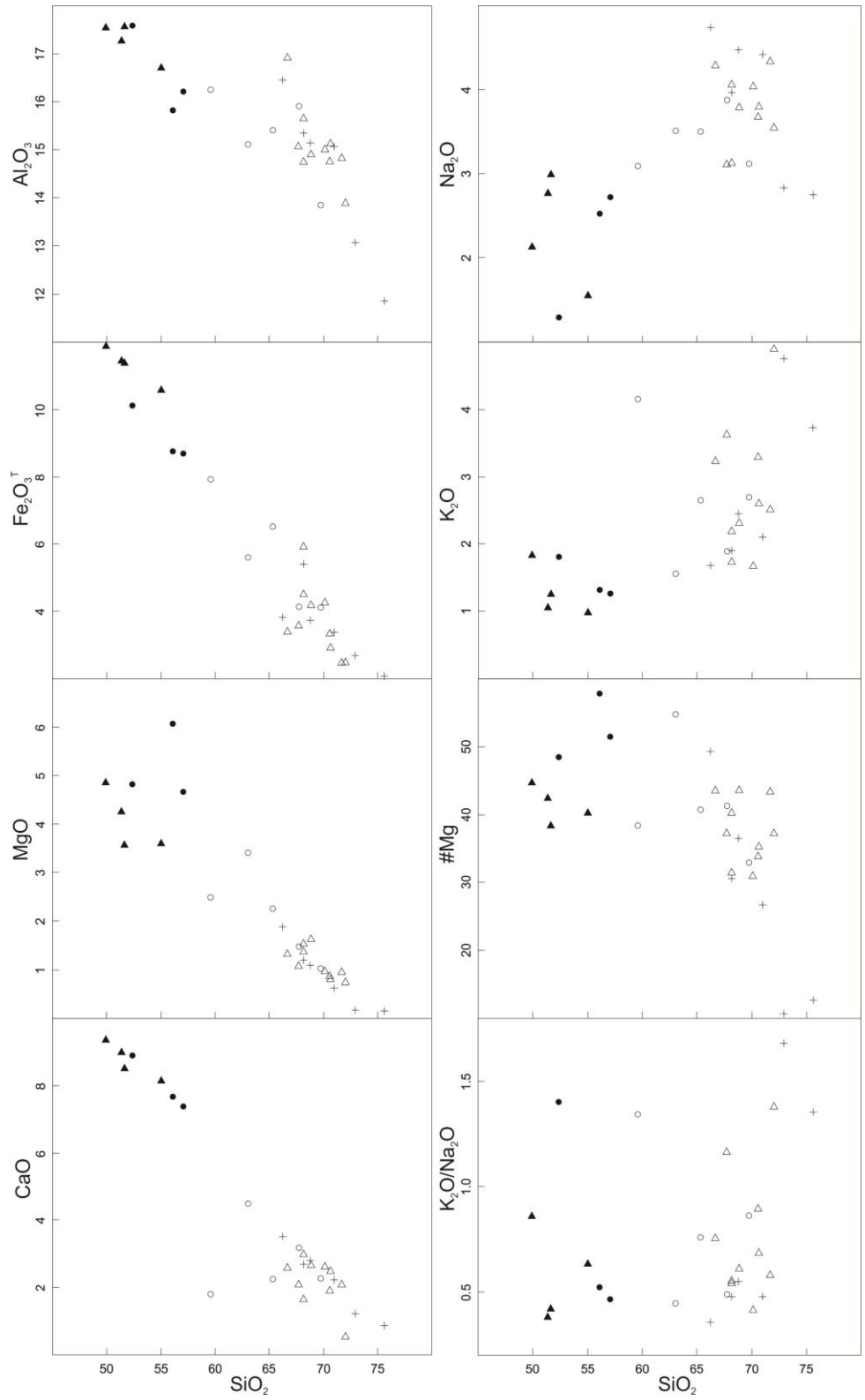

Figure 6 – Harker diagrams with SiO_2 as differentiation index for major elements of the Association 1 (circles), Association 2 (triangles) and Association 3 (crosses) of the Arroio dos Ratos Complex (ARC). For A1 and A2 rocks the full and empty symbols are the less differentiated mafic rocks, and the more differentiated felsic rocks, respectively. Major elements expressed as weight percent (%wt), number of magnesium as #Mg=100x{(MgO/40.3)/[(MgO/40.3)+(FeO^T/71.84)]} and $FeO^T=Fe_2O_3^T$x0.89. A1 data extracted from Gregory *et al.* (2011).

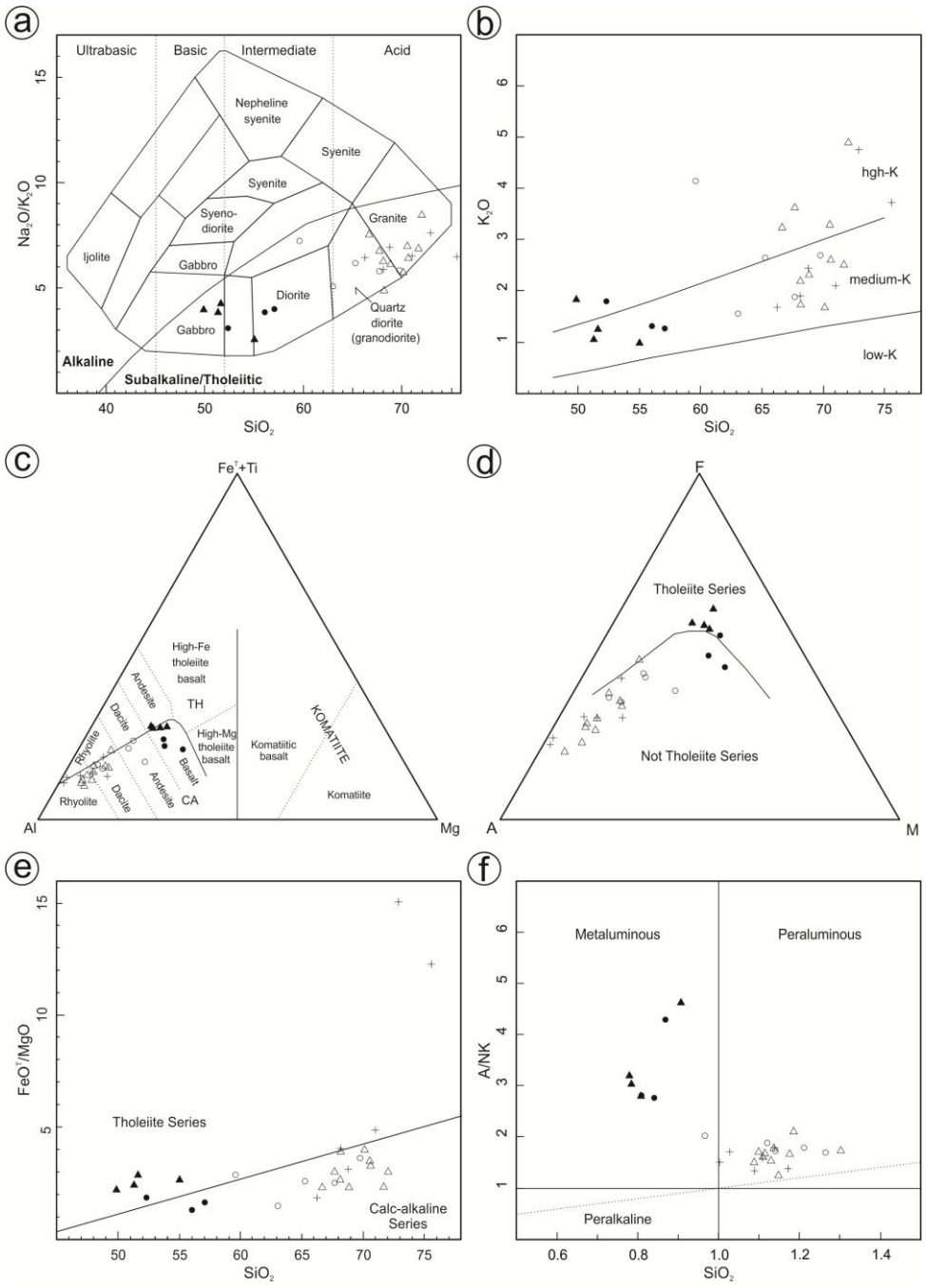

Figure 7 – Discrimination diagrams for ARC rocks. (a) TAS diagram of Cox *et al.* (1979) for plutonic rocks. (b) K_2O *vs* SiO_2 diagram of Le Maitre (2002). (c) Al-Fe+Ti-Mg diagram of Jensen (1976). (d) AFM diagram of Irvine & Baragar (1971). (e) FeO^T/MgO diagram of Miyashiro (1974). (f) A/(NK) *vs* A/(CNK) diagram suggested by Maniar and Piccoli (1989). Symbols as in figure 6.

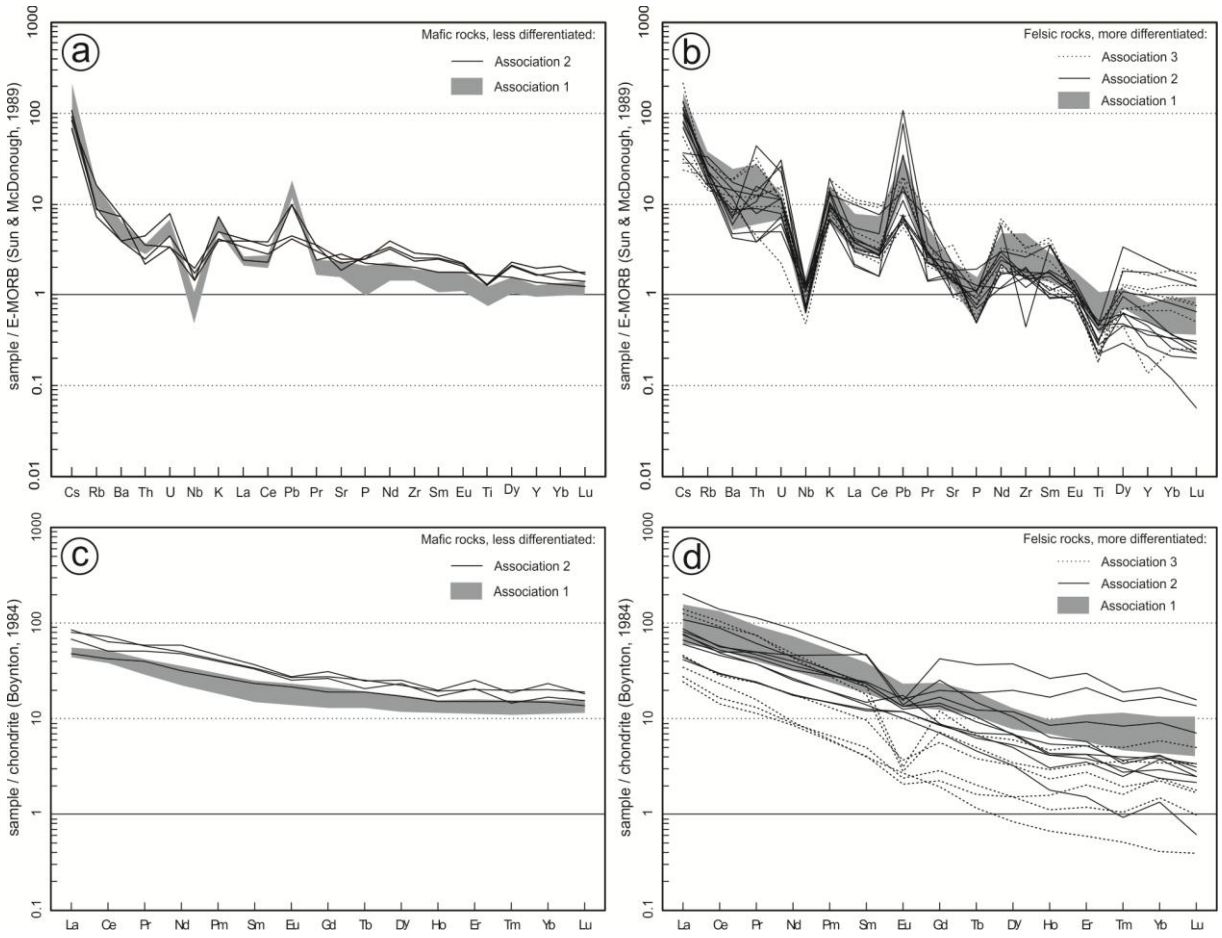

Figure 8 – Spidergrams for ARC A1 (gray field), A2 (full lines) and A3 (dashed line) samples. (a) A1 and A2 mafic rocks normalized to E-MORB values after Sun & McDonough (1989). (b) A1, A2 and A3 felsic rocks normalized to E-MORB values after Sun & McDonough (1989). (c) A1 and A2 mafic rocks normalized to REE chondrite values after Boynton (1984). (d) A1, A2 and A3 felsic rocks normalized to REE chondrite values after Boynton (1984).

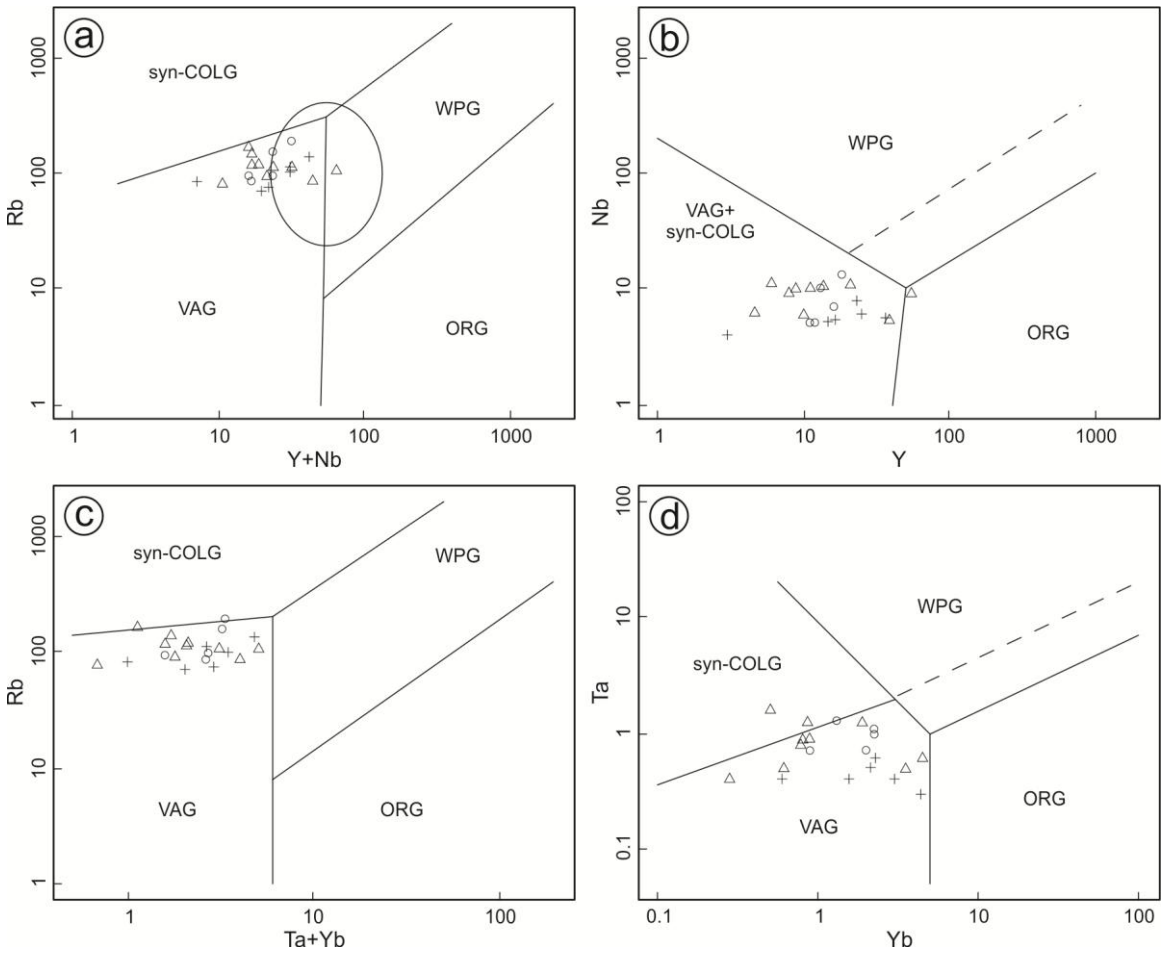

Figure 9 – The Arroio dos Ratos Complex felsic rocks in the tectonic setting discriminant diagrams for granitoids from Pearce *et al.* (1984), with post-collisional magmatism field indication (Fig. 9a, elliptical area) suggested by Pearce (1996),. Symbols as in figure 6.

Table 2 – Comparison of geochemical parameters reviewed by Condie (2005) for Adakites and Proterozoic TTG-type associations, with the A1, A2 and A3 associations of the Arroio dos Ratos Complex. La and Yb normalized to chondrite values from Haskin *et al.* (1968; La=0.32; Yb=0.186). #Mg corresponding to same formula as in figure 6.

Parameter	Adakites	TTGs	Association 1	Association 2	Association 3
SiO_2 (%wt)	62.43	63.7 – 70.9	63.05 – 69.75	66.67 – 72.04	66.24 – 75.6
Al_2O_3 (%wt)	17.05	15.02 – 16.58	13.85 – 15.91	13.89 – 16.92	11.85 – 16.46
Sr (ppm)	1,550	314 – 632	192 – 361	157.7 – 348.3	147 – 555
Y (ppm)	9.7	8.4 – 26.2	11 – 16	4.6 – 54.5	3 – 36.5
Yb (ppm)	0.81	0.47 – 2.19	0.9 – 2.2	0.28 – 4.46	0.6 – 4.43
Nb (ppm)	9.7	2.5 – 11.7	5 – 10	5.3 – 11	5.3 – 11
La_N/Yb_N	18.2	5.9 – 22.5	7.1 – 13	2.7 – 49.4	4.9 – 24
Sr/Y	160	7 – 67	12 – 30.1	3.9 – 64.3	4.2 – 185
Nb/Ta	16.1	3.2 – 16.6	3.8 – 10	6.9 – 15.3	9.2 – 19
#Mg	60.4	35.7 – 50.7	33.1 – 55	31.1 – 43.9	10.7 – 49.6
K_2O/Na_2O	0.33	0.31 – 0.81	0.44 – 0.86	0.41 – 1.38	0.4 – 1.7

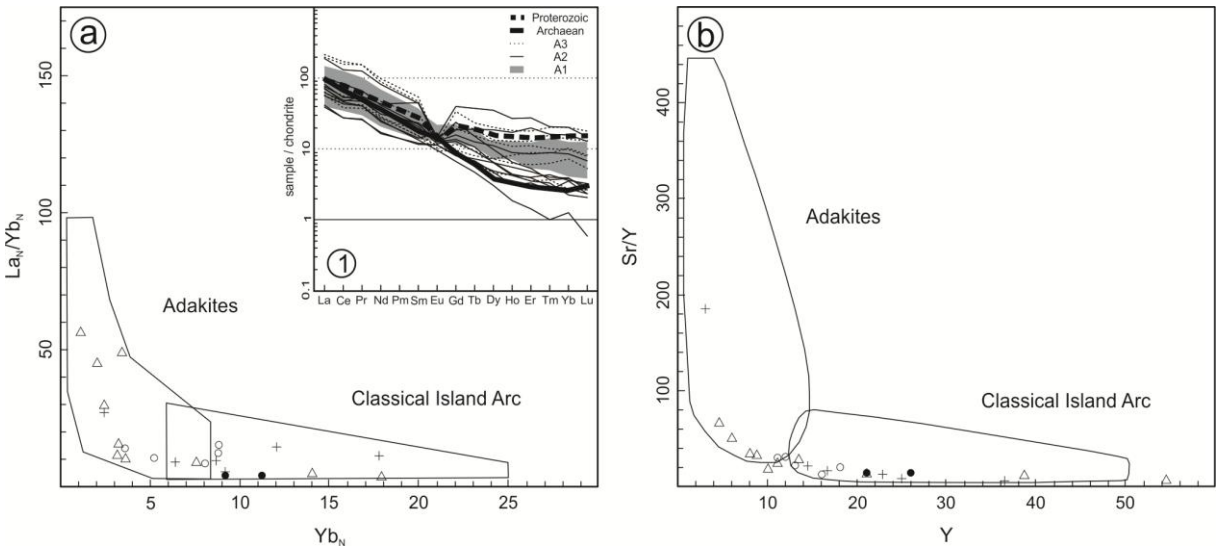

Figure 10 – Discriminant diagrams for adakites and classical island arc compositions for the ARC rocks (SiO_2 >56%). (a) $(La/Yb)_N$ *vs* Yb_N from Martin (1986). Inset corresponds to ARC rocks REE patterns normalized to chondritic values from Masuda *et al.* (1973), compared with Archaean TTG and post- 2.5 Ga continental crust (extracted from Moyen & Martin, 2012). (b) Sr/Y versus Y from Drummond & Defant (1990). Symbols as in figure 6. La and Yb normalized to chondrite values from Masuda *et al.* (1973; La=0.378; Yb=0.249).

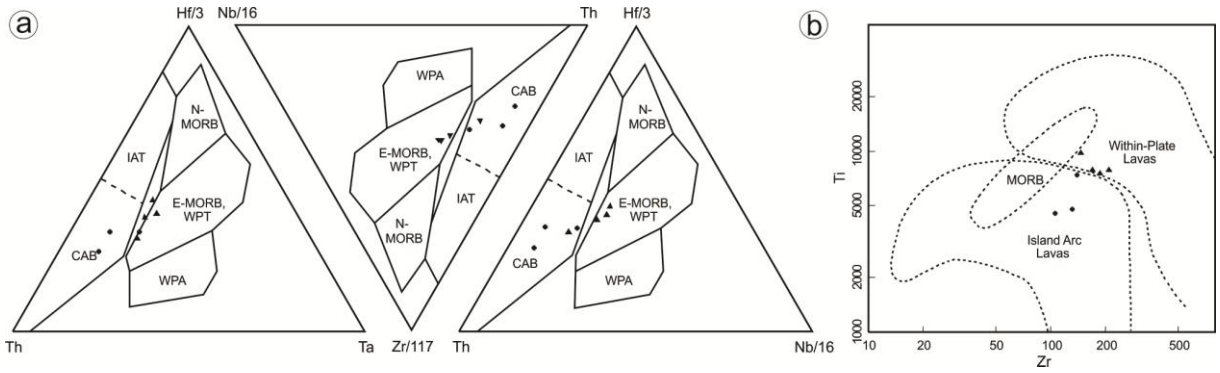

Figure 11 – Geotectonics settings discriminant diagrams for mafic rocks of the ARC. (a) Triangular diagrams of the Th-Hf-Ta-Zr-Nb system from Wood (1980). (b) Zr-Ti diagram for lavas from Pearce (1982). Symbols as in figure 6.

4.4. Isotope geochemistry

4.4.1 Total rock Rb-Sr and Sm-Nd isotopic data

The total rock Rb-Sr and Sm-Nd isotopic data of associations A1, A2, and A3 are given in Table 3. For the calculation of the isotopic parameters ($^{87}Sr/^{86}Sr_{(i)}$, $\varepsilon Nd_{(t)}$ and $^{143}Nd/^{144}Nd_{(i)}$) of each sample, the zircon U-Pb crystallization ages determined by laser ablation multi-collector inductively coupled mass spectrometry (LA-MC-ICP-MS) were obtained from Gregory *et al.* (submitted).

Table 3 –Rb-Sr and Sm-Nd isotopic data for the Arroio dos Ratos Complex.

sample	group	T (Ma)*	Rb (ppm)	Sr (ppm)	$^{87}Rb/^{86}Sr(c)$	$^{87}Sr/^{86}Sr$	error (2s)	$^{87}Sr/^{86}Sr(i)$	Sm (ppm)	Nd (ppm)	$^{147}Sm/^{144}Nd(c)$	$^{143}Nd/^{144}Nd$	error (2s)	εNd(0)	εNd(t)	T_{DM} (Ma)	$^{143}Nd/^{144}Nd(i)$
TG-01M	A1 - mtT	2,148±33	n.d.	n.d.	n.d.	n.d.	n.d.	n.d.	7.6	43.4	0.106	0.511441	0.000009	-23.4	1.53	2,272	0.509943
TG-01O	A1 - mtD	2,148±33	50	319	0.454020	0.716400	0.000030	0.702339	3.6	16.9	0.129	0.511835	0.000009	-15.7	2.95	2,172	0.510013
TG-01P	A1 - mtD	2,148±33	n.d.	n.d.	n.d.	n.d.	n.d.	n.d.	2.8	13.1	0.129	0.511874	0.000009	-14.9	3.59	2,112	0.510046
TG-02A	A1 - mtT	2,148±33	95	317	0.869213	0.729636	0.000027	0.702715	3.8	19.0	0.121	0.511648	0.000008	-19.3	1.45	2,300	0.509937
TG-02D	A1 - mtD	2,148±33	n.d.	n.d.	n.d.	n.d.	n.d.	n.d.	4.7	20.8	0.137	0.512031	0.000009	-11.8	4.61	2,002	0.510098
TG-05F	A1 - mtT	2,148±33	n.d.	n.d.	n.d.	n.d.	n.d.	n.d.	3.6	18.8	0.116	0.511584	0.000010	-20.6	1.62	2,278	0.509946
TG-01S	A2 - T	2,150±28	n.d.	n.d.	n.d.	n.d.	n.d.	n.d.	2.9	15.3	0.115	0.511652	0.000008	-19.2	3.28	2,144	0.510029
TG-02G	A2 - D	2,150±28	46	287	0.464232	0.715540	0.000038	0.701149	6.6	30.0	0.133	0.512009	0.000010	-12.3	5.19	1,953	0.510125
TG-06A	A3 - Ggn	2,077±13	101	147	2.001720	0.775079	0.000036	0.715163	9.6	56.6	0.103	0.511384	0.000009	-24.5	0.47	2,283	0.509981

mtT - metatonalite; mtD - metadiorite; T - tonalite ; D - diorite; Ggn - granodioritic gneiss.

* - LA-MC-ICP-MS Zircon U-Pb age data from Gregory *et al.* (submitted). n.d. - not determined. (c) - Isotopic ratio calculated from elemental data (not spiked). (i) - Initial ratio.
Sm-Nd T_{DM} calculated according DePaolo (1981).

The $^{87}Sr/^{86}Sr_{(i)}$ ratios of the ARC rocks (A1, A2 and A3) range from 0.701 to 0.715 and have a positive correlation with the silica content (Table 3; Fig. 12a). Associations A1 and A2 have the lowest ratios, ranging from 0.701 to 0.703, while the $^{87}Sr/^{86}Sr_{(i)}$ ratio of A3 is 0.715. The $\varepsilon Nd_{(t)}$ values are positive for the three associations, ranging from +0.47 to +5.19, and have a negative correlation with the SiO_2 content and $^{87}Sr/^{86}Sr_{(i)}$ ratio (Table 3; Fig. 12b, c). The evolution of the $\varepsilon Nd_{(t)}$ parameter as a function of T_{DM} follows a common evolution and reveals the sources for the three associations, with T_{DM} ages very close to the ages of igneous crystallization, indicating extraction from juvenile mantle material (Table 3; Fig. 12d).

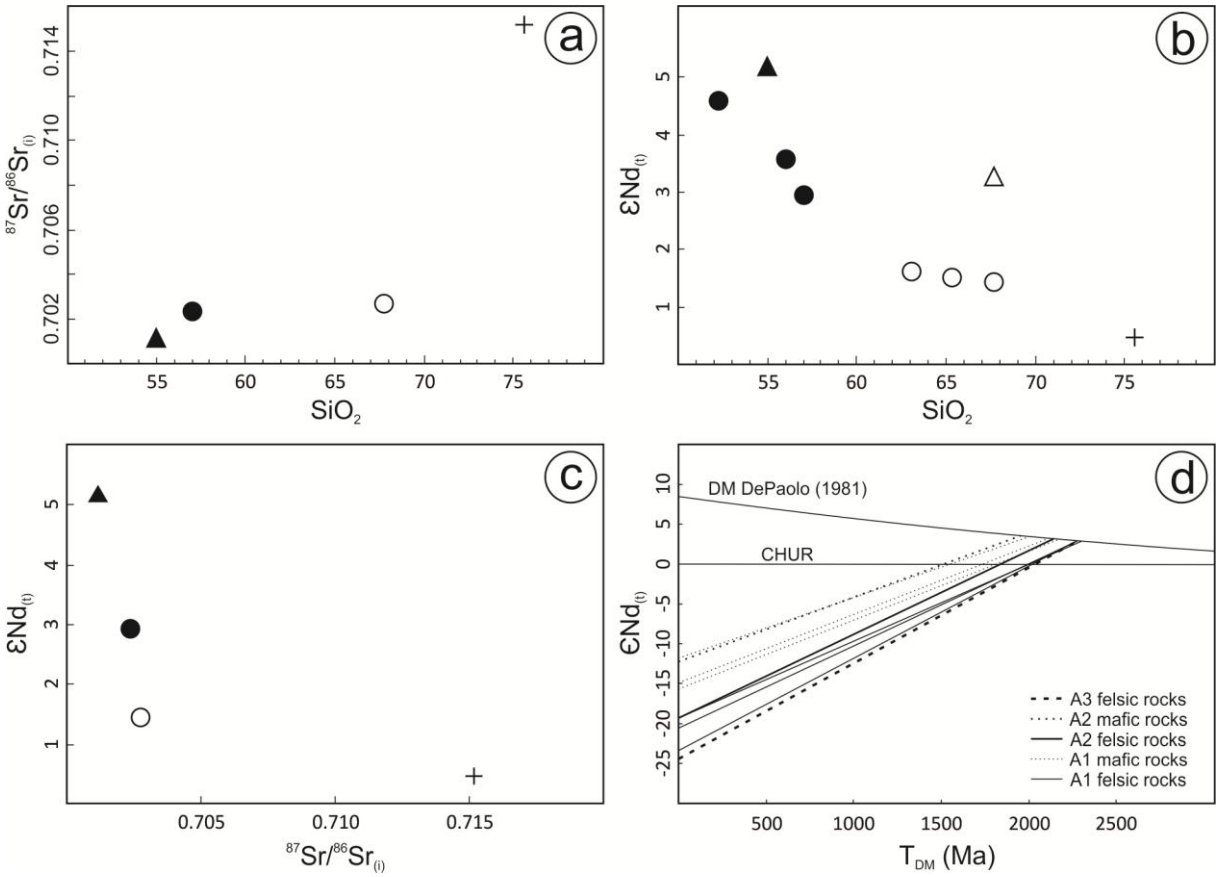

Figure 12 – Whole rock Rb-Sr and Sm-Nd isotopic data for the ARC. (a) Variation of $^{87}Sr/^{86}Sr_{(i)}$ relative to SiO_2. (b) Variation of $\varepsilon Nd_{(t)}$ relative to SiO_2. (c) Variation of $\varepsilon Nd_{(t)}$ relative to $^{87}Sr/^{86}Sr_{(i)}$. (d) Time evolution of $\varepsilon Nd_{(t)}$ as a function of T_{DM}, according to the evolution curves of the chondritic uniform reservoir (CHUR) and depleted mantle (DM) of DePaolo (1981). Symbols as in figure 6.

4.4.2 Pb-Pb in feldspars isotopic data

The results of the Pb isotopic data obtained directly from the K-feldspar in polished sections by LA-MC-ICP-MS are shown in Table 4.

The $^{208}Pb/^{204}Pb$, $^{207}Pb/^{204}Pb$, and $^{206}Pb/^{204}Pb$ ratios of A1 and A2 are similar and differ from A3. In associations A1 and A2, the $^{206}Pb/^{204}Pb$ ratio ranges from 18.0 to 18.2 and in A3 it is equal to 18.5. The $^{207}Pb/^{204}Pb$ ratio is similar among the three associations, ranging from 15.62 to 15.65. The $^{208}Pb/^{204}Pb$ ratio is also similar for associations A1 and A2, ranging from 37.3 to 37.6, and these values again differ from that of A3, $^{208}Pb/^{204}Pb = 37.1$.

Table 4 –Pb-Pb isotopic data obtained directly from feldspars in polished sections by LA-MC-ICP-MS.

sample	group	$^{206}Pb/^{204}Pb$	1σ	$^{207}Pb/^{204}Pb$	1σ	$^{208}Pb/^{204}Pb$	1σ
TG-01M	A1 metatonalite	18.192630	0.018300	15.621920	0.020500	37.413920	0.040600
		18.223150	0.005390	15.662580	0.007950	37.310290	0.018000
		18.266820	0.018400	15.656220	0.016900	37.486250	0.081600
		18.256250	0.008310	15.691370	0.012300	37.331680	0.017100
		18.254410	0.009930	15.651390	0.012500	37.540570	0.047600
	mean	18.238652	0.012066	15.656696	0.014030	37.416542	0.040980
TG-02A	A1 metatonalite	18.170660	0.025700	15.658150	0.013500	37.357430	0.021400
		18.096660	0.008120	15.634510	0.008200	37.321550	0.015400
		18.072050	0.009630	15.635650	0.006740	37.354720	0.014100
		18.059860	0.010700	15.622750	0.012100	37.354920	0.019200
		18.064850	0.009140	15.619090	0.011300	37.301950	0.021100
		18.096450	0.014200	15.647790	0.009240	37.369310	0.023800
	mean	18.093422	0.012915	15.636323	0.010180	37.343313	0.019167
TG-01S	A2 tonalite	18.097310	0.004380	15.631890	0.008440	37.504200	0.008650
		18.111880	0.004690	15.642840	0.007520	37.519850	0.010600
		18.181840	0.018000	15.623770	0.008690	37.404790	0.016200
		18.112140	0.012300	15.610540	0.012800	37.426070	0.025200
		18.142230	0.007690	15.642890	0.007950	37.512540	0.017400
		18.159220	0.010300	15.612910	0.012100	37.367720	0.027500
	mean	18.134103	0.009560	15.627473	0.009583	37.455862	0.017592
TG-02O	A2 tonalite	18.020950	0.008240	15.616270	0.011900	37.221700	0.020600
		18.086950	0.013400	15.634100	0.012500	37.347410	0.027200
		18.117950	0.009120	15.675040	0.007970	37.420560	0.021000
		18.016530	0.016300	15.605430	0.012000	37.247540	0.026400
		18.129420	0.012000	15.655220	0.011800	37.360820	0.025000
		18.079980	0.013100	15.629230	0.013800	37.303350	0.026600
	mean	18.075297	0.012027	15.635882	0.011662	37.316897	0.024467
TG-325A	A3 Tonalitic gneiss	18.518480	0.012000	15.631330	0.013000	36.993160	0.030200
		18.511850	0.014200	15.644650	0.023900	37.094190	0.037000
		18.515290	0.032700	15.646590	0.024500	37.079330	0.050200
		18.514280	0.010900	15.643260	0.012000	37.081310	0.019700
		18.532340	0.010700	15.669640	0.010800	37.099190	0.025300
		18.512230	0.014400	15.643950	0.012400	37.083740	0.024200
	mean	18.517412	0.015817	15.646570	0.016100	37.071820	0.031100

For the samples from associations A1 and A2, the results for the thorogenic (^{208}Pb) and uranogenic (^{207}Pb and ^{206}Pb) Pb isotopes indicate a common source that is compatible with the mantle (Fig. 13a) and orogen (Fig. 13b) evolution models according to Zartman & Haines (1988). The data for A3 indicate a source with a low Th/U ratio (Fig. 13a) and support the evolution of an uranogenic Pb reservoir, similar to what was found for associations A1 and A2 (Fig. 13b).

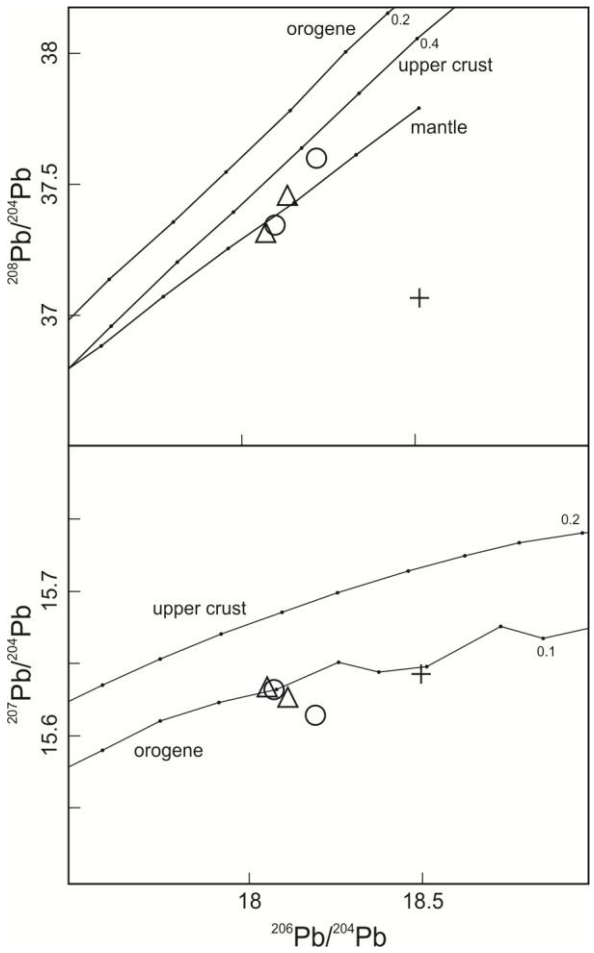

Figure 13 – Mean Pb-Pb isotopic data obtained directly from K-feldspars in polished sections by LA-MC-ICP-MS. (a) $^{208}Pb/^{204}$ *vs* $^{206}Pb/^{204}Pb$. (b) $^{207}Pb/^{204}$ *vs* $^{206}Pb/^{204}Pb$. Time intervals of 100 Ma (0.1 Ga). Symbols as in figure 6.

5. Sources and settings

The protoliths of associations A1, A2, and A3 of the ARC are interpreted as a record of igneous activity in a magmatic arc environment of an active continental margin, given their similar geochemical signature to the intermediate calc-alkaline and high-potassium series and their trace element patterns in tectonic discrimination diagrams. The tonalites, trondhjemites and granodiorites of these associations have a composition similar to those of TTG or adakitic associations from sources that are linked to the melting of a subducted plate, as discussed previously by numerous researchers (Barker, 1979; Jahn *et al.* 1981; Defant & Drummond, 1990; Springer & Seck, 1997; Martin, *et al.*, 2005), confirming the connection of the ARC rocks to a continental magmatic arc. The contemporaneity relationship with less differentiated magmas, represented by mafic-rich diorites and quartz-diorites, indicates that mantle sources played an important role in the evolution of the ARC magmatism.

The low $^{87}Sr/^{86}Sr_{(i)}$ ratios (0.701 to 0.703) of associations A1 and A2 are compatible with a mantle source that is poor in Rb and has limited influence of contamination by crustal material. The positive $\varepsilon Nd_{(t)}$ values (+1.45 to +5.19) and the T_{DM} ages close to the crystallization ages indicate their extraction from juvenile mantle material with a low crustal residence time. The Pb isotope ratios are similar between the two associations and compatible with the mantle and orogen evolutions (Fig. 13). The $^{87}Sr/^{86}Sr_{(i)}$ ratio of A3 (0.715) differs from those of A1 and A2. A3 has a lower $\varepsilon Nd_{(t)}$ value (+0.47) and a T_{DM} age that is close to its crystallization age. The Pb isotope ratio of A3 also differs

from those of associations A1 and A2 (Fig. 13) and indicate a source poor in Th (Fig. 13a). Furthermore, this association does not present a contemporaneity relationship with less differentiated magmas; A3 has lower contents of REEs (Fig. 8d) and is approximately 70 Ma younger. In addition, association A3 does not display inherited ages (Gregory *et al.*, submitted) and the composition, except for REE contents, is similar to those of the other ARC associations. Altogether, these characteristics indicate that the source that generated A3 was similar to the one that originated A1 and A2, although with some crustal contribution to A3 (as attested by its higher Rb content), but nonetheless related to the evolution of the same magmatic arc.

The correlation of the Nd isotopic parameters (Figs. 12b and 12d) with the differentiation suggests that the felsic rocks of associations A1 and A2 were subject to greater contamination by crustal material than the contemporary, less-differentiated rocks (diorites); this finding is also supported by the patterns of major and trace elements, such as the increase in the peraluminosity index, the enrichment in incompatible elements, and the strong depletion of heavy REEs (Fig. 6, 7 and 8). However, the contaminant material was not very different from the juvenile source that generated the less-differentiated rocks of the ARC. This finding is confirmed by the similar and progressive geochemical patterns, the similar and low values of the $^{87}Sr/^{86}Sr_{(i)}$ ratios (Figs. 12a and 12c), and the positive values of $\varepsilon Nd_{(t)}$ of mafic and felsic rocks of associations A1 and A2.

Although this contaminant material may have been assimilated during ascent and emplacement of magmas in the crust, given that the xenoliths found in the ARC rocks are derived from crustal rocks, the Pb isotope data indicate greater compatibility with the mantle and orogen evolutionary histories (Fig. 13). The hypothesis of contamination occurring in the lower crust, where the $^{87}Sr/^{86}Sr_{(i)}$ ratios are similar to the mantle, is also ruled out by the Pb isotope data, which discriminate between the two reservoirs (mantle and lower crust), as shown in figure 13. Thus, the contamination of juvenile magmas by crustal material could have occurred at greater depths, according to the classical models and to the conceptions of Castro (2014), who has postulated an "off-crust" model for the generation of magmas in the subduction zone. However, the "contaminant" source in question is isotopic and compositionally compatible with the ARC, or even with the evolution of basaltic magmas for the generation of the tonalitic crust or the magmatic arc crust. Thus, the influence of this source in the geochemical differentiation patterns of the ARC rocks could be masked. The isotope data confirm material with a low crustal residence time for associations A1 and A2, indicating that the contaminant could be derived from the assimilation of the crust itself, which is newly built by the arc magmatism and has a low crustal residence time, positive $\varepsilon Nd_{(t)}$ values, and low $^{87}Sr/^{86}Sr_{(i)}$ values, masking the juvenile character of the material. The existence of this "self-cannibalism" process is also reinforced by the zircon U-Pb data (collected by LA-MC-ICP-MS) obtained by Gregory *et al.* (submitted), which establish little inheritance and virtually equal ages, considering the error ranges, for associations A1 and A2, which display intrusive relations and structural differences.

According to Martin *et al.* (2014), the genesis of TTG-type associations requires the melting of LILE-enriched basalts, which is not compatible with melting of the oceanic crust or of depleted mantle. Those authors postulate that, in association with the melting of oceanic plates in subduction zone, these associations were generated by plumes rooted in the lower mantle (non-depleted mantle), generating an enriched mid-ocean ridge basalt (E-MORB). While the ARC rocks exhibit values close to the E-MORB (1 to 10), it is unlikely that they were generated from the partial melting of a rock with this composition, but very plausible that they have a source similar to one that generates this type of basalt, or an enriched mantle. Thus, the ARC rock composition closely resembles that of the E-MORB because of the enrichment of the metasomatized mantle wedge. The mixing with crustal melts (arc crust) imprinted the transitional character between the classic calc-alkaline arc associations (metasomatized mantle wedge melt) and the TTG/adakitic type (subducted plate melt) associations.

The complex intercalation of magma pulses in both time and space, with simultaneous local variations in the deformation field, has been demonstrated and interpreted by several authors (Bitencourt, 1996; Annen, 2011; Saint-Blanquat *et al.*, 2011; Menand *et al.*, 2011; Miller *et al.*, 2011; Vernon *et al.*, 2012; Florisbal *et al.*, 2012a, b) as the record of multi-scale events responsible for the building of plutons and batholiths in magmatic arcs or transpressive environments, and serves as a comparative base for the complex lithologic-structural-temporal relations that the ARC rocks display. Likewise, Ramos (2010) cites the abrupt changes in the subduction regime of the eastern Pacific coast of the Americas (contraction, neutral, extension) and their influence on the composition of volcanism, noting sensitive changes in magma composition caused by more or less opening of spaces and channels during each phase, as well as more or less decompression and melting of the lithospheric mantle. The intraplate slip regimes are also crucial in the evolution of continental arcs, as in the case of the intra-arc Liquiñe-Ofqui fault zone (Thomson, 2002) in the central Andes, where active volcanoes are aligned (Ramos, 2010). The structural variation observed between associations A1 and A2 is accompanied by a subtle change in the geochemical patterns of these associations, indicating that some petrogenetic changes accompanied this tectonic shift, though in the same type of environment, that is, a continental magmatic arc that was associated with oceanic plate subduction. This change is recorded both in the more-differentiated rocks (tonalites) and in the less-differentiated rocks (diorites) of both associations. The felsic rocks of A2 exhibit a greater variation in the degree of fractionation of the REEs compared to the A1 rocks, which could be attributed to the presence of garnet in the melt residue and would indicate sources at different depths or with different amounts of garnet. The mafic rocks of A2, on the other hand, exhibit characteristics that suggest a higher melting rate of the mantle, as evidenced by the slight enrichment of Nb and Ta in relation to the A1 rocks, which shifts these rocks from the graph field of calc-alkaline basalts towards the enriched intraplate MORB field or the tholeiitic field.

The three studied associations display two recrystallization episodes, one of high temperature and one of low temperature. The low temperature episode is compatible with the Neoproterozoic Southern Brazilian Shear Belt conditions. The high-temperature episode appears to have occurred prior to the SBSB, perhaps conditioned by the high-grade metamorphism related to a collision that is observed further west at the Várzea do Capivarita Complex (Martil *et al.*, 2011). The geochronological data obtained by Gregory *et al.* (submitted) indicate a thermal event at 635 ± 6 Ma, recorded as a metamorphic overgrowth in zircon crystals with an igneous core of Paleoproterozoic age.

6. Conclusions

The rocks of associations A1 and A2 of the ARC record the igneous activity of a magmatic arc of an active continental margin in the Paleoproterozoic. The geochemical data indicate melting of metasomatized lithospheric mantle in the subduction zone. The resulting magmas evolved by processes of assimilation and fractional crystallization. The contaminant agent is the crust itself, which was newly built by the magmatic arc, suggesting "self-cannibalism" of the arc. The different structural patterns and nearly identical ages indicate that the tectonic changes between the two associations occurred in a very short time interval, analogous to the temporal and spatial variations observed in the construction of plutons and batholiths. Although the similarity of the felsic rocks with the TTG-type associations indicates subduction plate melting, the data presented herein indicate that other processes were able to generate such a signature, such as the assimilation of and mixture with magmas derived from the melting of crust newly built by the magmatic arc.

The similar chemical composition and similar $\varepsilon Nd(t)$ values to those for associations A1 and A2 indicate that A3 has a source that is similar to the one that generated the felsic rocks of A1 and A2,

possibly the crust that was newly built by the arc. However, the different value for Pb and higher value of the $^{87}Sr/^{86}Sr_{(i)}$ ratio indicate that another crustal source was also active during the A3 magmatism. The greater degree of crustal participation, the lack of associated basic rocks, and the younger age possibly mark the more mature or late stages of the arc.

Acknowledgements

This work had partial financial support from the National Research Council (CNPq) to M.F. Bitencourt (Universal Project n. 471266/2010-8) and from the Rio Grande do Sul State Research Foundation (FAPERGS) to L. Nardi (Proc. n. 10.16039), as well as a PhD research grant from CNPq to T.R. Gregory.

References:

Almeida, F.F.M., Hasui, Y., Brito Neves, B.B. & Fuck, R.A. 1981. Brazilian structural provinces: an introduction. *Earth-Science Reviews*, *17*(1): 1-29.

Annen, C. 2011. Implications of incremental emplacement of magma bodies for magma differentiation, thermal aureole dimensions and plutonism-volcanism relationships. *Tectonophysics*. 500: 3-10.

Babinski, M., Chemale Jr., F., Hartmann, L.A., Van Schmus, W.R. & Silva, L.C. 1996. Juvenile accretion at 750-700 Ma in southern Brazil. *Geology*, 24(5):439-442.

Barker, E. 1979. *Trondhjemites, dacites, and related rocks*. New York, Elsevier, 659p.

Bitencourt, M.F. 1996. Granitóides sintectônicos da região de Porto Belo, SC: uma abordagem petrológica e estrutural do magmatismo em zonas de cisalhamento. Porto Alegre, 310p. Tese de doutorado, Programa de Pós-graduação em Geociências, Instituto de Geociências, Universidade Federal do Rio Grande do Sul.

Bitencourt, M.F., De Toni, G.B., Florisbal, L.M., Martil, M.M.D., Niessing, M., Gregory, T.R., Nardi, L.V.S., Heaman, L.M., Dufrane, S.A. 2011. Structural geology and U-Pb age of unusual Neoproterozoic syn-collisional syenite-tonalite association from southernmost Brazil. *In:* Seventh Hutton Symposium on Granites and Related Rocks, 2011, Avila. *Abstracts Book*. Avila: Universidad de Salamanca, v.u.p. 21-21.

Bitencourt, M.F. & Nardi, L.V.S. 1993. Late- to Post-collisional Brasiliano Magmatism in Southernmost Brazil. *Anais da Academia Brasileria de Ciências*, 65: 3-16.

Bitencourt, M.F. & Nardi, L.V.S. 2000. Tectonic setting and sources of magmatism related to the southern Brazilian shear belt. *Revista Brasileira de Geociências*, 30(1): 186-189.

Boynton, W.V. 1984. Cosmochemistry of the rare earth elements: meteoritic studies. *In*: Henderson, P. (ed.) *Rare Earth Elements Geochemistry*. Amsterdam, Elsevier, p. 63–114.

Camozzato, E., Philipp, R.P. & Chemale Jr., F. 2013. Idades Estaterianas e Calimianas no Domo da Vigia: Complexo Vigia e Porongos, Metagranito Seival e Anfibolito Tupi Silveira, Bagé, RS. *In*: XI Simpósio Nacional de Estudos Tectônicos. *Anais*...(CD). Ouro Preto, MG.

Castillo, P.R., Lonsdale, P.F., Moran, C.L. & Hawkins, J.W. 2009. Geochemistry of mid-Cretaceous Pacific crust being subducted along the Tonga–Kermadec Trench: Implications for the generation of arc lavas. *Lithos*, 112(1): 87-102.

Castillo, P.R. 2012. Adakite petrogenesis. *Lithos*, 134: 304-316.

Castro, A. 2014. The off-crust origin of granite batholiths. *Geoscience Frontiers*, 5(1): 63-75.

Condie, K.C. 2005. TTGs and adakites: are they both slab melts? *Lithos*, 80: 33-44.

Cox, K.G., Bell, J.D. & Pankhurst, R.J. 1979. *The interpretation of igneous rocks*. London, George, Allen and Unwin.

Defant, M.J. & Drummond, M.S. 1990. Derivation of some modern arc magmas by melting of Young subducted lithosphere. *Nature*, 347:662-665.

DePaolo, D.J. 1981. Neodymium isotopes in the Colorado Front Range and crust–mantle evolution in the Proterozoic. *Nature*, 29(1): 193–196.

D'Lemos, R.S., Brown, M. & Strachan, R.A. 1992. Granite magma generation, ascent and emplacement within a transpressional orogen. *Journal of the Geological Society of London*, 149:487-490.

Drummond, M.S., Defant, M.J. 1990. A model for trondhjemite-tonalite-dacite genesis and crustal growth via slab melting: Archaean to modern comparisons. *Journal of Geophysics Research*. 95: 21503-21521.

Fernandes, L.A.D. & Koester, E. 1999. The Neoproterozoic Dorsal de Canguçú strike-slip shear zone: its nature and role in the tectonic evolution of southern Brazil. *Journal of African Earth Sciences*, 1: 3-24.

Florisbal, L.M., Bitencourt, M.F., Janasi, V.D.A., Nardi, L.V.S. & Heaman, L.M. 2012a. Petrogenesis of syntectonic granites emplaced at the transition from thrusting to transcurrent tectonics in post-collisional setting: Whole-rock and Sr–Nd–Pb isotope geochemistry in the Neoproterozoic Quatro Ilhas and Mariscal Granites, Southern Brazil. *Lithos*, 153: 53-71.

Florisbal, L.M., Janasi, V.A., Bitencourt, M.F., Heaman, L.M. 2012b. Space-time relation of post-collisional granitic magmatism in Santa Catarina, southern Brazil: U-Pb LA-MC-ICP-MS zircon geochronology of coeval mafic-felsic magmatism related to the Major Gercino Shear Zone. *Precambrian Research*, 216-219: 132-151.

Frantz J.C., McNaughton N.J., Marques J.C., Hartmann L.A., Botelho, N.F., Caravaca, G. 2003. SHRIMP U-Pb zircon ages of granitoids from southernmost Brazil: constraints on the temporal evolution of the Dorsal de Canguçu Transcurrent Shear zone and the eastern Dom Feliciano Belt. *In:* IV South American symposium of isotope geology. *Short papers…*(p. 174–177). Salvador, Brazil.

Frost, B.R., Barnes, C., Collins, W.J., Arculus, R.J., Ellis, D.J. & Frost, C.D. 2001. A geochemical classification for granitic rocks. *Journal of Petrology*, 42: 2033-2048.

Garavaglia, L., Bitencourt, M.F. & Nardi, L.V.S. 2002. Cumulatic Diorites Related to Post-collisional, Brasiliano/Pan-African Mafic Magmatism in the Vila Nova Belt, Southern Brazil. *Gondwana Research*, 5:519-534.

Garavaglia, L., Koester, E., Bitencourt, M.F. & Nardi, L.V.S. 2006. Isotopic Signature of Late magmatic Arc to Post-collisonal Magmatism in the Vila Nova Belt, Southern Brazil. *In*: South-American Symposium on Isotope Geology, 5, 2006, Punta del Este. *Short Papers...*(p. 101-104). Punta del Este, Universidad de la Republica.

Gregory, T.R., Bitencourt, M.F., Nardi, L.V.S., Florisbal, L.M. & Chemale Jr., F. Geochronological data from TTG-type association of the Arroio dos Ratos Complex and implications for crustal evolution of southernmost Brazil in Paleoproterozoic times. *Journal of South American Earth Sciences* (*submitted*).

Gregory, T.R., Bitencourt, M.F. & Nardi, L.V.S. 2011. Caracterização estrutural e petrológica de metatonalitos e metadioritos do Complexo Arroio dos Ratos na sua seção-tipo, região de Quitéria, RS. *Pesquisas em Geociências*, 38(1): 85-108.

Hartmann, L.A., Leite, J.A.D., Silva, L.C., Remus, M.V.D., McNaughton, N.J., Groves, D.I., Fletcher, I.R., Santos, J.O.S. & Vasconcellos, M.A.Z. 2000. Advances in SHRIMP geochronology and their impact on understanding the tectonic and metallogenic evolution of southern Brazil. *Australian Journal of Earth Sciences*, 47:829-844.

Haskin, L.A., Haskin, M.A., Frey, F.A. & Wildeman, T.R. 1968. Relative and absolute terrestrial abundances of the REE. *In:* Ahrens, L.H. (Ed.). *Origin and Distribution of the Elements*. New York, Pergamon Press, p. 889-912.

Hidalgo, S., Gerbe, M.C., Martin, H., Samaniego, P. & Bourdon, E. 2012. Role of crustal and slab components in the Northern Volcanic Zone of the Andes (Ecuador) constrained by Sr–Nd–O isotopes. *Lithos*, 132: 180-192.

Irvine, T.N. & Baragar, W.R.A. 1971. A guide to the chemical classification of the common volcanic rocks. *Canadian Journal of Earth Sciences*, 8: 523-548.

Jahn, B.M., Glikson, A.Y., Peucat, J.J. & Hickman, A.H. 1981. REE geochemistry and isotopic data of Archean silicic volcanics and granitoids from the Pilbara Block, Western Australia: implications for the early crustal evolution. *Geochimica et Cosmochimica Acta*, 45: 1633-1652.

Jensen, L.S. 1976. A new cation plot for classifying subalkalic volcanic rocks. *Ontario Division of Mines, Miscellaneous Paper*, 6: 1-22.

Knijnik, D.B., Bitencourt, M.F., Gregory, T.R. 2013. A Zona de Cisalhamento Quitéria-Serra do Erval e o magmatismo sintectônico precoce do Cinturão de Cisalhamento Sul-brasileiro. *In*: XI Simpósio Nacional de Estudos Tectônicos. *Anais...*(CD) Ouro Preto, MG.

Knijnik, D.B., Bitencourt, M.F., Nardi, L.V.S., Pinto, V.M., Fontana, E. 2012. Caracterização Geoquímica do Granodiorito Cruzeiro do Sul: magmatismo shoshonítico pós-colisional neoproterozoico em zona de transcorrência, região de Quitéria, RS. Geol. USP, Sér. Cient., São Paulo, v. 12, n. 1, p. 17-38.

Koester, E., Chemale Jr., F., Porcher, C.C., Bertotti, A.L. & Fernandes, L.A.D. 2008. U-Pb ages of granitoids from Eastern Sul-riograndense Shield. *In*: VI South American Symposium on Isotope Geology. *Anais…*(p. 95). San Carlos de Bariloche, Argentina.

Kruhl, J.H. 1996. Prism- and basis-parallel subgrain boundaries in quartz: a microstructural geothermobarometer. *Journal of Metamorphic Geology*, 14: 581-589.

Le Maitre, R.W. 2002. *Igneous Rocks: A Classification and Glossary of Terms. Recommendations of the International Union of Geological Sciences, Subcommission on the Systematics of Igneous Rocks*. Cambridge University Press.

Machado, A., Chemale Jr, F., Conceição, R.V., Kawaskita, K., Morata, D., Oteíza, O. & Van Schmus, W.R. 2005. Modeling of subduction components in the genesis of the Meso-Cenozoic igneous rocks from the South Shetland Arc, Antarctica. *Lithos*, :82(3): 435-453.

Maniar, P. D. & Piccoli, P. M. 1989. Tectonic discrimination of granitoids. *Geological Society of America Bulletin*, 101: 635-643.

Martil, M.M.D., Bitencourt, M.F., Armstrong, R., Nardi, L.V.S., Chemale Jr., F. Geochronology of orthogneisses from the Várzea do Capivarita Complex thrust pile and implications for the timing of continental collision in southernmost Brazil. *Precambrian Research* (*submitted*).

Martil, M.M.D., Bitencourt, M.F. & Nardi, L.V.S. 2011. Caracterização estrutural e petrológica do magmatismo pré-colisional do Escudo Sul-rio-grandense: os ortognaisses do Complexo Metamórfico Várzea do Capivarita. *Pesquisas em Geociências*, 38(2): 181-201.

Martin, H. 1986. Effect of steeper Archaean geothermal gradient on geochemistry of subduction-zone magmas. *Geology*. 14: 753-756.

Martin, H. 1993. The mechanisms of petrogenesis of the Archaean continental crust – Comparison with modern processes. *Lithos*, 30: 373-388.

Martin, H. 1999. Adakitic magmas: modern analogues of Archaean granitoids. *Lithos*. 46: 411-429.

Martin, H., Smithies, R.H., Rapp, R., Moyen, J.F. & Champion, D. 2005. An overview of adakite, tonalite-trondhjemite-granodiorite (TTG), and sanukitoid: relationships and some implications for crustal evolution. *Lithos*, 79:1-24.

Martin, H., Moyen, J.F., Guitreau, M., Blichert-Toft, J. & Le Pennec, J.L. 2014. Why Archaean TTG cannot be generated by MORB melting in subduction zones. *Lithos*, 198: 1-13.

Masuda, A., Nakamura, N., Tanaka, T. 1973. Fine structures of mutually normalized rare earth patterns of chondrites. *Geoch. Cosmochim. Acta*. 37: 239-248.

Menand, T., Saint-Blanquat, M., Annen, C. 2011. Emplacement of magma pulses and growth of magma bodies. *Tectonophysics*. 500: 1-2.

Miller, C.F., Furbish, D.J., Walker, B.A., Claiborne, L.L., Koteas, G.C., Bleick, H.A., Miller, J.S. 2011. Growth of plutons by incremental emplacement of sheets in crystal-rich host: Evidence from Miocene intrusions of the Colorado River region, Nevada, USA. *Tectonophysics*. 500: 65-77.

Moyen, J.F., & Martin, H. 2012. Forty years of TTG research. *Lithos*, 148: 312-336.

Moyen, J.F., Martin, H., & Jayananda, M. 2001. Multi-element geochemical modelling of crust–mantle interactions during late-Archaean crustal growth: the Closepet granite (South India). *Precambrian Research*, 112 (1): 87-105.

Miyashiro, A. 1974. Volcanic rocks series in island arcs and active continental margins. *American Journal of Science*, 274: 321-355.

Nardi, L.V.S. & Bitencourt, M.F.A.S. 2007. Magmatismo granítico e evolução crustal no sul do Brasil. *In*: Iannuzzi, R. & Frantz, J.C. (Ed.). *50 Anos de Geologia. Instituto de Geociências. Contribuições.* Porto Alegre, Editora Comunicação e Identidade, CIGO e IG-UFRGS, p. 125-141.

Passchier, C.W. & Trouw, R.A. 2005. *Microtectonics*. Berlin, Springer, 366p, 2ed.

Pearce, J.A. 1982. Trace elements characteristics of lavas from destructive plate boundaries. *In:* Thorpe, R.S. (ed.), *Andesites*. Wiley, Chichester, p. 525-548.

Pearce, J.A. 1996. Sources and settings of granitic rocks. *Episodes*, 19(4):120-125.

Pearce, J.A., Harris, N.B.W. & Tindle, A.G. 1984. Trace element discrimination diagrams for the tectonic interpretation of granitic rocks. *Journal of Petrology*, 25: 956-983.

Peccerillo, A., Dallai, L., Frezzotti, M.L. & Kempton, P.D. 2004. Sr–Nd–Pb–O isotopic evidence for decreasing crustal contamination with ongoing magma evolution at Alicudi volcano (Aeolian arc, Italy): implications for style of magma-crust interaction and for mantle source compositions. *Lithos*, 78(1): 217-233.

Ramos, V.A. 2010. The tectonic regime along the Andes: Present-day and Mesozoic regimes. *Geological Journal*, 45 (1): 2-25.

Rapp, R.P., Shimizu, N., Norman, M.D. & Applegate, G.S. 1999. Reaction between slab-derived melts and peridotite in the mantle wedge: experimental constraints at 3.8 GPa. *Chemical Geology*, 160(4): 335-356.

Rapp, R.P., Watson, E.B. & Miller, C.F. 1991. Partial melting of amphibolites/eclogite and the origin of Archean trondhjemites and tonalites. *Precambrian Research*, 51: 1-25.

Saalmann, K., Gerdes, A., Lahaye, Y., Hartmann, L.A., Remus, M.V.D. & Läufer, A. 2011. Multiple accretion at the eastern margin of the Rio de la Plata craton: the prolonged Brasiliano orogeny in southernmost Brazil. *International Journal of Earth Sciences*, 100 (2-3): 355-378.

Saint-Blanquat, M., Horsman, E., Habert, G., Morgan, S., Vanderhaeghe, O., Law, R., Tikoff, B. 2011. Multiscale magmatic cyclicity, duration of pluton construction, and the paradoxical relationship between tectonism and plutonism in continental arcs. *Tectonophysics*. 500: 20-33.

Sato, K., Tassinari, C.C.G., Kawashita, K., Petronilho, L. 1995. O método geocronológico Sm-Nd no IG/USP e suas aplicações. *Anais da Academia Brasileira de Ciências*, 67: 315-336.

Schiano, P., Clocchiatti, R., Shimizu, N., Maury, R.C., Jochum, K.P. & Hofmann, A.W. 1995. Hydrous, silica-rich melts in the sub-arc mantle and their relationship with erupted arc lavas. *Nature*, 377(6550): 595-600.

Sommer, C.A., Philipp, R.P., Lima, E.F., Basei, M.S., Oliveira, D.S. & Filho, J.N. 2013. Geoquímica e geocronologia das rochas riolíticas associadas ao Batólito Pelotas, porção oriental do Escudo Sul-rio-grandense: dados preliminares. *In:* XIV Congresso Brasileiro de Geoquímica. *Anais...*(CD). Diamantina-MG.

Sorensen, S.S. & Grossman, J.N. 1989. Enrichment of trace elements in garnet amphibolites from a paleo-subduction zone: Catalina Schist, southern California. *Geochimica et Cosmochimica Acta*, 53(12): 3155-3177.

Springer, W. & Seck, H.A. 1997. Partial fusion of basic granulites at 5 to 15 kbar: implications for the origin of TTG magmas. *Contributions to Mineralogy and Petrology*, 127: 30-45.

Sun, S.S. & McDonough, W. 1989. Chemical and isotopic systematics of oceanic basalts: implications for mantle composition and processes.*Geological Society, London, Special Publications*, 42(1): 313-345.

Thomson, S.T. 2002. Late Cenozoic geomorphic and tectonic evolution of the Patagonian Andes between latitudes 42°S and 46°S: an appraisal based on fission- track results from the transpressional intra-arc Liquiñe-Ofqui fault zone. *Geological Society of America Bulletin*. 114 (9): 1159–1173.

Vernon, R.H., Collins, W.J., Cook, N.D.J. 2012. Metamorphism and deformation of mafic and felsic rocks in a magma transfer zone, Stewart Island, New Zealand. *Journal of Metamorphic Geology*. 30 (5): 473-488.

Wilson, M. 1989. *Igneous Petrogenesis*. Londres, Chapman & Hall, 466p.

Wood, D.A. 1980. The application of a Th-Hf-Ta diagram to problems of tectonomagmatic classification and to establishing the nature of crustal contamination of basaltic lavas of the British Tertiary volcanic province. *Earth Planet. Sci. Lett*. 50: 11-30.

Zartman, R.E. & Haines, S.M. 1988. The plumbotectonic model for Pb isotopic systematics among major terrestrial reservoirs – a case for bi-directional transport. *Geochimica et Cosmochimica Acta*, 52(6): 1327-1339.

3.3 Artigo 3 submetido à revista Gondwana Research

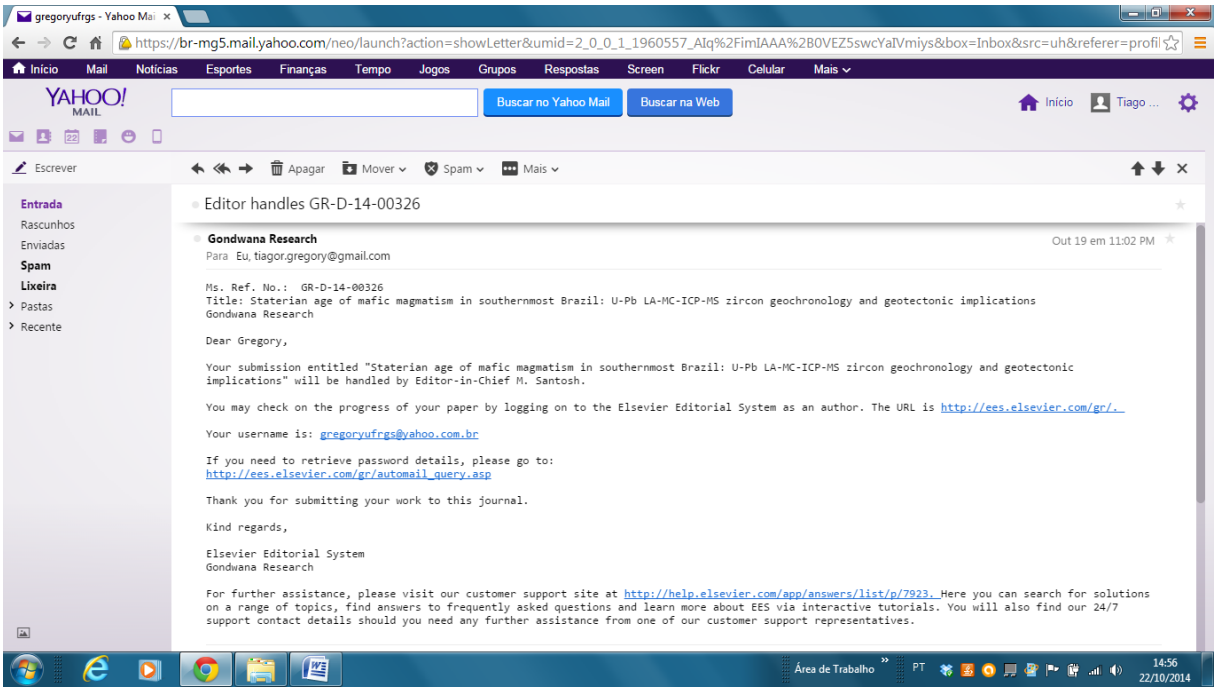

Staterian age of mafic magmatism in southernmost Brazil: U–Pb LA-MC-ICP-MS zircon geochronology and geotectonic implications

Gregory, T.R.[1]*, Bitencourt, M.F.[1], Florisbal, L.M.[2] & Nardi, L.V.S.[1]

[1] Instituto de Geociências, Universidade Federal do Rio Grande do Sul, Av. Bento Gonçalves, 9500, Porto Alegre, RS, Brasil. CEP 91501-970

[2] Serviço Geológico do Brasil - CPRM. Rua Costa, 55 - Cerqueira César - São Paulo - SP - Brasil. CEP 01304-010

* Corresponding author. Tel.: +15 51 9725 1566

E-mail address: gregoryufrgs@yahoo.com.br (T.R. Gregory)

Keywords

Staterian mafic magmatism, mafic dykes, anorogenic environment, Sul-rio-grandense Shield.

Highlights

A Staterian igneous age value (1,716 ± 72 Ma) was obtained in zircons from an amphibolite that crosscuts Paleoproterozoic high-grade paragneisses.

Dated amphibolite is interpreted as a former mafic dike and correlated to the Florida dyke swarm in Uruguay.

The mafic magmatism signals a Staterian anorogenic to taphrogenic period in southernmost Brazil.

Abstract

This paper presents U-Pb LA-MC-ICP-MS zircon ages from a mafic rock intrusive in the Paleoproterozoic Arroio dos Ratos Complex (ARC), southernmost Brazil. The ARC is part of the basement for the Neoproterozoic granitic magmatism related to the Southern Brazilian Shear Belt, a lithospheric-scale transcurrent structure active between 650 and 580 Ma. The largest volume of ARC rocks corresponds to metamorphosed TTG-type rock associations with igneous age ranging from 2150 to 2070 Ma. A subordinate volume comprises high-grade paragneisses, mostly pelitic but also calc-silicate, which exhibit similar structural relations as observed in the orthometamorphic varieties. The studied rock was taken from a discordant amphibolite body interpreted as a former mafic dyke. The selected zircon crystals are dark-coloured, metamict and have no apparent zoning. Despite the high discordance, the results provide an upper intercept discordia age of 1,716 ± 72 Ma interpreted as the protholith magmatic crystallization age. The lower intercept discordia age of 635 ± 130 Ma is attributed to the amphibolite facies metamorphism. This metamorphic age is also identified in a concordant $^{207}Pb/^{206}Pb$ 624 ± 7 Ma age obtained in one of the clear zircon crystals. The data presented here are the first Staterian age value obtained from mafic rocks in southern Brazil, and they are correlated in age and composition with the well-known Florida dyke swarm in Uruguay, interpreted as tholeiitic, anorogenic to taphrogenic magmatism. The ARC is here interpreted to represent the register of a mid- to late Rhyacian continental magmatic arc, followed by a Staterian anorogenic, or maybe

even a taphrogenic stage. Unlike previous interpretations, the Staterian record identified in southern Brazil is here interpreted to most likely correspond to juvenile accretion in a within-plate environment.

1. Introduction

The southern portion of the Mantiqueira Province (Fig. 1) (Almeida et al., 1981) corresponds to an extensive Neoproterozoic mobile belt which registers the collision between the Kalahari and Rio de la Plata cratons and eventually led to the amalgamation of West Gondwana supercontinent. The eastern part of this crustal segment features a wide shear belt comprised of several, anastomosing shear zones that extends from the state of Santa Catarina (south Brazil) to Uruguay. In southern Brazil, this set of translithospheric structures is designated Southern Brazilian Shear Belt (SBSB) and its discontinuities are thought to have conditioned Neoproterozoic post-collisional magmatism (Bitencourt & Nardi, 1993; 2000; Florisbal et al., 2012) under transcurrent kinematics between 630 and 580 Ma. To the west, a supracrustal metamorphic belt separates the SBSB from Neoproterozoic rock sequences attributed to mature continental magmatic arc environment (Garavaglia et al., 2002; 2006) of 704 ± 13 Ma (U-Pb in zircon – Babinski et al., 1996) that are partially hidden under Cambrian to Neoproterozoic volcanosedimentary cover sequences. As part of this metamorphic belt, the country rocks for the SBSB granitoids are represented by the Varzea do Capivarita Complex (as defined by Martil et al., 2011), comprised of a multi-scale interleaving of ortho- and paragneisses metamorphosed at ca. 650 Ma, where the igneous protoliths represent a mature magmatic arc association of ca. 790 Ma (Martil et al., submitted), and ca. 640 Ma syntectonic syenite magmatism (Bitencourt et al., 2011). This unit is interpreted as a thrust pile by Martil et al. (submitted) and signals the main collisional episode at 650 Ma in southern Brazil. Further to the west and southwest, Archaean and Paleoproterozoic associations are found within the remnants of the Rio de la Plata Craton in Brazil and Uruguay, as pointed out by Hartmann et al. (2000).

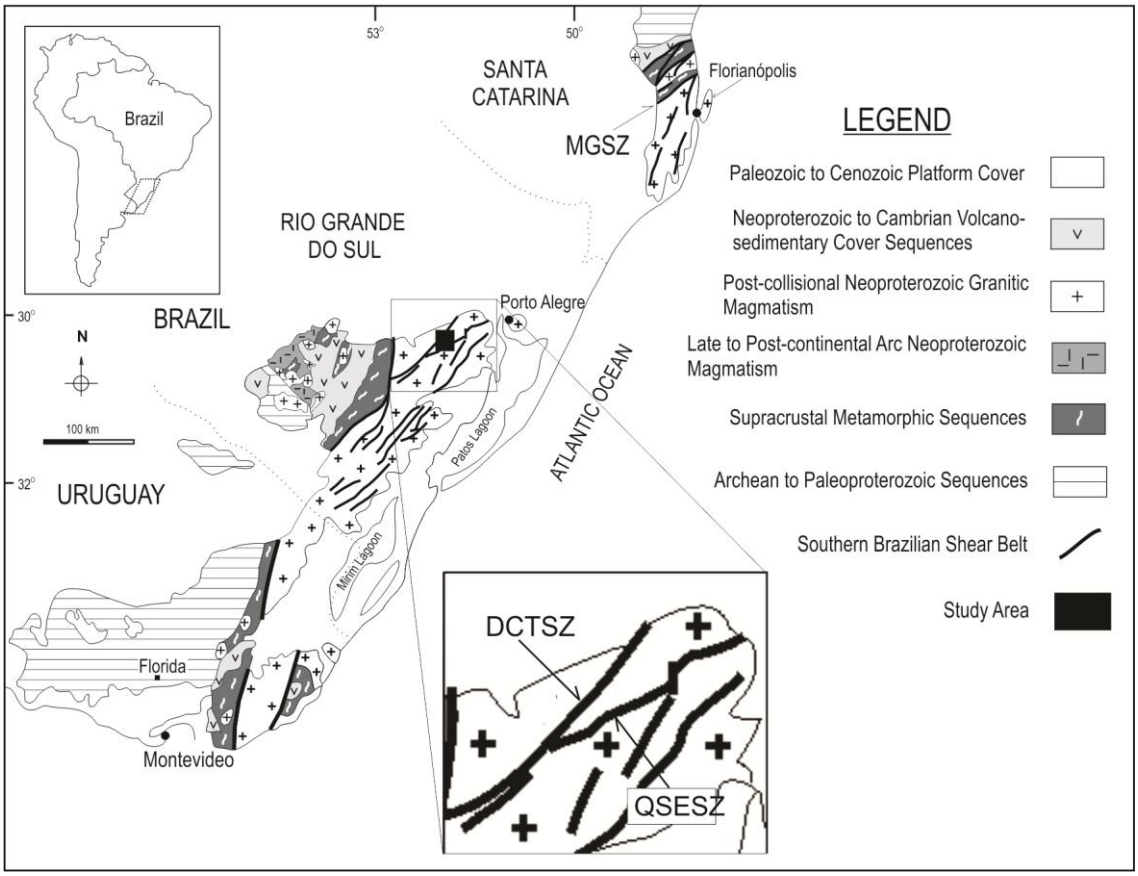

Figure 1 – Main geotectonic units from southern Brazil and Uruguay, with location of the study area (modified from Nardi & Bitencourt, 2007). MGSZ – Major Gercino Shear Zone; DCTSZ – Dorsal de Canguçu Transcurrent Shear Zone; QSESZ – Quitéria-Serra do Erval Shear Zone.

The Transamazonian (2.26-2.00 Ga) and Brasiliano (900-535 Ma) orogenic cycles are the main record of geological activity in this crustal segment, as recognized by several authors (*e.g.* Chemale Jr, 2000; Hartmann *et al.*, 2007). The Paleoproterozoic record is present mainly on the western side of Rio Grande do Sul shield areas, known as the Sul-rio-grandense Shield (SrgS) (Fig. 1), where the Santa Maria Chico Granulite Complex has yielded magmatic ages of 2.5 to 2.1 Ga (zircon U-Pb SHRIMP – Hartmann *et al.*, 2007). Paleoproterozoic rock sequences are also found in the northern part of Santa Catarina, as the *ca.* 2.16 Ga Camboriú Complex (Silva *et al.*, 2000).

References to Paleoproterozoic rocks in the Central and Eastern portions of this Mantiqueira Province segment are scattered, and the latter one features mainly the record of Neoproterozoic Brasiliano / Pan-African Cycle. In the central portion of the SrgS, the Paleoproterozoic record is found in the basement remnants of a supracrustal metamorphic belt (Fig. 1), as TTG-type rock associations, where igneous age values are referred by Chemale Jr. (2000 – 2,263 ± 18 Ma and 2,363 ± 6 Ma, U-Pb SHRIMP), Saalmann *et al.* (2011 – 2,234 ± 28 Ma, U-Pb LA-ICP-MS) and Camozzato *et al.* (2013 – 2,112 ± 22 Ma and 2,153 ± 20 Ma, U-Pb LA-MC-ICP-MS). Additional data on Paleoproterozoic rocks of the eastern part are provided by Leite *et al*. (2000 – 2,078 ± 13 Ma) and Gregory *et al.* (submitted a – 2,150 to 2,070 Ma).

The occurrence of late Paleoproterozoic (Staterian) to Mesoproterozoic tectono-stratigraphic units is rare in the SrgS. However, provenance studies carried out in Neoproterozoic basins have demonstrated the presence of Mesoproterozoic and late Paleoproterozoic (1,434 to 1,149 Ma – Bicca

et al., 2013; 1,782 to 1,352 Ma – Hartmann *et al.*, 2008) zircon grains whose source-rocks have yet to be found, or are only rarely mentioned.

Mesoproterozoic and Late Paleoproterozoic ages are also found in inherited zircons belonging to Neoproterozoic volcanic rocks (900 to 1,100 Ma and 1,777 ± 26 Ma – Almeida *et al.*, 2012; 1,323 ± 61 Ma and 1,836 ± 23 – Janikian *et al.*, 2012). Sm-Nd data obtained in volcanic rocks from the eastern part of the Neoproterozoic basin by Janikian *et al*. (2012) point to a single source, of Paleoproterozoic model age. Provenance studies by Gruber *et al*. (2011) in metasedimentary rocks, central part of the SrgS, indicate a wide range of Mesoproterozoic (1,000 to 1,600 Ma) and Late Paleoproterozoic (1700 a 1900 Ma) detrital zircon ages.

A Mesoproterozoic U-Pb zircon igneous age (LA-MC-ICP-MS) of 1,573 ± 21 Ma is reported by Chemale Jr. *et al.* (2011) in the Capivarita Anorthosite, and a similar, igneous value (1,567 ± 21 Ma; LA-MC-ICP-MS) is found in nearby amphibolites (Camozzato *et al.*, 2013). In the central supracrustal metamorphic belt (Fig. 1), the same authors report two Staterian U-Pb zircon age (LA-MC-ICP-MS) values of 1,785 ± 42 Ma and 1,768 ± 24 Ma from metagranites intrusive in orthogneisses, and one value of 1,764 ± 29 Ma from a mylonitic granitoid lying concordant within the supracrustal rocks.

In the extension of these shield areas into Uruguay (Fig. 1), Halls *et al.* (2001) present a U-Pb baddeleyite age value of 1,790 ± 5 Ma for the mafic dyke swarm that crosscuts Archaean to Paleoproterozoic rocks in the region of Florida.

This paper presents a new, U-Pb zircon Staterian age value obtained from a mafic dyke within the Arroio do Ratos Complex (Gregory *et al.*, 2011). Since this is the first Staterian age value obtained in mafic dykes from the Sul-rio-grandense Shield, the results are compared with the ones obtained in similar rocks from Uruguay in order to investigate possible correlations and implications for Paleoproterozoic geotectonic environment and crustal evolution in southernmost Brazil.

2. Local geology

The Arroio dos Ratos Complex (ARC) is mostly comprised of Paleoproterozoic (2,150 ± 28 to 2,077 ± 13 Ma) TTG-type rock associations with coeval mafic magmatism bearing a continental magmatic arc geochemical signature, as defined by Gregory *et al*. (submitted a, b). In the study area it is limited by two shear zones (Fig. 2 and inset of Fig. 1) along which Neoproterozoic post-collisional granites are positioned. The Dorsal de Canguçu (Fernandes & Koester, 1999) and Quitéria-Serra do Erval shear zones (Knijnik *et al.*, 2013) have their minimum interval of activity (658 to 605 Ma) limited by the magmatic age of their syntectonic granites, as determined by Frantz *et al.* (2003), Koester *et al.* (2008), and Knijnik *et al.* (2012). Later reactivation of these shear zones, possibly under lower-temperature and shallower conditions, are marked by quartz-mylonites and phyllonites in discontinuous ridges (Fig. 2) currently under investigation, whose movement ages are not yet precisely determined. To the southeast of these structures (Fig. 2) several undeformed plutonic, hypabyssal and volcanic rock sequences signal the late magmatic phases of post-collisional setting with a large volume of extensional, alkaline magmatism at ca. 580 Ma, as pointed out by Sommer *et al.* (2013).

The ARC also contains less voluminous, high grade paragneisses, mostly pelitic, but locally represented by plagioclase-rich calc-silicate varieties. They exhibit similar structural relations as observed in the TTG rock associations, but detailed structural and geochronological studies have yet to be performed in these rocks. The studied rock is an amphibolite found as meter-wide tabular bodies, discordantly intrusive in the paragneisses. Although the original geometry is somewhat modified by

further deformation, a small angle between the mafic rock and the main foliation of the paragneisses, together with their approximately tabular geometry, indicate that they are former dykes (Fig. 3). Additional structural and field work may lead to the definition of a dyke swarm, most of them being now concordant with the host-rock structure due to regional deformation and metamorphism.

The amphibolite is a fine-grained, foliated rock composed of plagioclase (60%), common hornblende (30%), garnet (7%) and opaque minerals (3%) with very small amounts of quartz, and zircon as the only accessory phase. Remnant nuclei of clinopyroxene are locally identified. A polygonal granoblastic texture is typical, and a microscale gneissic banding is given by alternating amphibole-rich mafic bands and plagioclase-rich felsic ones. Poikiloblastic garnet is visible in hand sample (~1mm) and found in both, mafic and felsic bands. The host paragneisses contain plagioclase, quartz, sillimanite, garnet, cordierite, biotite, monazite and opaque minerals.

Preliminary data from the mafic rocks indicate that their geochemical characteristics are similar to the ones of tholeiitic basalts, as the FeoO/MgO ratio of *ca*. 2.8 and Al_2O_3 contents lower than 15 wt%, for SiO_2 contents of *ca*. 49 wt%.

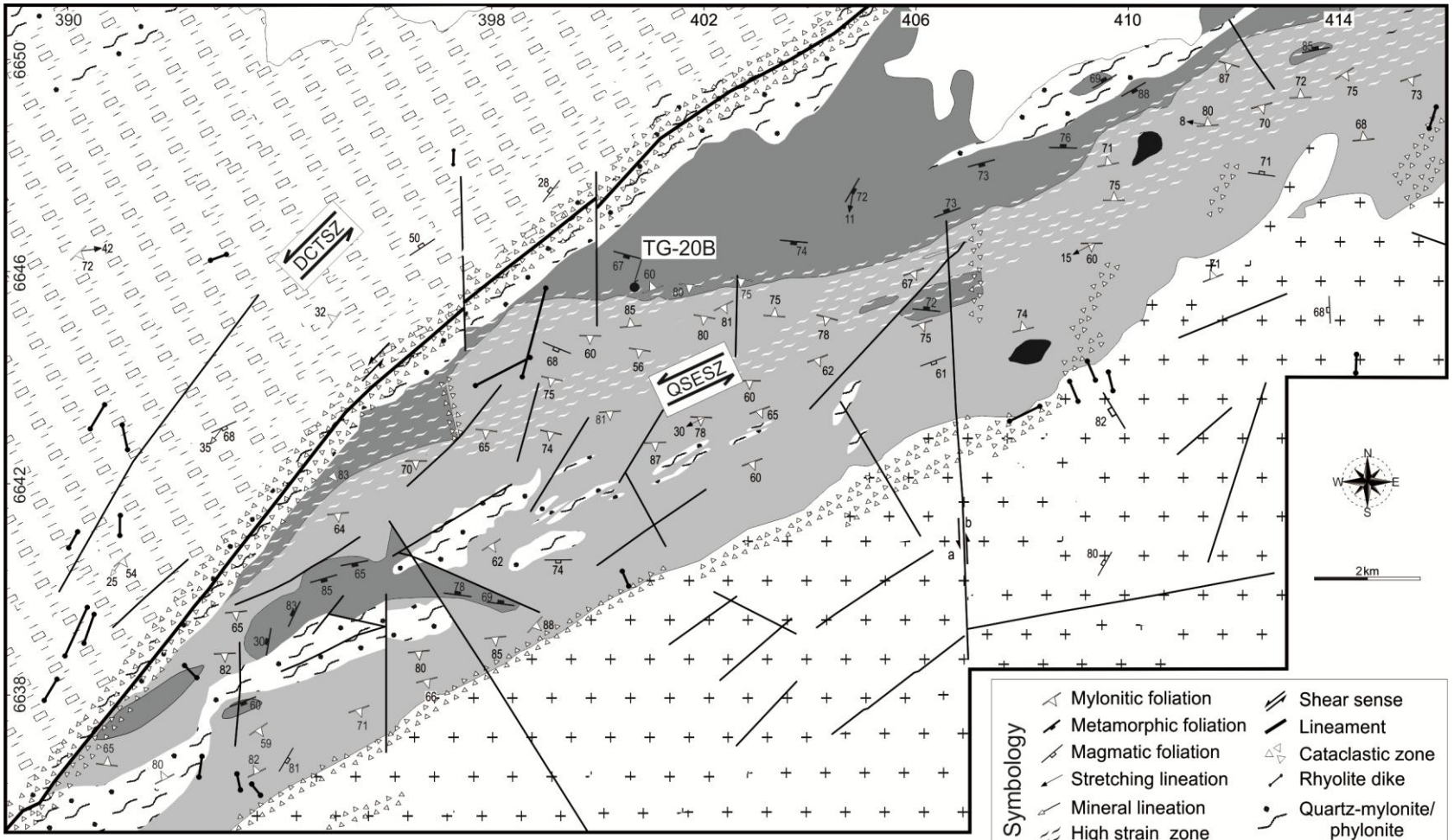

LEGEND

- Paleozoic Sedimentary Cover
- Quitéria-Serra do Erval Syntranscurrent Granitoids ~630 Ma
- High-grade Parametamorphic Rocks
- Late Transcurrent Plutonic and Hypabyssal Rocks ~580 Ma
- Dorsal de Canguçu Syntranscurrent Granitoids 658-605 Ma
- Arroio dos Ratos Complex

Figure 2 – Geological map of Quitéria-Serra do Erval region (modified from Gregory *et al.*, 2011), with location of dated sample point. DCTSZ – Dorsal de Canguçu Transcurrent Shear Zone; QSESZ – Quitéria-Serra do Erval Shear Zone.

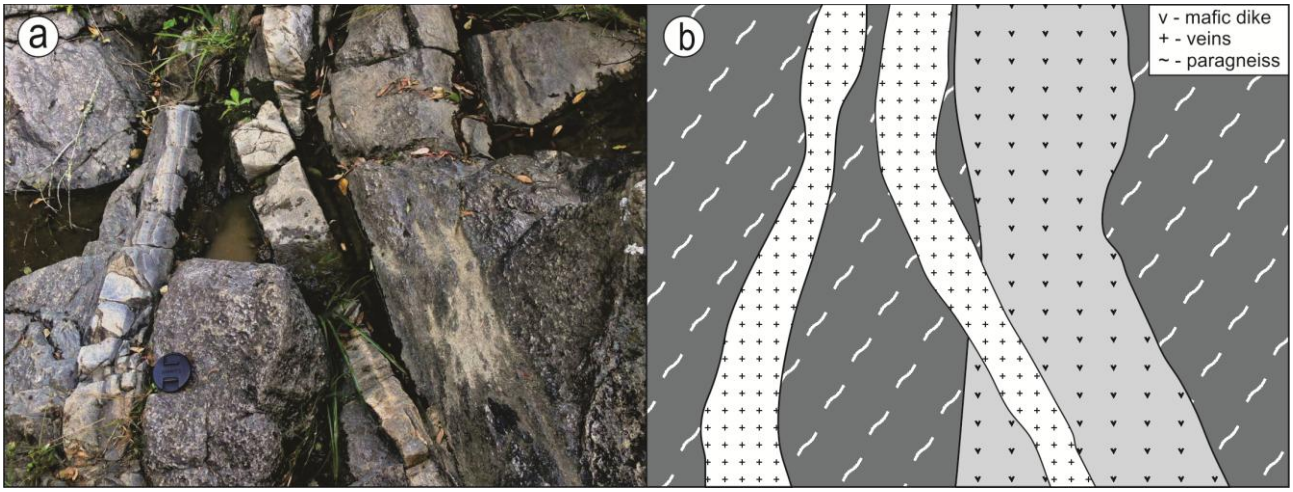

Figure 3 – Photograph (a) and sketch (b) of mafic rock field relations at sample site. The mafic rock discordantly crosscuts high-grade paragneisses as a dyke. Later granitic injections crosscut both.

4. Materials and methods

About 27 crystals were selected from the least magnetic zircon fraction and then secured and polished in a standard epoxy mount. The mount was initially carbon-coated for CL e SE image study with a JEOL JSM-5800 scanning-electron microscope (SEM) at the Centro de Microscopia Eletrônica of the Universidade de São Paulo, Brazil, using 15 kV accelerating voltage and 10 nA current.

The U-Pb isotopic analyses were performed on zircon grains using a Thermo-Finnigan Neptune MC-ICP-MS coupled with a Nd:YAG UP213 New Wave laser ablation system, installed in the Laboratory of Geochronology at the University of Brasília. The U-Pb analyses on zircon grains were carried out using the standard-sample bracketing method (Albarède & Beard, 2004) using the GJ-1 standard zircon in order to control the fractionation. Four detrital zircons have been analyzed between GJ-1 standard analyses, and $^{207}Pb/^{206}Pb$ and $^{206}Pb/^{238}U$ ratios have been time corrected. The raw data were processed off-line and reduced using an Excel worksheet (Bühn *et al.*, 2009). Analyses were performed using spot size of 30 µm and laser induced fractionation of the $^{206}Pb/^{238}U$ ratio was corrected using the linear regression method (Kosler *et al.*, 2002).

Data and diagrams were performed using the Isoplot/Ex software (Ludwig, 2003). About 11 of the 27 analysed crystals were selected for the age calculation. The selected crystals were the least metamict and least fractured ones. Results with discordance level above 30% were discarded, as well as the ones with error in U/Pb and Pb/Pb isotope ratios above 5%.

5. Geochronology

The selected zircon crystals are dark coloured, metamict and have no apparent zoning. They are subhedral to euhedral, and rarely have bipyramidal terminations or rounded edges. Crystal size varies around 90-200 µm, with aspect ratio of 3:1 to 5:1. Fractures are not common, although some

transgranular fractures may be very expressive (Fig. 4). Brighter spots and irregular brighter zones are concentrated in such fractured zones. No overgrowths or distinct rims are observed.

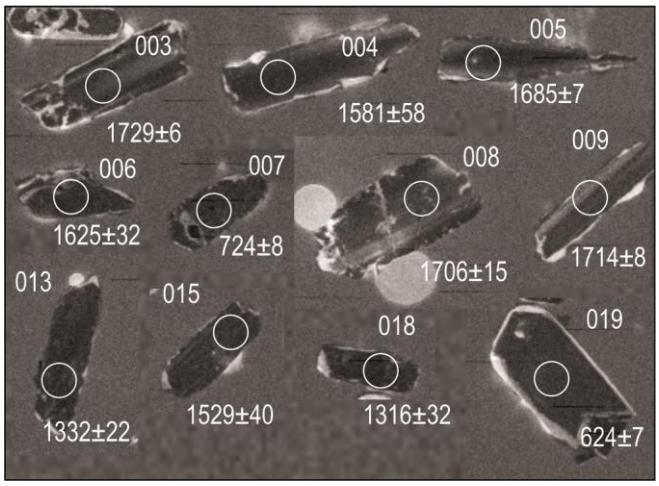

Figure 4 – Cathodoluminescence images (CL) of zircon grains from sample TG-20B. 30 μm spots marked in the analysed sites with $^{207}Pb/^{206}Pb$ ages highlighted (Ma; errors in 1σ).

Table 1 – Results of LA-MC-ICP-MS analyses in zircon crystals used to calculate the age of sample TG-20B.

TG-20B*	Isotopic Ratio							Age and error (Ma, 1σ)							Th/U
spot	$^{207}Pb/^{235}U$	error (%,1σ)	$^{206}Pb/^{238}U$	error (%,1σ)	rho	$^{207}Pb/^{206}Pb$	error (%,1σ)	$^{206}Pb/^{238}U$	error	$^{207}Pb/^{235}U$	error	$^{207}Pb/^{206}Pb$	error	% Disc	
003	4.002870	0.974147	0.274253	0.922071	0.941143	0.105857	0.314242	1562	13	1635	8	1729	6	9.65	0.954
004	3.795052	3.819767	0.281612	2.394761	0.623659	0.097738	2.975859	1599	34	1592	31	1581	58	-1.14	0.476
005	3.521592	0.773201	0.247085	0.688603	0.868825	0.103369	0.351663	1423	9	1532	6	1685	7	15.55	0.508
006	3.306351	2.358797	0.239737	1.653206	0.884032	0.100026	1.682508	1385	21	1483	19	1625	32	14.73	2.293
007	0.969529	0.743983	0.110774	0.643120	0.833639	0.063478	0.374040	677	4	688	4	724	8	6.49	0.286
008	4.360367	1.665663	0.302625	1.455012	0.868797	0.104500	0.810787	1704	22	1705	14	1706	15	0.07	0.695
009	3.918547	2.022123	0.270717	1.981214	0.979490	0.104980	0.404692	1544	27	1618	17	1714	8	9.89	0.554
013	1.944058	2.303549	0.164487	2.015201	0.872424	0.085719	1.115932	982	18	1096	16	1332	22	26.29	0.485
015	3.268866	2.543748	0.249449	1.493719	0.578553	0.095042	2.058994	1436	19	1474	20	1529	40	6.10	1.433
018	1.840540	2.363318	0.157002	1.729789	0.726303	0.085023	1.610312	940	15	1060	16	1316	32	28.57	0.420
019	0.854292	0.662520	0.102279	0.588005	0.854277	0.060578	0.305259	628	4	627	3	624	7	-0.55	0.003

* - coordinates 400,696 mE and 6,645,703 mN, fuse 22J, datum Córrego Alegre.

For age calculation purposes 11 zircon crystals were selected (Fig. 4; Tab. 1) that yield an upper intercept discordia age of 1,716 ± 72 Ma (Fig. 5), interpreted as the magmatic crystallization age of the protolith. The $^{207}Pb/^{206}Pb$ weighted mean average age of 1,706 ± 120 Ma (Fig. 5) calculated from data with <16% discordance is in agreement with the upper intercept discordia age. The spots aligned along the discordia line illustrate progressive Pb loss and these spots have variable U/Th ratios (0.420-2.293), which points to opening of the U-Th-Pb system.

The lower intercept discordia age is 635 ± 130 Ma. The only two spots set in the lower intercept and aligned to the discordia line have Th/U ratios of 0.003 and 0.286. This lower intercept age can either have geological meaning or represent progressive Pb loss. However, the individual 624 ± 7 Ma $^{207}Pb/^{206}Pb$ age (spot 19, Tab.1; Fig. 4) is a concordant spot that anchors the discordia line (Fig. 5). This age was obtained in a crystal core with Th/U = 0.003, well preserved, slightly fractured and clearer in comparison with the other zircon grains. On the other hand, the other Neoproterozoic age of 724 ± 8 Ma age, with Th/U = 0.286 (spot 007, Tab.1; Fig. 4) is not set in the concordia line, but aligned over the discordia line delineated by the whole dataset (Fig. 5). This age was obtained in a

metamict crystal core and close to a fractured zone (Fig.4). Taking all this into account, the 624 ± 7 Ma age is intepreted as the metamorphic age of the amphibolite facies event identified in the rock. This interpretation is based on the fact that this is a concordant data, with low Th/U ratio, obtained in a clean and non-fractured crystal and by the correlation of this metamorphic age with the thermal event linked to the massive Neoproterozoic sintectonic granite emplacement in the region. By contrast, the 724 ± 8 Ma age, was obtained in a very fractured, metamict grain, with higher discordance and that does not have any potential correlation with a known regional geological event. Therefore, it is interpreted as a result of progressive Pb loss, which is also verified in a large part of the discordant data for this sample.

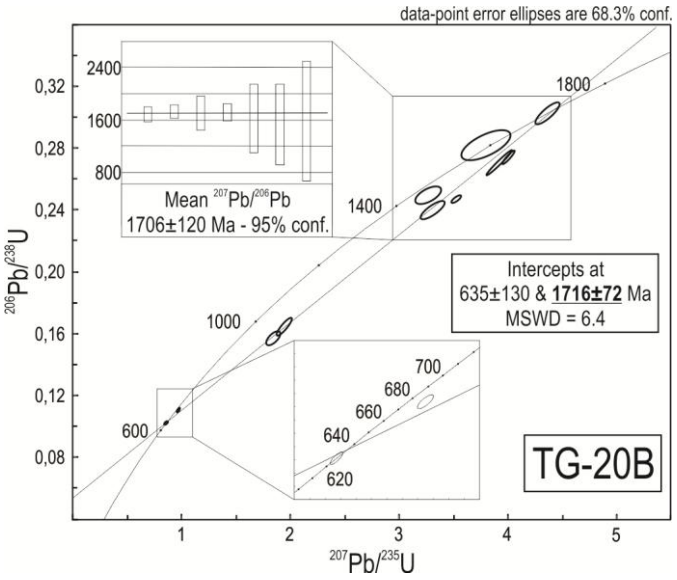

Figure 5 – Concordia plot for sample TG-20B. Upper intercept discordia age interpreted as magmatic crystallization age, lower intercept discordia age intepreted as metamorphic amphibolite facies event. Upper inset in the figure shows the $^{207}Pb/^{206}Pb$ weighted mean average age calculated. The lower inset in the figure is a detail of the Neoproterozoic ages identified in the sample.

6. Discussion and Conclusions

The calculated age of 1,716 ± 72 Ma corresponds to the Paleoproterozoic Staterian period (1,800 to 1,600 Ma), rarely identified in the Sul-rio-grandense Shield. Furthermore, Staterian ages have never been identified in mafic rocks from these shield areas.

The Staterian amphibolitic rocks studied in this paper may be correlated to the mafic rocks of the Florida (UY) dyke swarm in terms of their composition and age although, unlike the Florida swarm, the presently studied rocks are strongly deformed and recrystallized.

The Florida dyke swarm studied by Bossi *et al.* (1993) and Mazzucchelli *et al*. (1995) comprises unmetamorphosed basalts and andesitic basalts oriented EW which crosscut Archaean and Paleoproterozoic cratonic rocks. In the studied case, the mafic dykes are discordantly intrusive in paragneisses which have been metamorphosed and deformed together with Paleoproterozoic rocks, but of which the precise age is still unknown.

The Florida dykes are interpreted as resulting from either anorogenic or taphrogenic intraplate tholeiitic magmatism by Bossi *et al.* (1993) and Mazzucchelli *et al*. (1995) based on their chemical characteristics. The mafic rocks presently described are not yet well characterized from a geochemical

viewpoint, but the few available analyses indicate FeO/MgO ratio and alumina contents compatible with a tholeiitic affinity as well. The basic composition of the studied dikes points out to juvenile accretion during this Staterian event in southern Brazil. The 1,716±72 Ma age value presently obtained in zircon is very similar to the age of 1,790±5 Ma obtained from baddeleyite in the Florida dikes by Halls *et al.* (2001).

The Staterian (1,785 ± 42 Ma and 1,768 ± 24 Ma, LA-MC-ICP-MS) deformed granitoids reported by Camozzato *et al.* (2013) are interpreted by these authors as representing the evolution of a Paleoproterozoic continental margin arc. Considering the age interval of activity of the continental magmatic arc described by Gregory *et al.* (submitted a) from 2,150 to 2,070 Ma, the ARC is interpreted to represent the register of a mid- to late Rhyacian magmatic arc, followed by a Staterian anorogenic, or maybe even taphrogenic stage. Thus, it is here suggested that the Staterian record identified in the eastern part of the Sul-rio-grandense Shield corresponds to a within-plate environment, different from the interpretation of Camozzato *et al.* (2013) for chrono-correlated units in the central part of the Shield.

The evolutionary trend presently admitted for the ARC rocks, with development of a magmatic arc followed by a *ca.* 200 Ma-long period of tectonic stagnation, eventually leading to taphrogenesis, is similar to the common evolution verified in the Paleoproterozoic terranes of South America, whose agglutination in the Atlantica Supercontinent (Rogers, 1996) would have culminated in the so-called Staterian Taphrogeneis (Brito Neves, 1999; Almeida *et al.*, 2000).

The metamorphic age of 624±7 Ma is correlated to the syntectonic magmatism along the QSESZ (*ca* 630 Ma – Knijnik *et al.*, 2012), and coincides within error with the *ca* 635 Ma age reported by Gregory *et al.* (submitted a) for metamorphic borders developed over Paleoproterozoic igneous zircons in a tonalite.

The very fact that the ARC paragneisses are crosscut by Staterian mafic dykes indicates that they are not to be correlated with the Várzea do Capivarita Complex studied by Martil *et al.* (submitted) high-grade paragneisses of Neoproterozoic age, but represent an older supracrustal gneissic sequence, possibly metamorphosed under similar conditions in Neoproterozoic times. The presence of pre-Staterian supracrustal rocks reinforces the observations of Gregory *et al.* (2011) who report xenoliths of calc-silicate gneisses in the ARC Paleoproterozoic tonalites probably formed in an active continental margin.

Acknowledgments

We are grateful to prof. Márcio Martins Pimentel for his help with obtaining part of the isotope data. This work had partial financial support from the National Research Council (CNPq) to M.F. Bitencourt (Universal Project n. 471266/2010-8) and from the Rio Grande do Sul State Research Foundation (FAPERGS) to L. Nardi (Proc. n. 10.16039), as well as a PhD research grant from CNPq to T.R. Gregory.

References

Albarède, F. & Beard, B. 2004. Analytical methods for non-traditional isotopes. *Reviews in mineralogy and geochemistry*, 55(1): 113-152.

Almeida, D.P.M., Chemale Jr, F. & Machado, A. 2012. Late to post-orogenic Brasiliano-Pan-African volcano-sedimentary basins in the Dom Feliciano Belt, southernmost Brazil. *Petrology – New Perspectives and Applications*, 2012: 73-130.

Almeida, F.F.M., Brito Neves, B.B. & Dal Ré Carneiro, C. 2000. The origin and evolution of the South American Platform. *Earth-Science Reviews*, 50(1): 77-111.

Almeida, F.F.M., Hasui, Y., Brito Neves, B.B. & Fuck, R.A. 1981. Brazilian structural provinces: an introduction. *Earth-Science Reviews*,*17*(1): 1-29.

Babinski, M., Chemale Jr., F., Hartmann, L.A., Van Schmus, W.R. & Silva, L.C. 1996. Juvenile accretion at 750-700 Ma in southern Brazil. *Geology*, 24(5):439-442.

Bicca, M.M., Chemale Jr, F., Jelinek, A.R., de Oliveira, C.H.E., Guadagnin, F. & Armstrong, R. 2013. Tectonic evolution and provenance of the Santa Bárbara Group, Camaquã Mines region, Rio Grande do Sul, Brazil. *Journal of South American Earth Sciences*, 48: 173-192.

Bitencourt, M.F., De Toni, G.B., Florisbal, L.M., Martil, M.M.D., Niessing, M., Gregory, T.R., Nardi, L.V.S., Heaman, L.M., Dufrane, S.A. 2011. Structural geology and U-Pb age of unusual Neoproterozoic syn-collisional syenite-tonalite association from southernmost Brazil. *In:* Seventh Hutton Symposium on Granites and Related Rocks, 2011, Avila. *Abstracts Book*. Avila: Universidad de Salamanca, v.u.p. 21-21.

Bitencourt, M.F. & Nardi, L.V.S. 1993. Late- to Post-collisional Brasiliano Magmatism in Southernmost Brazil. *Anais da Academia Brasileria de Ciências*, 65: 3-16.

Bitencourt, M.F.A.S. & Nardi, L.V.S. 2000. Tectonic setting and sources of magmatism related to the southern Brazilian shear belt. *Revista Brasileira de Geociências*, 30(1): 186-189.

Bossi, J., Campal, N., Civetta, L., Demarchi, G., Girardi, V.A.V., Mazzucchelli, M. & Molesini, M. 1993. Early Proterozoic dike swarms from western Uruguay: geochemistry, Sr-Nd isotopes and petrogenesis. *Chemical Geology*, 106(3): 263-277.

Brito Neves, B.B. 1999. América do Sul: quatro fusões, quatro fissões e o processo acrescionário andino. *Brazilian Journal of Geology*, 29(3): 379-392.

Bühn, B., Pimentel, M.M., Matteini, M.& Dantas, E.L. 2009. High spatial resolution analysis of Pb and U isotopes for geochronology by laser ablation multi-collector inductively coupled plasma mass spectrometry (LA-MC-ICP-MS). *Anais da Academia Brasileira de Ciências*, 81(1): 99-114.

Camozzato, E., Philipp, R.P. & Chemale Jr., F. 2013. Idades Estaterianas e Calimianas no Domo da Vigia: Complexo Vigia e Porongos, Metagranito Seival e Anfibolito Tupi Silveira, Bagé, RS. *In*: XI Simpósio Nacional de Estudos Tectônicos. Anais...(CD) Ouro Preto, MG.

Chemale Jr., F. 2000. Evolução Geológica do Escudo Sul-rio-grandense. *In*: Holz, M. & De Ros, L.F. (Eds.). *Geologia do Rio Grande do Sul*. Porto Alegre, CIGO/UFRGS, p. 13-52.

Chemale Jr., F., Phillip, R.P., Dussin, I.A., Formoso, M.L.L., Kawashita, K. & Berttotti, A.L. 2011. Lu–Hf and U–Pb age determination of Capivarita anorthosite in the Dom Feliciano Belt, Brazil. *Precambrian Research*, 186, 117–126.

Fernandes, L.A.D. & Koester, E. 1999. The Neoproterozoic Dorsal de Canguçú strike-slip shear zone: its nature and role in the tectonic evolution of southern Brazil. *Journal of African Earth Sciences*,1: 3-24.

Florisbal, L.M.F., Janasi, V.A., Bitencourt, M.F., Heaman, L.M. 2012. Space-time relation of post-collisional granitic magmatism in Santa Catarina, southern Brazil: U-Pb LA-MC-ICP-MS zircon geochronology of coeval mafic-felsic magmatism related to the Major Gercino Shear Zone. *Precambrian Research*, 216-219: 132-151.

Frantz J.C., McNaughton N.J., Marques J.C., Hartmann L.A., Botelho, N.F., Caravaca, G. 2003. SHRIMP U-Pb zircon ages of granitoids from southernmost Brazil: constraints on the temporal evolution of the Dorsal de Canguçu Transcurrent Shear zone and the eastern Dom Feliciano Belt. *In:*IV South American symposium of isotope geology. *Short papers…*(p. 174–177). Salvador, Brazil.

Garavaglia, L., Bitencourt, M.F. & Nardi, L.V.S. 2002. Cumulatic Diorites Related to Post-collisional, Brasiliano/Pan-African Mafic Magmatism in the Vila Nova Belt, Southern Brazil. *Gondwana Research*, 5:519-534.

Garavaglia, L., Koester, E., Bitencourt, M.F. & Nardi, L.V.S. 2006. Isotopic Signature of Late magmatic Arc to Post-collisonal Magmatism in the Vila Nova Belt, Southern Brazil. *In*: South-American Symposium on Isotope Geology, 5, 2006, Punta del Este. *Short Papers*...(p. 101-104).Punta del Este, Universidad de la Republica.

Gregory, T.R., Bitencourt, M.F. & Nardi, L.V.S. 2011. Caracterização estrutural e petrológica de metatonalitos e metadioritos do Complexo Arroio dos Ratos na sua seção-tipo, região de Quitéria, RS. *Pesquisas em Geociências*, 38(1): 85-108.

Gregory, T.R., Bitencourt, M.F., Nardi, L.V.S. & Florisbal, L.M. Petrogenesis of Paleoproterozoic TTG-type mafic and felsic rock associations from southernmost Brazil, based on elemental and isotopic geochemistry. Lithos (*submitted b*).

Gregory, T.R., Bitencourt, M.F., Nardi, L.V.S., Florisbal, L.M. & Chemale Jr., F. Geochronological data from TTG-type association of the Arroio dos Ratos Complex and implications for crustal evolution of southernmost Brazil in Paleoproterozoic times. *Journal of South American Earth Sciences* (*submitted a*).

Gruber, L., Porcher, C.C., Lenz, C. & Fernandes, L.A.D. 2011. Proveniência de metassedimentos das sequências Arroio Areião, Cerro Cambará e Quartzo Milonitos no Complexo Metamórfico Porongos, Santana da Boa Vista, RS. *Pesquisas em Geociências*, 38(3): 205-223.

Halls, H.C., Campal, N., Davis, D.W. & Bossi, J. 2001. Magnetic studies and U–Pb geochronology of the Uruguayan dyke swarm, Rio de la Plata craton, Uruguay: paleomagnetic and economic implications. *Journal of South American Earth Sciences*, 14(4): 349-361.

Hartmann, L.A., Chemale Jr., F. & Philipp, R.P. 2007. Evolução Geotectônica do Rio Grande do Sul no Pré-Cambriano. *In*: Iannuzzi, R. & Frantz, J.C. (Eds.). *50 anos de Geologia: Instituto de Geociências. Contribuições*. Porto Alegre, Instituto de Geociências, Universidade Federal do Rio Grande do Sul, p. 97-124.

Hartmann, L.A., Leite, J.A.D., Silva, L.C., Remus, M.V.D., McNaughton, N.J., Groves, D.I., Fletcher, I.R., Santos, J.O.S. & Vasconcellos, M.A.Z. 2000. Advances in SHRIMP geochronology and their impact on understanding the tectonic and metallogenic evolution of southern Brazil. *Australian Journal of Earth Sciences*, 47:829-844.

Hartmann, L.A., Schneider, J.O. & McNaughton, N.J. 2008. Detrital Zircon U-Pb Age Data, and Precambrian Provenance of the Paleozoic Guaritas Formation, Southern Brazilian Shield. *International Geology Review*, 50(4): 364-374.

Janikian, L., Almeida, R.P., Fragoso-Cesar, A.R.S., Martins, V.T.S., Dantas, E.L., Tohver, E., McReath, I. & D'Agrella-Filho, M.S. 2012. Ages (U–Pb SHRIMP and LA ICPMS) and stratigraphic evolution of the Neoproterozoic volcano-sedimentary successions from the extensional Camaquã Basin, Southern Brazil. *Gondwana Research*, 21(2): 466-482.

Knijnik, D.B., Bitencourt, M.F., Gregory, T.R. 2013. A Zona de Cisalhamento Quitéria-Serra do Erval e o magmatismo sintectônico precoce do Cinturão de Cisalhamento Sul-brasileiro. *In*: XI Simpósio Nacional de Estudos Tectônicos. Anais...(CD) Ouro Preto, MG.

Knijnik, D.B., Bitencourt, M.F., Nardi, L.V.S., Pinto, V.M., Fontana, E. 2012. Caracterização Geoquímica do Granodiorito Cruzeiro do Sul: magmatismo shoshonítico pós-colisional neoproterozoico em zona de transcorrência, região de Quitéria, RS. *Geologia USP*, 12(1): 17-38.

Koester, E., Chemale Jr., F., Porcher, C.C., Bertotti, A.L. & Fernandes, L.A.D. 2008. U-Pb ages of granitoids from Eastern Sul-riograndense Shield. *In*: VI South American Symposium on Isotope Geology. *Anais…*(p. 95). San Carlos de Bariloche, Argentina.

Košler, J., Fonneland, H., Sylvester, P., Tubrett, M. & Pedersen, R.B. 2002. U–Pb dating of detrital zircons for sediment provenance studies—a comparison of laser ablation ICPMS and SIMS techniques. *Chemical Geology*, 182(2): 605-618.

Leite, J.A.D., Hartmann, L.A., Fernandes, L.A.D., McNaughton, N.J., Soliani Jr, E., Koester, E., Santos, J.O.S. & Vasconcellos, M.A.Z. 2000. Zircon U-Pb SHRIMP dating of gneissic basement of the Dom Feliciano Belt, southernmost Brazil. *Journal of South American Earth Sciences*, 13: 739-750.

Ludwig, K.R. 2003. *User's manual for Isoplot 3.00: A geochronological toolkit for Microsoft Excel* (No. 4). Kenneth R. Ludwig.

Martil, M.M.D., Bitencourt, M.F. & Nardi, L.V.S. 2011. Caracterização estrutural e petrológica do magmatismo pré-colisional do Escudo Sul-rio-grandense: os ortognaisses do Complexo Metamórfico Várzea do Capivarita. *Pesquisas em Geociências*, 38(2): 181-201.

Martil, M.M.D., Bitencourt, M.F., Armstrong, R., Nardi, L.V.S., Chemale Jr., F. Geochronology of orthogneisses from the Várzea do Capivarita Complex thrust pile and implications for the timing of continental collision in southernmost Brazil. Precambrian Research (*submitted*).

Mazzucchelli, M., Rivalenti, G., Piccirillo, E.M., Girardi, V.A.V., Civetta, L. & Petrini, R. 1995. Petrology of the Proterozoic mafic dyke swarms of Uruguay and constraints on their mantle source composition. *Precambrian Research*, 74(3): 177-194.

Nardi, L.V.S. & Bitencourt, M.F. 2007. Magmatismo granítico e evolução crustal no sul do Brasil. *In*: Iannuzzi, R. & Frantz, J.C. (Ed.). *50 Anos de Geologia. Instituto de Geociências. Contribuições.* Porto Alegre, Editora Comunicação e Identidade, CIGO e IG-UFRGS, p. 125-141.

Rogers, J.J. 1996. A history of continents in the past three billion years. *The journal of geology*, 104: 91-107.

Saalmann, K., Gerdes, A., Lahaye, Y., Hartmann, L.A., Remus, M.V.D. & Läufer, A. 2011. Multiple accretion at the eastern margin of the Rio de la Plata craton: the prolonged Brasiliano orogeny in southernmost Brazil. *International Journal of Earth Sciences*, 100 (2-3): 355-378.

Silva, L.C., Hartmann, L.A., McNaughton, N.J. & Fletcher, I.R., 2000. Zircon U/Pb SHRIMP dating of a Neoproterozoic overprint in Paleoproterozoic graniticgneissic terranes, southern Brazil. *American Mineralogist*, 85: 649-667.

Sommer, C.A., Philipp, R.P., Lima, E.F., Basei, M.S., Oliveira, D.S. & Filho, J.N. 2013. Geoquímica e geocronologia das rochas riolíticas associadas ao Batólito Pelotas, porção oriental do Escudo Sul-rio-grandense: dados preliminares. *In:* XIV Congresso Brasileiro de Geoquímica. *Anais…*(CD). Diamantina-MG.